Alma Mater Studiorum – University of Bologna

SCIENCE UNIVERSITY

Department of Industrial Chemistry "Toso Montanari"

Master's Degree in

Industrial Chemistry

Class LM-71 – Science and Industrial Chemistry Technology

Electrodeposition of actives species on carbonaceous materials for energy applications

CANDIDATE

Diana Elena Ciurduc

SUPERVISOR

Illustrious Professor: Marco Giorgetti

CO SUPERVISOR

Illustrious Professor: Eduardo Enciso Rodrìguez

Dino Tonti

Academic Year 2016-2017

Session II

Abstarct

The thesis work focuses on the electrosynthesis of active species on carbonaceous materials, their characterization and energy applications. Two protocols of electrochemical synthesis that lead to two forms of hexacyanoferrate copper (CuHCF) with different composition and structure, were applied. The procedure used is a "two – step" method that involves the deposition of metallic copper and the subsequent anodization in the presence of ferricyanide ion, using as support graphite sheet, carbon cloth and carbon toray paper. Another protocol was that of electrosynthesis of double layer hydroxide (LDH) containing cobalt as bivalent cation and aluminium or iron as trivalent metal, using as support graphite sheet, carbon cloth, carbon toray paper and nickel foam. After studying the correlation between the electrodeposition time and the masses obtained, the specific capacities of the deposited materials were calculated. The last used protocol was the electrochemical synthesis of nickel hexacyanoferrate on nickel foam. All the film obtained were electrochemically characterized by cyclic voltammetry. SEM – EDX and XRD analyses were performed on some samples in order to obtain morphological and chemical informations.

Some tests were conducted using the supports or some of the electrodeposited samples as cathodes in lithium – air batteries, to understand their potential as sources of energy. After performing oxygen and argon cyclic voltammetries, controlling in what way the potential change at different current density and carrying out full discharge at constant current density (0.02 mA/cm^2), it was found that the carbon tissue was the one that produced the best results. So it was decided to study in deep the behaviour of this support when active species are electrodeposited above it.

As a parallel work, attempts were made to obtain porous carbon from hair, with the intention of using it as a support, in a slurry for example, for testing electrodepositions of active species mentioned above. Despite the porosity being tested through nitrogen adsorption isotherms and good results have been achieved, it has not been enough time to find the right slurry with which to conduct the electrodepositions.

Sommario

Chapter 1: Introduction

The purpose of this introduction is to give a comprehensive overview of the techniques and tools used to develop this thesis work.

1.1 Hexacyanoferrate of transition metals

When we talk about hexacyanoferrate of transition metals we refer to a category of inorganic compounds of general formula $A_xM_y[Fe(CN)_6] * zH_2O$, with M = metal of transition, A = countercation, belonging to the largest family of compounds called hexacyano metallates.

1.1.1. Prussian Blue

In this class of compounds, the first and most studied is the hexacyanoferrate (II) of iron (III), also known as Prussian Blue (PB). Its synthesis is reported in the literature of the early 18th century (1), making it one of the first coordinating compounds to be obtained synthetically and one of the oldest inorganic pigments produced industrially (2).

The "soluble" $KFe^{III}Fe^{II}(CN)_6$ form is obtained when $K_4[Fe(CN)_6]$ is mixed in a 1 : 1 solution with Fe^{3+} [1.1] or inversely when $K_3[Fe(CN)_6]$ is put in solution with a Fe^{2+} salt [1.2]. The structure thus obtained is the more regular and free from defects even if in both cases a colloidal solution is obtained. The soluble term was introduced by paint manufacturers, referring to the easiness with which Potassium salts form colloidal solutions (peptization).

$$Fe^{3+} + K_4[Fe^{II}(CN)_6] \rightarrow 3K^+ + K[Fe^{III}Fe^{II}(CN)_6] \qquad [1.1]$$

$$Fe^{2+} + K_3[Fe^{III}(CN)_6] \rightarrow 2K^+ + K[Fe^{III}Fe^{II}(CN)_6] \qquad [1.2]$$

The "insoluble" form $Fe_4[Fe(CN)_6]_3$ is obtained when Fe^{3+} or Fe^{2+} salts are added in excess to a solution of anions $[Fe(CN)_6]^{4-}$ or $[Fe(CN)_6]^{3-}$, obtaining in the first case the Blues of Prussia and in the second the Blue of Turnbull (3). It has been demonstrated, through XRD analysis and electron diffraction, as the two compounds possess the same structure (4). The tonal difference resides purely in the precipitation method, which affects the size of the particles and the content of impurities.

The soluble and insoluble terms, however, should not be understood in the real sense of terms, but rather refer to the ability or not to form colloidal solutions. Such propriety is due to the presence or not, respectively, of interstitial cavity. (5)

The first to study the structure of the copper hexacyanoferrate were Keggin and Milles (6) through X-ray diffraction. The structure in Figure 1.1 is a face centered cubic structure (fcc) where Fe^{2+} and Fe^{3+} ions are connected via bridges of $-C \equiv N -$ forming a bond of type Fe^{II} – CN – Fe^{III}. The cell length is about 10 Å. Studies by IR and Mössbauer have made it possible to establish definitively that in ferric ferrocyanide the iron atom coordinated to the carbon is a low spin Fe^{2+}, while the iron coordinated to the nitrogen is a high spin Fe^{3+} (7) (8).

The structure of the insoluble form was determined by Ludi et all (9). They found it a greater structural disorder caused by the fact that a quarter of the sites destined to ferrocyanide is not occupied. The sites that present deficiencies of $[Fe(CN)_6]^{4-}$ ions are occupied by water molecules. The structure contains three different coordination iron sites: $Fe^{II}C_6$, $Fe^{III}N_6$ and $Fe^{III}N_4(H_2O)$ in a 3 : 1 : 3 ratio.

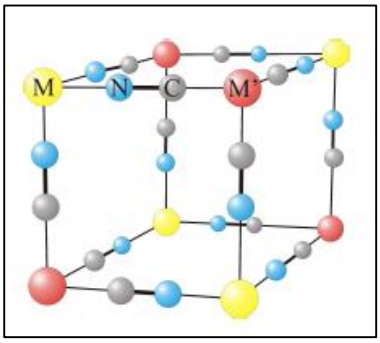

Figura 1.1: In the figure, a part of the cubic lattice characterictic of hexagonal metal. The possible defect and intercalated molecules or ions are not shown. When M = Fe^{III} and M' = Fe^{II}, we obtain the classic idealized structure of Prussian Blue.

The intense blue color is due to the transfer of electrons between the ions $[Fe^{II}(CN)_6]^{4-}$ and Fe^{3+}. In fact if the centers of Fe^{3+} are completely reduced to Fe^{2+} we obtain the white salt of $K_4F_4^{III}[Fe^{II}(CN)_6]_3$, called Prussian White (PW) or Everitt's salt. If on reverse the centers of Fe^{2+} are oxidezed at Fe^{3+} we obtain $Fe_4^{III}[Fe^{III}(CN)_6]_3$, called also Prussian Yellow (PY). A partial oxidation leads to Green of Berlin (BG).

The interest in this category of compounds rised thanks to Neff's electrochemical studies (10), he deposited for the first time a slim film of Prussian Blue attached to a conductive material. He observed how the deposit could be oxidezed and reduced in response to a variation in the electrochemical potential.

Electronic transfer reactions are accompanied by transfer of cations inside and outside the structure so the charge balance is kept neutral. In the case of Prussian Blue, the reduction of iron centers involves the insertion of alkali metal cations in the inserstitial positions. [1.3]

$$Fe_4^{III}[Fe^{II}(CN)_6]_3 + 4e^- + 4K^+ \leftrightarrow K_4Fe_4^{II}[Fe^{II}(CN)_6]_3 \qquad [1.3]$$

During oxidation, alkaline metal cations leave the lattice and go back in solution. Going from Prussian White to Prussian Blue, the cations go out of the grid, for this reason it is believed that further oxidation to Green of Berlin and Prussian Yellow involves the insertion of anions. (11) [1.4]

$$Fe_4^{III}[Fe^{II}(CN)_6]_3 + 3e^- + 3A^- \leftrightarrow Fe_4^{III}[Fe^{II}(CN)_6A]_3 \qquad [1.3]$$

Prussian Blue films were deposited for simple dipping (10) (12), electrochemical deposition in galvanostatic way (13), potentiodynamic (14), potentiostatic (15) (16) (17) (18), and through plasma techiques combined with electrochemical methods (19). The different deposition mechanisms of Prussian Blue on a conductive support are reported in literature by some authors (12) (20) (21). In the non – electrochemical process it has been hupothesized that the formation of Prussian Blue is associated with the oxidation of the conductive support due to the complex $Fe^{III}[Fe^{III}(CN)_6]$. The immersion of a conductive support in a solution like $FeCl_3$ e $K_3Fe(CN)_6$ has a very positive OCP which is not achieved in a solution contaning only one of these two salts. We can conclude that the solution consisting of both salts is a strong oxidant.

The potentiodynamic deposition is believed to be based on two mechanisms: in the first the potential of +0.7V is reached in the cathodic direction and the Prussian Blue is deposited thanks to the reduction of the $Fe^{III}[Fe^{III}(CN)_6]$ complex, while in the second at a potential of +0.4V the Fe^{3+} ions are reduced to Fe^{2+} ions on the nude electrode. The Fe^{2+} reacting with the ferricyanide ions caused the precipitation of Prussian Blue.

A furher strategy is to deposit a metallic iron film on the conducting substrate, oxidazing it in a solution of $K_4Fe(CN)_6$ by the potentiostatic or potentiodynamic way (22). The supersaturation of the Fe^{3+} ion that is created near the surface of the electrode allows the deposition of the Prussian Blue. It is also possible to deposit Prussian Blue from a solution containing only $[Fe(CN)_6]^{3-}$. By favoring the acid pH condition, the ferrocyanide anion dissociates; the Fe^{3+} is reduced to Fe^{2+} on the surface of the electrode forming Prussian Blue (23). Galvanostatic methods are based on the same mechanisms as the previous ones; apply one determined current density for a certain period of time, during which the potential of the electrode changes. The driving force is never the same and the film that is

formed coould have different shapes or structures when compared with the methods that allow to controle the potential.

The interest for this compound has led to the synthesis of countless analogies where Fe^{3+} ion is replaced by transition metals such as Cu (24), Pd (25), In (26), Pt (27), Cr (28), Ni (29), Co (30), V (31), Zn (32), Ga (33), Mn (34). In addition to the possibility of create hexacyanoferrates of mixed metals, such as CuPdHCF (35), CuCoHCF (36), NiPdHCF (37), NiCoHCF (38), FeRuHCF (39), recently have also been synthesized compounds based on rare earths (40).

1.1.2. Copper Hexacyanoferrate

The copper hexacyanoferrate (CuHCF) is one of the most studied Prussian Blue's analogs. Its synthesis is reported in literature from the end of the XIX century, and with this synthesis they performed perhaps the oldest semi-permeable membrane for studies on osmotic equilibrium (41). In the article of 1963 by Keggin and Miles (6) the structure in the Figure 1.2 is common to that of the Prussian Blue. The structure can be referred to CuHCF in the "soluble" form or in the "insoluble" one. The "soluble" form has a typical face centered cubic structure, in which the iron is bonded to the carbon while the copper is bonded to the nitrogen ($Fe - C \equiv N - Cu$). The "insoluble" form has a similar cubic structure to the previously described one, but with a quarter of the sites for $[Fe(CN)_6]^{4-}$ unused and water molecules in the empty positions to complete the coordination shell of Cu (42).

The substitution of Fe^{3+} with Cu^{2+} produces a distorted and more opened structure that the Prussian Blue one. This feature has raised the interest in this compound since it is capable of interacting with a wider range of ions and for the ability to exploit the couple Cu^{2+}/Cu^{+} for the electrocatalysis of many compounds.

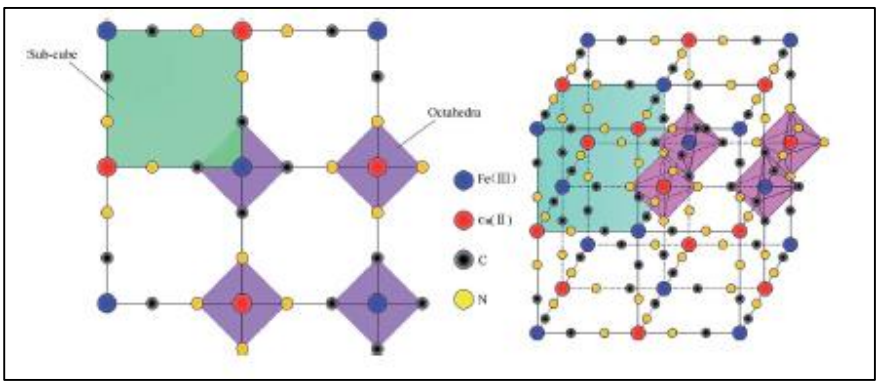

Figure 1.2: Structure of CuHCF **(43)** a_0 around 10 Å, and it is twice the distance between the Fe and Cu metals

The molecular formula is generally represented as $Cu_3^{II}[Fe^{III}(CN)_6]_2 * xH_2O$ for the oxidized species and $K_2Cu_3^{II}[Fe^{II}(CN)_6]_2 * xH_2O$ for the reduced species. The results obtained from Ayrault et al (44) (45) show how the reduced form of CuHCF is composed of two different components: $Cu_2^{II}[Fe^{II}(CN)_6]$ and $K_2Cu^{II}[Fe(CN)_6]$. The oxidized form and the first of the two reduced ones were determined by X-ray diffraction (XRD), the second reduced one remained indeterminate since one singe crystal cannot be obtained.

The CuHCF was deposited for the first time on a glassy carbon electrode by Siperko and Kuwana (24), who identified by cycling voltammetry the set of peaks at about +0.7V corresponding to the oxidation and reduction of the iron from the hexacyanoferrate.

Subsequently Shankaran (46) observed a second electrochemical process with more negative potentials belonging to the pair of Cu^{2+} / Cu^{+}, confirmed later by Makowski (47). The redox processes, as for the other hexacyanoferrate occur with the participation of cations, although, through studies with EQCM and PBD in situ was hypothesized the participation of anions and/or solvents to a lesser extent (27). The reducing semi-reaction of a CuHCF film can be represented in general as follows:

$$Cu_3[Fe^{III}(CN)_6]_2 + 2e^- + 2K^+ \rightarrow K_2Cu_3[Fe^{II}(CN)_6]_2 \qquad [1.5]$$

1.1.3 Synthesis of Copper Hexacyanoferrate

In general for the synthesis of CuHCF, we can distinguish between precipitation in the "bulk" of the solution and precipitation preferentially on a conducting substrate.

Synthesis in Bulk

- **Precipitation method**: this method is most used and has many variants depending on the starting salts present in the solution. In general, the precipitation occurs by mixing a solution of Cu^{2+} salt with a solution of hexacyanoferrate (II) or (III) ions derived from the alkali metallic salts of from the ferrocyanide acid. It is important to pay attention to the ratio between cations and hexacyanoferrate ions that leads, as appropriate, to compounds with different structure. The normal procedure consists in add the solutions of the two salts to a third one, in order to control the selected stoichiometry.

  Starting from hexacyanoferrate (II) salts we obtain a compound with a cubic shape, which present a $Cu_3^{II}[Fe^{III}(CN)_6]_2$ formula which represents its oxidized form. In this form we can find cations intercalated in the structure and water molecules in variable quantity. Instead, starting from hexacyanoferrate (II) salts, we obtain the

reduced form $Cu_2^{II}[Fe^{II}(CN)_6]_2$ which presents a greater amount of intercalated cations. Using lithium salts we are able to obtain the pure compound in this stage, since they don't intercalate into the structure (44).

- **Method through Local Growth:** For this kind of synthesis you can follow two procedures:
    - The hexacyanoferrate crystals of an alkaline metal are added in a concentrate solution of copper nitrate or copper sulphate
    - Copper sulphate crystals are added to a concentrated solution of an alkaline metal hexacyanoferrate. An insoluble film of the hexacyanoferrate is formed around the growing crystal that grows thick until the starting solid is completely consumed. This method results in a greater amount of potassium ions in the lattice, and we are able to obtain the pure phase $K_2Cu^{II}Fe^{II}(CN)_6$.

At the end of both the synthesis we proceed with decantation or centrifugation, then the precipitate is filtered, washed and left to dry. With bulk synthesis we can get more material and this method is often used when we need to get a fair amount of substance. The powders obtained with this procedure can be used as modifiers of a conducting substrate. Some precipitate granules can be immobilized on the electrode surface through some techniques which can go from simple abrasion to the use of PIGE (graphite electrodes impregnated with paraffin) (48) or mixed with graphite powder and with a "binder" in order to produce a "carbon paste" electrode (49). There are also cases where the Layer Deposition Layer (LBL) technique was used (50).

Synthesis on a conductive substrate

- **Dilute solution of starting salts** (51)**:** A conducting substrate is immersed in a solution which contains the hexacyanoferrate ion, the copper ion and a support electrolyte usually formed by salts of sodium or potassium (52). The deposition is done via potentiodynamic, through potential cycles. The film's growth can follow two ways: the first one provides the meeting between Cu^{2+} with $[Fe(CN)_6]^{3-}$ when the ferrocyanide is reduced on the surface's electrode at $[Fe(CN)_6]^{4-}$ during cathodic scan, while the second way occurs through the coagulation process that begins when the two ions Cu^{2+} with $[Fe(CN)_6]^{3-}$ are in contact in the same solution. Is must be paid attention to the time between the beginning of the voltammetric cycles and the time of insertion of the electrode, since as soon as the electrode in

immersed in the solution deposition is already able to start slowly at OCP's potential. Also the concentration of the two ions is a fundamental parameter, if too high the precipitation in the bulk of the solution will happen quickly and, contrariwise if the concentration would be too low, the coagulation and formation time of the CuHCF film may be excessive. This kind of synthesis has the advantage of being able to adjust the thickness of the film. It is reported that CuHCF can be deposited by potentiodynamic way in solutions that contains cations other than potassium (53).

- Metallic deposition of Cu and anodization in presence of $[Fe(CN)_6]^{3-}$ (54) (47) (55): The precipitation occurs during the oxidation of the previously deposited copper film on the surface of the electrode, in presence of $[Fe(CN)_6]^{3-}$. The dissolution of the film can be done potentially, galvanostatic as well as potentiodynamic. By doing in this way, a supersaturated layer of Cu^{2+} is formed near the electrode surface that allows the precipitation of CuHCF on the conductive material. Even in this process the time between the application of the potential and immersion of the electrode must be minimized. The advantage of this method is to obtain a film of remarkable thickness in a short time with the disadvantage of having less reproducibility than other methods.
- **Open circuit deposition:** No potential is applied to the working electrode and deposition occurs spontaneously on the electrode surface. The synthesis occurs only by coagulation and can be performed through different methods. The conductive substrate can be immersed in a solution of the two starting salts for a certain period of time, or you can immerse the electrode in a solution of $[Fe(CN)_6]^{3-}$ after the deposition of a metallic copper film on the same electrode.

1.1.4 Electrochemical and morphological characterization

Transition metal hexacyanoferrate can be characterized by numerous techniques. Below we report an overview of those used in this thesis work.

Electrochemical characterization

In order to characterize the sample electrochemically is necessary to anchor it to a conductive support in one of the ways described in the preceding paragraphs.

Redox processes: Studying redox processes within the film is definitely the most used method of characterization, which claim speed and simplicity of execution. By polarizing

the electrode on which the hexacyanoferrate is anchored, the redox reactions within the solid that occurs at precise potentials are stimulated, and they allow the recognition of hexacyanoferrate. The most used technique is cyclic voltammetry (CV), whose response consists of a voltammogram with a characteristic form that change according to the type of cation present in the solution (53). In some cases too spacious cation inhibit electrochemical activity, because they are incapable to intercalate in the lattice.

Morphological characterization

To characterize the morphology of hexacyanoferrates Electronic Scanning Microscopy (SEM) (42) was used. The scanning electronic microscopy uses as light source a linear beam of electrons that interact with the surface of the sample creating an image that reflects the surface characteristics of the material. The observation of the images obtained with this technique allows to identify and to interpret the texture of the resins and coals; and although thus technique provides preliminary information of great utility about the shape and dimensions of the material's porosity.

1.2 Nickel Hexacyanoferrate

One of the others analogues of Prussian Blue is the nickel hexacyanoferrate (NiHCF) and it results particularly indicated for the capture of the cesium (56) (57) (58) because the three-dimensional open structure allows the transport of cations of different sizes to ensure the charge balancing during redox reactions (59). For this reason a number of studies have been carried out on the possible synthesis methods of this compound. Nickel hexacyanoferrate has an adsorptive capacity of 48 %, that means that it succeeds to intercept 0.48 moles of cesium for each mole of NiHCF (60) (61). After discovering the possibility of depositing it electrochemical in a similar way that the one used for the Prussian Blue (62), its structure has been studied and always new materials have been used as substrates to improve their quality and proprieties.

From the structural point of view it has been shown that depending on the synthesis method and the experimental conditions that are used is possible to obtain different products. These studies have been generally conducted in presence of potassium, even if NiHCF can be also successfully deposited using sodium as a counter cation (62). The NiHCF film obtained by electrochemical deposition or by precipitation, are solid solution of two different compounds containing greater or lower quantity of counter cations. While considering the use of potassium, the first is written normally as $K_2Ni[Fe^{II}(CN)_6]$ while for

the second the approximate formula $KNi_{1.5}[Fe^{II}(CN)_6]$ is used. The prevailing structure depends from the preparation method of the film; the maintenance of a certain constant potential or the application of a variable potential, in fact, lead to obtain respectively the poor structure or a rich one in cation.

Also the time of application of the potential can affect the final product as it has been reported in the literature that at short time correspond the compound $K_2Ni[Fe^{II}(CN)_6]$, replaced by the other one when the time increases (59). NiHCF may be electrodeposited mainly on inert carriers such as Glassy Carbon (57) (58), gold electrodes and gold plated plastic electrodes (59), or on nickel electrodes of various shapes and sizes (59) (63) (64).

By depositing the compound on materials with a high superficial area, it is possible to check the electroactive area and improving its ion exchange capacity. Therefore, NiHCF can be prepared using as electrodes carbon nanotubes coated with a thin film of porous polyaniline (57) or foam Nickel (58).

1.3 Layered double hydroxides

The hydrotalcites (HT) or layered double hydroxides (LDH) are inorganic solids consisting of a layered octahedral structure formed by mixed hydroxides of a bivalent and a trivalent metal (such ad Mg^{2+} and Al^{3+}). Each layer has an excess of positive charge that is neutralized by intercalated anions in the interlayer space, in conjunction with water molecules, as shown in the figure 1.3.

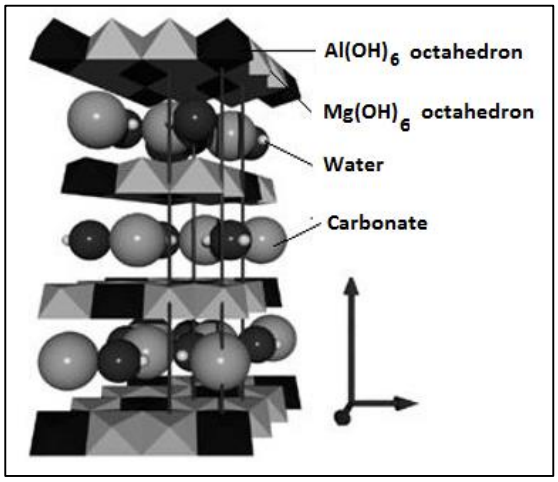

Figura 1.3: Schematic representation of the LDH structure.

The LDH derived from the natural hydrotalcite, having the formula $Mg_6Al_{12}(OH)_{12}(CO)_3 * 4H_2O$, have general formula:

$$\left[M^{II}_{1-y}L^{III}_{y}(OH)_2\right]^{y+}[X^{n-}]_{\frac{y}{n}}[H_2O]_z$$

Where M and L are respectively the bivalent and trivalent metal that form the octahedral lamellar structure, while X is the intercalated anion in the interstate. LDHs can be synthesized from numerous bivalent and trivalent metals, if they have adequate radius.

Of crucial importance are the size of the ion because it should be able to be located in the brucitic layer structure and make octahedral coordination to bind with six hydroxides. For this reason, metallic ions of valence II and III must have similar dimensions to those of Mg^{2+} and Al^{3+} and possess electronic characteristics compatible with the octahedral symmetry.

Hydrotalcite compounds are formed by trivalent ion with radius ranging from 0.5 to 0.8 Å and by bivalent ion with radius between 0.65 and 0.80 Å (Table 1). The only exception is Cu^{2+}, which, because of its electronic configuration, doesn't assume an octahedral symmetry, but forms compounds characterized by tetragonal distortion, for Jahn-Teller effect. In hydrotalcite compounds is possible to insert also metals with inappropriate characteristics, if they are in small percentage. Hydrotalcite compounds can be synthetize with Cu^{2+} side by side to the bivalent metal that presents the appropriate characteristics for the hydrotalcitic structure.

M (II)									
Be	Mg	Cu	Ni	Co	Zn	Fe	Mn	Cd	Ca
0.30	0.65	0.69	0.72	0.74	0.74	0.76	0.80	0.97	0.98

M (III)									
Al	Ga	Ni	Co	Fe	Mn	Cr	V	Ti	In
0.50	0.62	0.62	0.63	0.64	0.66	0.69	0.74	0.76	0.81

Table 1: Ionic rays (Å) of some bivalent and trivalent metal ions.

The ratio between M and L can vary in a relatively large range, because the two ions assume a random distribution in the hydrotalcytic layers. But a pure hydrotalcitic phase can be obtained only if X is between 0.2 and 0.33 because otherwise there would be a hydroxide phase of the excess ion in conjunction with the hydrotalcitic phase. A specific literature (65) as reference point on the molar ratios of the metals is available.

In this work hydrotalcites has been prepared with cobalt, aluminium and iron. It is also important to choose the anion to intercalate in the interstate whose size and nature determine the amplitude of the interstate itself. Since it has to occupy the clay interstates with variable dimensions, the anion used may be of various nature. CO_3^{2-} is the most common anion present in natural clay, and it establishes strong bond with hydrotalcytic

layers. Because of these strong interactions, we must make sure that carbonate doesn't contaminate synthesized hydrotalcite with different anions.

Other anions employed and known in the literature are:

- Inorganic anions: F^-, Cl^-, Br^-, I^-, ClO_4^-, NO_3^-, ClO_3^-, IO_3^-, OH^-, CO_3^{2-}, SO_4^{2-}, SO_4^{2-}, $S_2O_3^{2-}$, WO_4^{2-}, CrO_4^{2-}, $[Fe(CN)_6]^{3-}$, $[Fe(CN)_6]^{4-}$, $[SiO(OH)_3]$;
- Iso and heteropolyanions such as $(PMo_2O_{40})^{3-}$,, $(PW_{12}O_{40})^{3-}$, $(V_{10}O_{28})^{6-}$;
- Anions of organic acids: adipate, oxalate, succinate, malonate;
- Anionic metalorganic compounds.

It is possible to synthesize different hydrotalcites for compositional characteristics and structural variables that thus have different reactivity and applications. If we modify, for example, the intercalated anions, it is possible to obtain hydrotalcite with a variable amplitude of the interlayer spacing. The thickness depends on the number, size, orientation and strength of the bonds between the anion and the oxydriles in the brucite layer.

1.3.1 Synthesis methods of double layer hydroxide

LDH electrodes for analytical purposes are mainly prepared are thin films that cover the surface of the working electrode. This approach is used as an alternative to the construction of prepared electrodes by pressing the active material mixture a metal grid. Typically a drop of chemically synthesized colloidal suspension of LDH is deposited on the electrode and let to dry in the air, sometimes using a spin-coating procedure.

LDH can also be prepared by direct synthesis by coprecipitating a metal hydroxide mixture from a solution containing the anion located in the interlayer and, by the so called reconstruction method, consisting in the resuspension of the solid obtained by calcination into a solution containing the intercalated anion.

One of the main problems of physical deposition is the poor adhesion of LDH to metallic support, sometimes it can be detached from the surface of the electrode. Better adhesion can be achieved by reducing the particle size of LDH. A synthesis method exploits microemulsions, which allow nanostructural particle size control. Microemulsion can be considered as nanometric reaction chambers suitable for controlling nucleation and growth of inorganic precipitates.

Recently, it has been studied the possibility to grow very stable LDH films through chemical electrode deposition. This process takes place in one step and at room temperature. When a cathodic potential is applied to a nitrate solution, various reactions

occur, leading to the disappearance of H^+ ions and the generation of OH^- ions, which contribute to the precipitation of hydrotalcites on the surface of the electrode. The reaction involved in the consumption of H^+ ions are as follows:

$$H^+ + e^- \rightarrow H_{ads}$$

$$2H^+ + 2e^- \rightarrow H_2 \qquad E^\circ = 0.0V$$

$$NO_3^- + 2H^+ + 2e^- \rightarrow NO_2^- + H_2O \qquad E^\circ = 0.93V$$

$$NO_3^- + 10H^+ + 8e^- \rightarrow NH_4^+ + 3H_2O \qquad E^\circ = 0.36V$$

$$2H_2O + 2e^- \rightarrow H_2 + 2OH^- \qquad E^\circ = -0.83V$$

$$NO_3^- + H_2O + 2e^- \rightarrow NO_2^- + 2OH^- \qquad E^\circ = 0.01V$$

All of these reactions contribute to the formation of the metal hydroxide on the electrode surface and adjacent to it, according to the reaction:

$$M_n^+ + nOH^- \rightarrow M(OH)_n \downarrow$$

Among the above mentioned reactions it is difficult to determine which influence more the pH evolution on the surface of the electrode. This kind of electrochemical synthesis can be carried out on galvanostatic or potentiostatic way. In the first case, experiments can be carried out by monitoring the rate of involved reduction reactions, allowing to obtain films with good adhesion and with the desired morphology. The current flow through the working corresponds to the flow of electrons needed to reduce the interested species. However, such synthesis can lead to significant variations in potential, which may thus favour "parasitic" reactions, such as direct reduction of the metals considered, leading to unwanted phases of production. Potentiostatic synthesis is carried out in a classical three electrode cell by applying a suitable potential, measured respect to the reference electrode, to the working electrode. In this case we generally have a decrease in the current, mostly due to the rate of ion's diffusion from the bulk to the electrode surface. Depending on the applied potential it is possible to deposit individual stages with a good degree of purity.

This technique offers several advantages over the methods previously described for the synthesis of hydrotalcitic compounds. First all the reactions occur next to the electrode and the products are deposited in the form of thin layers whose thickness can easily be varied from about 100 nm to come μm by acting on the synthesis time. Secondly, the solid – liquid interface allows the growth of homogenous coating on any type of support without any form limitations, if the material of which the support is formed is an electrical conductor. The use of a proper counter electrode allows to obtain a uniform polarization of the working electrode, uniformizing the start of electrochemical reactions considered

throughout the surface. This is also a technique that doesn't require high temperatures, allows kinetic control of the reaction by controlling the current through the electrodes and allows thermodynamic control by applying a suitable potential. Experiment don't require long or difficult preparations and the necessary tools are readily available and relatively inexpensive.

There are, however, some disadvantages, such as the fact that at room temperature this electrochemical technique leads to the formation of unclear phases and hence difficult to identify. In conclusion we can say that the success of this synthesis method depends on several parameters, the choice of electrodes, cell type, electrochemical technique used, composition and concentration of solution, working temperature and pH, both the initial working solution that the one developed on the surface of the electrode.

The advantage of electrochemical deposition is the short time required to obtain LDH films, the ability to coat also supports with a complex geometry and the modulation of electrolytic bath and synthesis time. These considerations are essential for obtaining films of different thickness and different molar ration between M(II) and M(III).

1.4 Conductor substrates

We want to provide in this paragraph a brief introduction to the conductor substrates which were used during this thesis work. The main materials used as electrode materials in addition to noble metals, as platinum, gold and silver, are the carbonaceous materials. Carbon and graphite electrodes are used as working electrodes mainly in the fields of anodic potentials, where they are considered inert for the reduction of the H_3O^+ ion, that at the GC electrode have a Standard Reduction Potential E° of – 2.1 V vs NHE and can be used as rotating or stationary electrode. (66)

1.4.1 Graphite sheets

The graphite sheet material is in the form of a sheet prepared from graphite. Examples of graphites are usual graphite and expanded graphite. Usual graphite is the most known type. Expanded graphite is produced from natural or synthetic flasky graphite by treating the graphite with an oxidizing agent in order to form an interlayer compound between the graphite layers constituting graphite particles and subsequently heating the graphite at a high temperature abruptly, to rapidly expand the graphite. This process expands the graphite particles perpendicularly to the plane of the layer to rapidly increase the volume

usually about 100 to about 250 times. The oxidizing agent to be used is one capable of forming an interlayer compound, as a mixture of sulfuric acid and nitric acid, or a mixture of sulfuric acid and an oxidizing agent, such as sodium nitrate or potassium permanganate. The treated graphite is then heated to a high temperature of at least 500 °C, preferably about 600 °C to about 1000 °C.

Impurities are removed from the expanded graphite to reduce the impurity content to not higher than 100 ppm, preferably not higher than 50 ppm. The expanded graphite is made into sheet by compression or roll forming.

1.4.2. Carbon Paper Gas Diffusion Layers (GDL)

A typical piece of carbon paper consists of a sheet of paper that has been impregnated with carbon and sandwiched between two sheets of regular paper. All components are standard, except for the coated sheet that performs the reprography. Its coating is made up of several materials, the most important of which is carbon black. Carbon black is a very fine, spherical, amorphous form of carbon that isn't as crystalline as graphite. Mostly carbon, but it also contains small amounts of oxygen, hydrogen and sulfur. The carbon black adheres to the paper with the help of various waxes.

Carbon Paper Gas Diffusion Layers (e.g. Sigracet, Freudenberg, Toray) tend to be thinner and more brittle than Carbon Cloth Gas Diffusion Layers. Each type has a different mass transport, hydrophobicity, conductivity and porosity. Paper such as Toray are quite hard and brittle, with very low compressibility.

Gas Diffusion Layer	**Toray Paper 060**
Type	Paper
Thickness (mm)	0.190
Bulk density (g/cm^3)	0.44
Electrical resistivity (mΩcm)	80
Tensile strength (N/cm)	50
Flexural modulus (mPa)	40
Porosity	78%

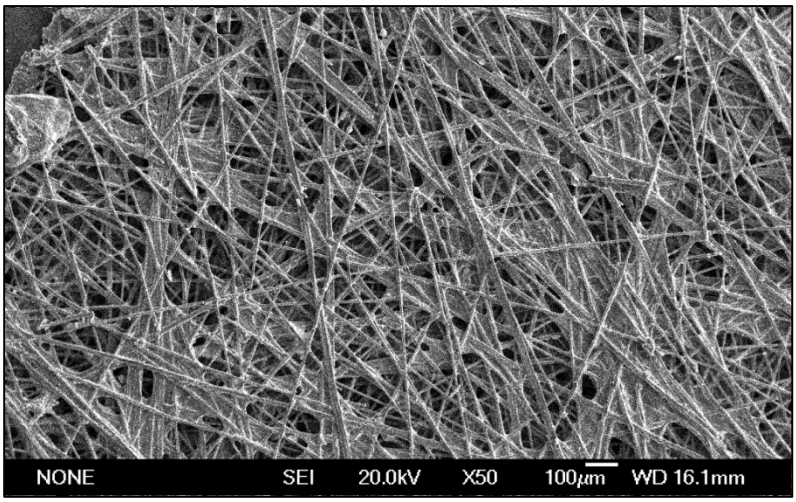

Figure 1.4: Image of Carbon Paper acquired at SEM

1.4.3. Carbon Cloth Gas Diffusion Layers

Spools of carbon fiber are taken to a weaving loom, where the fibers are then woven into fabrics. The two most common types of weaves are “plain weave” and “twill”. Plain weave is a balanced checker board pattern, where each strand goes over then under each strand in the opposite direction. Whereas a twill weave looks like a wicker basket. Both twill and plain weaves have an equal amount of carbon fiber going each direction, and their strengths will be very similar. The difference is primarily an aesthetic appearance. The carbon cloth are the most flexible and are generally quite mechanically robust, but are also the thickest.

Gas Diffusion Layer	Carbon Cloth 060
Type	Cloth
Thickness (mm)	0.38
Bulk density (g/cm^3)	1.75
Carbon content %	99
Tensile strength (N/cm)	10

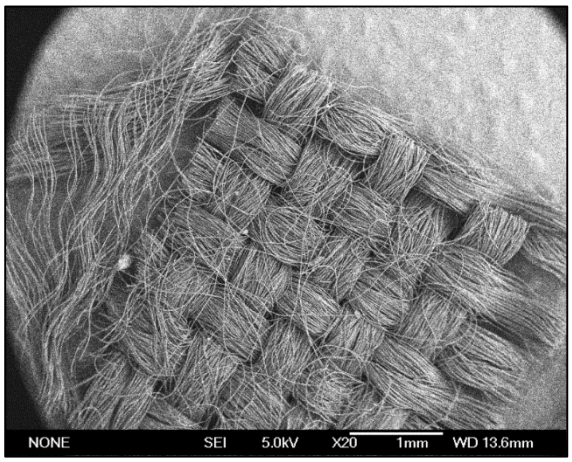

Figura 1.5: Image of Carbon Cloth acquired at SEM

1.4.4. Glassy Carbon

The most commonly used are glassy carbon electrodes (GC) and carbon paste electrode (CPE). The glassy carbon electrodes boast a low electrical resistance, high resistance to chemicals and impermeability to gases and liquids. (67) The production takes place through the pyrolysis of thermosetting resins, where between the most used ones are polyurethane and phenol formaldehyde. (67) From a structural point of view this material is completely in sp2 configuration and the more acclamaid shape is the one proposed by Jenkins and Kawamura (68), a form of interlaced ribbons (Figure 1.6).

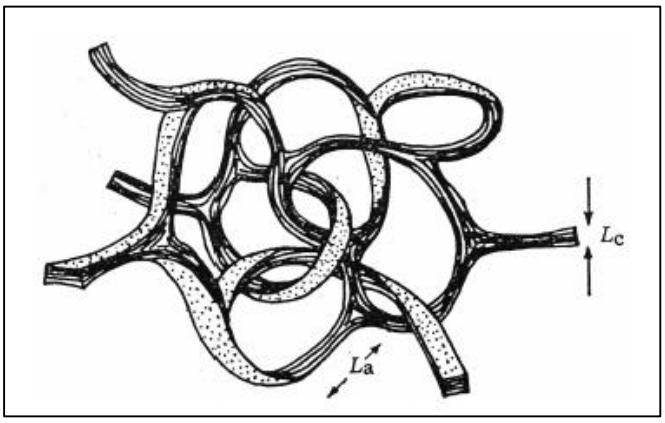

Figura 1.6: Model proposed by Jenkins-Kawamura. L_a represents the length of the graphite layers while L_c is the thickness.

The foundation on which it is based assumes that there is a memory effect and that the final product structure is based on that of the starting polymeric precursor. However, the proposed model fails to explain aspects such as high impermeability and low reactivity, since the described structure would be porous and with many more reactive atoms to the edges that the carbon atoms on the plane. Other studies have suggested that this material has a structure related to fullerenes. (69)

1.4.5. Nickel foam

Nickel foam has high porosities, around 75-95% of volume is empty space. Nickel foams are produced by injecting gas or mixing a foaming agent into molten metal which creates a froth that is stabilized by a high temperature foaming agent. Nickel foams are cellular structures made with a large volume fraction of pores. Foams traits include low density, high stiffness, high energy absorbance, low thermal conductivity, low magnetic permeability and fire resistance.

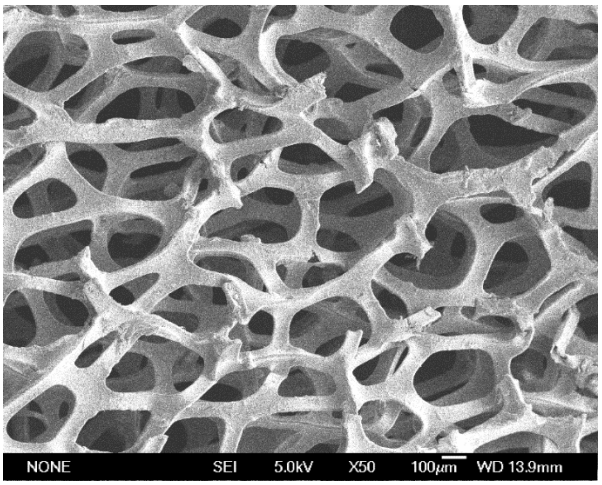

Figure 1.7: Image of Nickel Foam acquired at SEM

Type	Foam
Thickness (mm)	1.6
Elongation (≥ %)	20
Electrical resistivity (μΩm)	7.6
Purity	≥ 99.8 %
Porosity	97 %

1.5 Hair

Lately, the synthesis of carbon materials derived from organic waste for energy applications has been attracting much interest because of the increasing scarcity of fossil fuels. Waste material including agricultural wastes, foods and even animal products have been utilized as carbon precursors. Human hair, an easy available waste, has become commercially available to crop producers in the past few years. The composition of hair comprises about 51% carbon, 17% nitrogen, 21% oxygen, 6% hydrogen, 5% sulfur and trace amounts of iron, magnesium, arsenic, chromium and various minerals. (70)

1.6 Applications

1.6.1 Batteries

A battery is a device that has the ability to convert chemical energy into electrical one. There is a distinction between primary and secondary cells: the primary cell coverts the energy of a chemical reaction, during which the reactants are consumed in a single discharge process, while a secondary one, through a current that passes in the opposite sense to that of the spontaneous discharge reaction, can be restored. A secondary cell is

known also as a rechargeable cell and could hold less energy and last for less time but it can provide several cycles of discharge/charge.

The secondary battery should have: ability to undergo several discharge/charge cycles with high efficiency and reversibility, a high power/mass or power/volume ratio.

Lithium secondary cells consists of lithium metal as negative electrode, an active material (AM) as positive electrode, and a non-aqueous lithium-ion solution which enables ion transfer between the electrodes. The electrode material should undergo a reversible reaction with lithium ions: reduction occurs during discharge and oxidation during charge:

$$xLi^+ + AM(s) + xe^- \underset{charge}{\overset{discharge}{\leftrightarrow}} Li_xAM\ (s)$$

The lithium – ion batteries require to be assembled or even disassembled inside inert gas filled chambers. Lithium and the electrolyte solution are air and moisture sensitive and can cause fire hazards.

The ability to intercalate ions within the structure is also an exploited feature in the field of batteries, using hexacyanoferrates such as cathodes or anodes. It is established that the copper hexacyanoferrate has a sufficiently more open structure than the Prussian Blue (71) (72) to allow better input and output flow to a group of larger cations. Its use with lithium and sodium ions is reported in literature (43) and there are some applications as host material for divalent (73) and trivalent cations (74). If the host ion is able to carry two more charges, the stored energy increases inside the structure, which is an advantage in comparison to the monovalent cation batteries.

The Li-air battery potentially has much higher gravimetric energy storage density compared to all other battery chemistries and this has led to strong interest in the last period. The basic principle behind the operation of metal – air batteries, or better metal – O_2 drawn from air is used, is well known. But there are some immense challenges in order to make these technologies practical and to have the promised step – change in energy storage. The operation of Li – O_2 batteries consists of the conversion of stored chemical energy in lithium and oxygen into electrical energy through the formation of reaction products containing lithium ions and reduced oxygen species. (75) Here are incorporated operational elements of a fuel cell, for example reduction of gaseous O_2 from the environment during discharge, with that of a battery, as storage of electrons and Li^+ in the oxygen electrode. This represents a departure from conventional Li – ion positive electrode

development. In Li – O_2 batteries oxygen is reduced to solid Li_2O_2, filling the pore spaces of the electrode in nonaqueous electrolytes and soluble LiOH in aqueous electrolytes.

The difference in the morphology and surface chemistry of Li_2O_2 particles can be explained by the following elementary reaction in nonaqueous electrolytes:

$$O_2 + e^- \rightarrow O_2^-$$

$$Li^+ + O_2^- \rightarrow LiO_2$$

$$2LiO_2 \rightarrow Li_2O_2 + O_2$$

Or

$$Li^+ + LiO_2 + e^- \rightarrow Li_2O_2$$

There is the appearance of LiO_2 as an intermediate, followed by a disproportion or a second electron transfer reaction to form Li_2O_2.

1.6.2 Electrochemical Capacitors

Electrochemical capacitors are devices with a specific capacity of the order of F/g or F/cm^3, extremely high compared to the most common electrostatic capacitors, whose capacity is of the order of magnitude of pico, nano or micro Farad for mass or volume units. For this reason, these are called "supercapacitors". It is commonly referred to supercapacitors with the acronym EDLC (electric double layer capacitor) to highlight the specific feature of supercapacitors, in other words the property of creating a double layer of charge separation within the dielectric. The electrochemical capacitor, as seen in the figure 1.7, is characterized by a construction very similar to that of a battery. It has substantially two electrodes, and a permeable ion separator, placed among the electrodes, which contains the electrolyte.

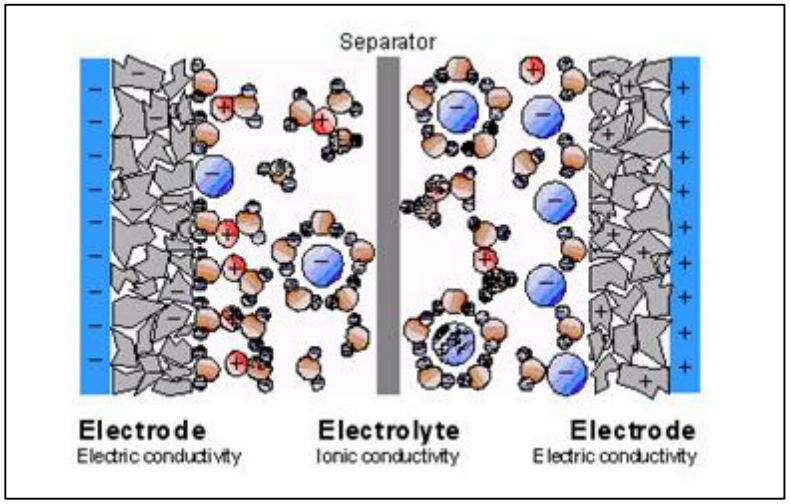

Figure 1.8: Elemental schematisation of a supercapacitor that emphasizes the mobility of the electrolytic ions, surrounded by solvent, in this case water.

Porous electrodes are immersed in an electrolytic solution. Applying a small potential difference to the electrode leads to a charge separation process induced by the presence of an electric field. The area where these charges are concentred is also called double layer, right from where the supercapacitors are called “double layer”. Electrochemical capacitors thus store energy in the double layer, also referred to as Helmoholtz’s layer, which is formed at the electro-electrolyte interface. Here, positively or negatively charged ions accumulate at the electrode-electrolyte interface and are compensated by electrons located on the surface of the electrode. The thickness of this layer depends on the concentration of the electrolyte and the size of the ions. Typically, we have thicknesses of the order of 2 – 10 Å. (76) The electrodes are designed to form a high surface and are made of porous material having pores of the diameter nanometer order to maximize the surface of the double layer.

The supercapacitors are equipped with a high specific capacity thanks to the reduced intermolecular distance between the opposite electrical charge points on the electrolyte-electrode interface, and to the high surface area of the electrode realized through the deposition of carbon with a nanomolecular structure. In addition to the capacity resulting from the separation of charges that is obtained in the double layer there is also a contribution from reactions that can occur on the surface of the coal. Such reactions give rise to an additional accumulation of electricity. In the double layer supercapacitor it has been observed that the principle of operation is mainly based on the separation of charges due to the application of a potential difference between the two electrodes; electrons between electrodes and electrolyte are therefore not transferred.

Pseudo-capacitors

Pseudo-capacitors are hybrids between a battery and a double-layer electric capacitor (EDLC). Due to this configuration, we can leverage the bigger storage capacity of a battery combined with the rapid release of energy of an EDLC. In a supercapacitor one of the two carbon electrodes is replaced by conductive polymers or metal oxides, this involves two different electrodes charging mechanism: the classic double layer electrode and a combination of reactions on the modified one. This combination produces a charge transfer that is dependent on the applied potential, so the device behaves like a normal condenser.

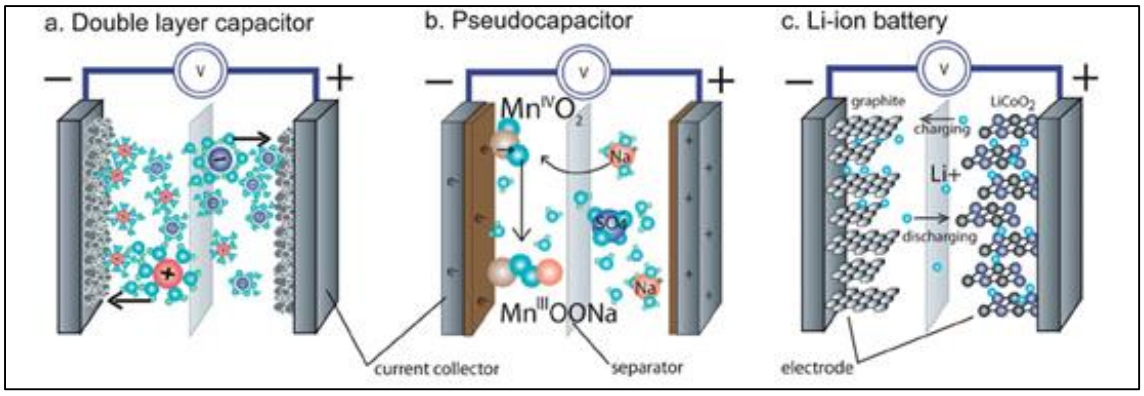

Figure 1.8: Basic scheme for (a) doble – layer capacitor (EDLC), (b) a pseudo-capacitor with MnO_2 base, (c) a lithium ion battery. All devices have an active material (carbon, MnO_2, $LiCoO_2$), current collector, separation membrane and electrolyte.

Chapter 2: Motivation

The main purpose of this thesis was to test the various protocols developed on different substrates and compare them to see which one has the best performance, even in terms of energy storage capabilities.

This thesis work regards studies on copper hexacyanoferrate (CuHCF), one of the most important analogies of the Prussian Blues, with the aim to test the "two-step" electrochemical deposition method: metallic deposition of Cu and anodizing in the presence of $[Fe(CN)_6]_3$. The method brings with it some advantages, including the short duration of the steeps and the high ratio of deposited material and depositing time. The "one step" methods have the advantage of being able to check the thickness of the film but the synthesis process takes grater time than the "two-step" method. This justifies the interest in deepening and in the improvement of the "two-step" method as an alternative method. Two distinct synthesis protocols, method A and method B, were used during the work and their reproducibility was checked. These two methods lead to obtain different characteristic cyclovoltamograms. Diversity in the form of these traces indicates that the products obtained contain structural differences.

Another goal of this work was the electrochemical synthesis of Co/Al and Co/Fe double layer hydroxides on supports of different nature, with the aim of studying its electrochemical proprieties and in particular the specific capacity for their possible use as supercapacitors. Various tests have been conducted for each support to demonstrate on which the best deposition can be obtained and also the LDH mass obtained for electrosynthesis was evaluated. By varying the deposition time, the correlation between LDH and deposition time was studied.

As far as hair is concerned the purpose of this preparation is to obtain porous carbon from biomass, in this case hair that is a renewable source, and that has become more and more attractive for its abundance, low cost, easy accessibility and environmental friendliness compared with other carbonaceous precursors.

Chapter 3: Experimental Part

3.1 Cleaning of electrode surface

Usually research activities involving electrochemical deposition tests are made on electrodes with a low capacitive current and reusable, as carbonaceous materials and metals such as gold, silver and platinum. There is a need to bring the surface back to the same initial condition and every type of material needs a pretreatment protocol. The cleaning treatment has the purpose of erasing the possible traces of previous uses and providing to the external surface a renovated microstructure. There is the possibility to use a conductive substrate that can be hardly reused or there is no need of a pretreatment, such as graphite sheet.

3.1.1 Graphite Sheets

The samples are obtained by cutting rectangles from a A4 graphite sheet having a width of 5 mm and a sufficient height to allow the application of a scotch layer and leave sufficient space to attach the sample to the instrument with a crocodile. The layer of scotch serves to delimit the surface and ensure the reproducibility of the measurements, creating a square with a side of 5 mm. Regarding the cleaning treatment, the graphite sheet has been left to soak in ethanol for about 10 minute. The graphite sheets were provided by VED.

3.1.2 Carbon Cloth, Carbon Paper and Nickel foam

Even in this case the samples are obtained by cutting rectangles having a sufficient height to allow the application of a scotch layer and leave sufficient space to attach the sample to the instrument with a crocodile. The layer of scotch serves to delimit the surface and ensure the reproducibility of the measurements, creating a square with a side of 5 mm. No cleaning treatment was carried out. The carbon cloth and carbon toray paper were provided by Quintech, while the nickel foam was provided by Xiamen Tob New Energy Technology Co.

3.1.3 Glassy Carbon Electrode (GCE)

The use of a glassy carbon electrode not damaged and in good condition is recommended. The cleaning process is done by removing the visible naked eye deposit abrading on 0.05 mm alumina powder (Al_2O_3) damped on the polishing cloth. The chafe act is executed by drawing an eight until the surface is polished to mirror and rinsed thoroughly.

3.2 Materials, substances and instrumentation

The following tables show the tools and reagents used to carry out the tests described in the previous paragraphs.

	Features	Manufacturer
Reference Electrode	Ag/AgCl	CH Instruments, Inc
Counter Electrode	Platinum Wire	
Potentiostat		BioLogic VSP
Horizontal tubular furnace	Temperature control	Energon HLT-40-0/12, H1269
Porosity Analyser		Micromeritics ASAP 2020
Cycler		MTI BST8
SEM		Quanta 650 FEG
XRD		Bruker-AXS, model D8 Advance

	Chemical formula	Manufacturer
Hexayanoferrate of iron (III), or ferricyanide	$K_3Fe(CN)_6$	Riedel de Haen
Sulphate of copper (II)pentahydrate	$CuSO_4 * 5H_2O$	Carlo Erba
Potassium sulphate	K_2SO_4	Sigma Aldrich
Potassium nitrate	KNO_3	Sigma Aldrich
Sodium nitrate	$NaNO_3$	Sigma Aldrich
Cobalt nitrate hexaydrate	$Co(NO_3)_2 * 6H_2O$	Sigma Aldrich
Aluminium nitrate nonahydrate	$Al(NO_3)_3 * 9H_2O$	Sigma Aldrich
Iron nitrate nonahydrate	$Fe(NO_3)_3 * 9H_2O$	Riedel de Haen
Potassium hydroxide	KOH	Sigma Aldrich
Zinc nitrate hexaydrate	$Zn(NO_3)_2 * 6H_2O$	Sigma Aldrich

3.3 Copper Hexacyanoferrate

Cronoamperometry and cyclic voltammetry (CV) have been used for the electrodeposition and electrochemical characterization processes.

3.3.1 Deposition of metallic Cu and anodization in presence of ferricyanide ion

- Medium potentials and long time of application (Method A)
    - *1° step Deposition of copper metal film:* In this step a solution of $CuSO_4$ 0.05M and K_2SO_4 0.05M. Once assembled the equipment of counter electrode, reference electrode and working electrode, the deposition was carried out through cronoamperometry applying a potential of -0.80 V for 20 seconds.
    - *2° step Dissolution of copper film and subsequent precipitation of the low soluble salt (CuHCF) on the electrode surface:* Once the electrodes have been rinsed are now immersed in a solution of $K_3Fe(CN)_6$ 1 mM and K_2SO_4 0.25 M. using the cronoamperometry applying a potential of 0.6 V for 300 seconds and we can observe a sharp drop in current due to the formation of CuHCF on the surface electrode. After an average of 40 seconds it is normal to observe precipitation in bulk represented by a trail that moves from the electrode to the solution.
- Extreme potential and short time of deposition (Method B)
    - *1° step Deposition of copper metal film:* Also for this passage a solution of $CuSO_4$ 0.05 M in KSO_2 0.05 M is used. Once assembled the equipment of counter electrode, reference electrode and working electrode, the deposition was carried out through cronoamperometry applying a potential of -1 V for 4 seconds.
    - *2° step Dissolution of copper film and subsequent precipitation of the low soluble salt (CuHCF) on the electrode surface:* Once the electrodes have been rinsed are now immersed in a solution of $K_3Fe(CN)_6$ 1 mM and K_2SO_4 0.25 M. using the cronoamperometry applying a potential of 1 V for 15 seconds and we can observe a sharp drop in current due to the formation of CuHCF on the surface electrode.

3.3.2 Electrochemical Characterization

The characterization of CuHCF films was performed by cyclic voltammetry in solution of KNO_3 0.1 M with the same instrumental configuration used for the deposition, cycling the potential between -0.2 V and 1.05 V. Normally 10 voltammetric cycles at the scan rate of 10 mV/s and 100 mV/s and 3 voltammetric cycles at the scan rate of 1 mV/s were performed. All operations were performed at a room temperature.

3.4 Nickel Hexacyanoferrate

Nickel hexacyanoferrate electrosynthesis was performed in a three electrode cell by applying a constant potential.

The three electrodes were immersed in a glass cell containing a solution of $K_2Fe(CN)_6$ 5 mM and KNO_3 0.1 M for 300 seconds, subsequently applying a potential oh 1.0 V for another 300 seconds. The thus deposited NiHCF was then characterized by cyclic voltammetry in NaNO3 1.0 M, KNO3 0.1 M, $Al(NO_3)_3 * 9H_2O$ 0,1 M or $Zn(NO_3)_2 * 6H_2O$ 0,1 M. At first a constant potential of 0.25 V was applied at the electrode for 120 seconds. After this a cyclic voltammetry was conducted at a scan rate of 50 mV/s in a potential window between -0.1 V and 0.8 V. All operations were performed at a room temperature.

3.5 Layered double hydroxides (LDH)

All electrochemical tests were performed using a single cell with three electrodes: reference electrode, counter electrode and working electrode. These tests were first depositing a Co/Al LDH and a Co/Fe LDH, according to the electrodeposition procedures that will be described below. All operations were performed at a room temperature.

3.5.1 Co/Al LDH

The three electrodes were introduced into a $Co(NO_3)_2 * 6H_2O$ and $Al(NO_3)_3 * 9H_2O$ solution with a total concentration of 0.03M and in 3:1 ratio to allow deposition by applying a potential of -1.15V for 30 seconds. Characterization by cyclic voltammetry was conducted in a KOH 1M solution between 0V and 0.5V by running 10 cycles at a scan rate of 10 mV/s and 50 mV/s and 2 cycles at a scan rate of 1 mV/s.

3.5.2 Co/Fe LDH

The three electrodes were introduced into a $Co(NO_3)_2 * 6H_2O$ and $Fe(NO_3)_3 * 9H_2O$ solution with a total concentration of 0.03M and in 3:1 ratio to allow deposition by

applying a potential of -1.15V for 30 seconds. Characterization by cyclic voltammetry was conducted in a KOH 1M solution between -0.4V and 0.2V by running 10 cycles at a scan rate of 10 mV/s and 50 mV/s and 2 cycles at a scan rate of 1 mV/s.

3.6 Hair

The hair was washed with soap and dried. Once dried they were placed in ceramic bowls and introduced into the oven. Here, a stabilization treatment has taken place up to a temperature of 300 °C in presence of oxygen with an increase in temperature of 1 °C per minute. Once reached the temperature of 300 °C this was maintained for 1 hour, after which the temperature was lowered to 20 °C with a ramp of 5 °C per minute. Small amounts of stabilized hair mixture and KOH were prepared in different ratios (1 to 2, 1 to 1.25, 1 to 1, 1 to 0.5, 1 to 0.25 and 1 to 0). KOH immersing leads to a homogeneous mixture of them, and KOH oxidatively reacts with carbon at high temperature to generate H2, CO2 and CO gas and thus produce the pores. The activation mechanism of KOH is as below (77):

$$6KOH + 2C \rightarrow 2K + 3H_2 + 2K_2CO_3$$

$$K_2CO_3 \rightarrow K_2O + CO_2$$

$$CO_2 + C \rightarrow 2CO$$

$$K_2CO_3 + 2C \rightarrow 2K + 3CO$$

$$K_2O + C \rightarrow 2K + CO$$

After mixing well in a mortar, they were reintroduced into the oven and subjected to activation treatment that bring to a temperature of 900 °C with an increase ramp of 3 °C per minute, keeping it for 3 hours and then bring it back to 20 °C with a ramp of 5 °C per minute, all in the presence of nitrogen with a flow of 28/30 bubbles every quarter of a minute. Taken out of the oven before it was neutralized with a solution of HCl 2M until it reached a pH of about 6, after which it was washed twice with water using a centrifuge.
On the samples thus obtained were made nitrogen absorption isotherms to obtain information on porosity and other parameters such as volume and microporous area.

3.6.1 Adsorption isotherms

It is very important to quantify the surface of porous carbons in order to carry out a comparative study between structure and proprieties. The study of the microporous and macroporous structure of the material with the synthesis parameters and the storage capacity of the material. This textural analysis was carried out by adsorption – desorption

isotherms measurements of N_2 at -196°C using a Micromeritics ASAP 2020 porosity analyser. To obtain these data, a protocol of preparation and measurements was followed which involves several steps and it is described below:

- Degassing: before introducing the sample into the equipment is necessary to ensure the pores don't contain air, moisture or other volatile components derived from the synthesis. The sample, between 50 and 100 mg, are collocated in a glass holder, which is closed using a plug with an O – ring to seal. It is placed in the degassing port and kept in a vacuum for 3 hours, heating with a blanket at 180°C. Although mass losses in degasification were not large, the holder with the degassed sample was always weight and the resulting mass is taken into account for subsequent calculations. Like all the carbons developed an important microporosity in some cases was required the study of adsorption in the area of low relative pressures. For this, another degassing at a much larger vacuum (0.1 μm) for 3 hours.
- Analysis: After having the degassed sample, it is placed in the measurement port and the equipment begins to measure according to the program previously assigned to it. In our case points at relative pressures were selected (pressure respect to the pressure of condensation at the temperature at which measurements are conducted) between 0.005 and 1 covering the whole area of mesopores and macropores where the nitrogen is capable to condensing. When the analysis was performed at low relative pressure (below 0.005) you have to select manually the nitrogen dose for each point.
- Surface of mesoporous: the most commonly used methods for obtaining mesoporous surface parameters in porous material are applied on the adsorption – desorption isotherm. Some modifications were made to the Langmuir kinetic model to evaluate the external area of material, until 1935, when Brunauer and Emmett developed the model BET (Brunauer – Emmett – Teller) (78). Now the BET model is one of the most used models for the determination of the surface area of adsorbents, catalyst and porous materials, although the underlying model is not very realistic since it is based on several assumptions.
- Surface of microporous: a first value of the microporosity parameters was already obtained with the adsorption – desorption isotherms, but to obtain information on the microporous filling there is the need to measure at lower relative pressures because when the interaction of the pore with the adsorbent is strong the adsorption

is produced at lower relative pressures. The obtaining of the textural parameters is carried out with mathematical analysis of the isotherms adsorption that uses models based on different theoretical foundations. For data processing the most used model is the Dubinin – Radushkevich (79) which is semi – empirical, since it doesn't underlie any theory but assumes some of the assumptions that appear in other theoretical models, part of the idea that the total occupation of the micropores doesn't occur after the formation of multi-layered, as occurs with mesopores.

- Calculation of the pore distribution: the BJH model was used for the calculation of the mean mesopore size, the volume of mesopore and the mesopore distributions of both adsorption and desorption were calculate with the BJH method.

3.7 Electrochemical techniques used

3.7.1 Chronoamperometry

Chronoamperometry is a potentiostatic electrochemical technique with which the current passing through an electrode is measured, depending on time. Chronoamperometry is particularly useful in all cases where the redox process that we want to monitor is governed by the diffusion occurring in the region at a d distance from the electrode's surface. It is necessary that the analytical solution, that contains the redox pair, is not subject to agitation and the temperature must be kept constant.

When the potential applied to the working electrode is the same of the equilibrium one of the redox pair ($E_{WE} = E_{eq}$), there is no current passage, because the two reactions, of oxidation and reduction, continue at the same speed. If the potential that we apply to the working electrode is different from the equilibrium one, there is a progressive increase of the current that can be due to the oxidation (anodic current, i_a) and reduction (cathodic current, i_c) of the redox pair present in the solution. In conclusion, applying a suitable potential and assuming that in the solution is present the specie A_{ox}, is possible to register a discharge current. Applying a potential different from the one of equilibrium the concentration of A_{ox} next to the electrode surface decrease fast, and also the faradic current. After the A_{ox} species near the electrode has been consumed, a concentration gradient is created and it causes a spontaneous diffusion of the species towards the electrode. Since the solution is quiet and the reduction continues the A_{ox} species have to spread from far distances and this causes a constant decrease in current from the starting value to a constant value. The current associated to the process decays as described by Cottrell's law:

$$i(t) = \frac{n * F * A * C_b * \sqrt{D_0}}{\sqrt{\pi * t}}$$

In which:

- n = number of exchanged electrons
- F = Faraday constant (96485 C/mol)
- A = the area of the electrode surface (cm^2)
- D_0 = diffusion coefficient of the active species (cm^2/s)
- C_b = concentration of the analyte in the solution bulk (mol/L)

If we know the coefficient diffusion and we check the circulating current, is possible to obtain alternatively the area of the electrode surface or the concentration of the analyte. The respond is a current-time graph.

3.7.2 Cyclic Voltammetry

Cyclic voltammetry is useful to detect the redox reactions and the potential at which they occur. The working electrode is immersed is a no agitated solution, where the potential varies linearly with a velocity, said scanning speed, generally measured in volts per second (V/s). The potential is measured between the reference electrode, constant potential, and the working electrode, while the current is measured between the working electrode and the counter electrode. The current (i) is reported against the applied potential (E) to give the so called cyclovoltammogram. This cyclovoltammogram has a particularly closed loop, whose shape varies considerably in relation to the reversibility of the redox system. A substantially reversible system produces a trace where the anodic peak and the cathodic peak are distant by a a quantity equal to:

$$\Delta E_p = E_{pa} - E_{pc} \cong \frac{0.059}{n}$$

Where n is the number of involved electrons.

The more the system behaves in an irreversible way and greater will be the ΔE. It is possible to obtain both the standard potential (E°) and the half wave potential ($E_{1/2}$). It can be demonstrate that:

$$E^{\circ} \cong E_{1/2} \cong \frac{(E_{pa} + E_{pc})}{2}$$

The I_p current peak can be expressed as a function of the scan rate by the equation of Randles – Sevcik, and at 298.15 K can be approximated to:

$$I_p = 2.686 * 10^5 * n^{3/2} * A * \sqrt{D * v} * C$$

Where:

- C = concentration of the analyte in solution (mol/cm^3)
- v = scan rate of the potential (V/s)
- D = diffusion coefficient of the analyte (cm^2/s)
- A = electrode area (cm^2)
- n = number of exchanged electrons
- I_p = intensity of the current peak (A)

From this equation it is possible to calculate the diffusion coefficient of the analyte if we know its concentration and vice versa. This technique is very important in the study of electrode reaction because of the easy access to the value of ΔE, that represents a useful parameter to understand the reversibility of the system. Its use in quantitative analysis is secondary, because other techniques provide better performance. This technique is very used for the study of redox species dispersed in solution but also of solids immobilized on the surface of the electrode.

3.8 Chemical and morphological characterization

3.8.1 SEM – EDX

The electronic scanning microscope or SEM is a type of electronic microscope. The image is taken by hitting the sample with a beam of focused electrons, scanning a little rectangular area. The primary electron beam hits the sample and numerous particles are emitted, including secondary electrons. These secondary electrons are captured by a special detector and converted into electrical impulses. The sample is placed is a room under high vacuum (10^{-5} Torr) for increase the average free walk of electrons and avoid diffusion phenomena due to air – electron interactions. Furthermore, the sample must conduct electricity or be metallized, if not production of electrostatic charges would disturb the detection of secondary electrons.

The energy dispersion spectroscopy or EDX exploits the X - ray characteristic emitted by the accelerated electron beam incident on the sample. With this technique we are able to recognize the chemical elements that constitute the sample and with a SEM microscope we can combine the morphological and compositional characterization.

3.8.2 XRD – X Ray Diffraction

The X rays are generated by a cathode tube and filtered to produce monochromatic radiation, collimated to concentrate and after directed toward the sample. The interaction of these incident rays with the sample produces constructive interference and a diffracted ray when the Bragg's law is satisfied:

$$n\lambda = 2d \sin\theta$$

This law relates the wavelength of electromagnetic radiation to the diffraction angle and the lattice spacing in a crystalline sample. The characteristic X ray diffraction pattern generated is a unique "fingerprint" of the crystals present in the sample. By comparison with standard reference patterns and measurements, this fingerprint allows identification of the crystalline form.

3.9 Batteries

All the components used for assembling the batteries were first cleaned and then put into the oven to eliminate any traces of water. The internal parts of the battery were sonicated in acetone for 10 minutes, except the active material, the separators and the lithium disks. The Teflon support was cleaned with the help of a paper soaked in acetone, while the valves were cleaned with a stream of nitrogen. Once dried all in the oven, it was introduced into the glove box where the assembly was carried out. The separators, the lithium foil and the electrolyte were already inside. The batteries were assembled as follows and as shown in the picture (Figure 3.9.1): a nickel collector, two lithium disks, two separators, ten electrolyte drops, the active material, a fine grid, a large grid, a large spring and closed with the valve. This is the trim in the large part of the Teflon support the one that represent the cathode. On the other side, a smaller spring, a screw, is placed and it is also closed with a valve. This represent the anode of the battery.

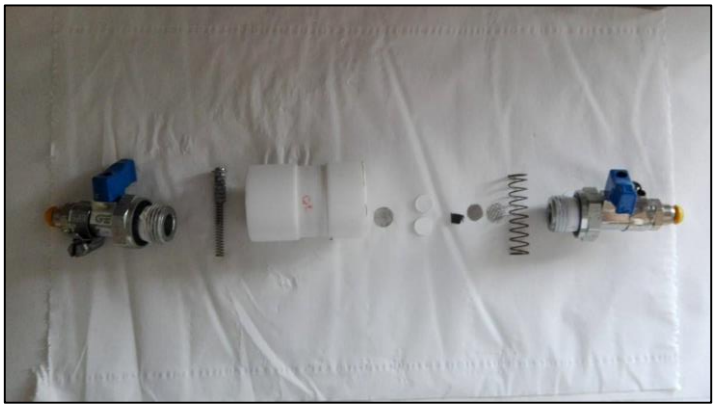

Figure 3.9.1: The various battery components

When assembled the batteries were pulled out of the glove box and a cyclic voltammetry in argon was first conducted between a potential of 2 and 4.2 V at a scan rate of 20 mV/s. after which a flux of oxygen was passed into the battery for 15 seconds and another cyclic voltammetry was carried out under the same conditions to measure the effect of oxygen vs the argon blank. At the end the battery has been subjected to a multiple current test and a full discharge test.

1M lithium triflate salt (CF_3SO_3Li) in a solvent of diethylene glycol dimethyl ether (DEGDME), and in the other case 0.6M lithium triflate salt in a solvent of ionic liquid (PYR14TFSI). Then the same protocol of the first case was applied only that in the case of ionic liquid the batteries were kept at 60°C for all the duration of the test.

3.10 Data processing

All data and graphics have been processed with Origin 9.0, Excel and Igor Pro (WaveMetrics).

Chapter 4: Results and discussion

4.1 Metallic Cu deposition and anodization in presence of ferricyanide ion (CuHCF)

This technique was thoroughly studied by the Bologna research team and my job was to apply it to different substrates and then compare the results, in order to understand which one was better in terms of performance. Two reproducible protocols have been identified to two different voltammograms. The two procedures are identified as Method A and Method B. For graphoil testing, in this case a sheet with graphite on one side was used, while the other side was covered with a conductive polymer of the manufacturer Cixi Weilite Sealing Material Co.

METHOD A

DEPOSITION

In this procedure, the electrode is immersed in the solution for longer times but at moderate potentials respect to Method B. The first step consists in deposition of metallic copper (Cu^0), through potentiostatic way, at - 0.8V vs Ag/AgCl for 20 seconds (Figure 4.1.1a). for this method the amount of deposited metallic copper is higher than that of Method B. In the second step the copper film dissolution is potentiostatically performed at a potential of +0.6V for 300 seconds (Figure 4.1.1b) in ferrocyanide potassium ($K_4Fe(CN)_6$) 1mM solution.

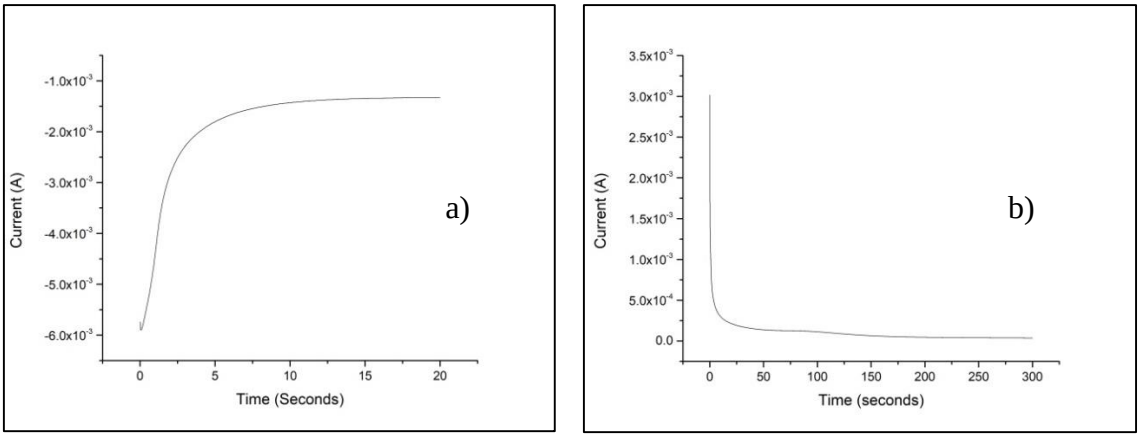

Figure 4.1.1: a) Chronoamperogram of metalic copper deposition process (-0.8 V for 20 seconds) in $CuSO_4$ 0.05 M + K_2SO_4 0.05 M solution. b) Chronoamperogram of the dissolution process of the film (+0.6 V for 300 seconds) in a solution of $K_3[Fe(CN)_6]$ 1 mM + K_2SO_4 0.25 M. Support: graphoil.

ELECTROCHEMICAL CHARACTERIZATION

Figure 4.1.2 shows the CV characterization of a sample deposited on graphoil in KNO_3 0.1 M. The first segment in the anodic direction has a higher current intensity value that tends to decrease until stability, and this indicates that the deposition process doesn't produce a finite film. The cathodic peak at about 0.0 V has the same behaviour and it is assumed that there are two related processes. The scan rate at which the cyclic voltammetry was done is 10 mV/s.

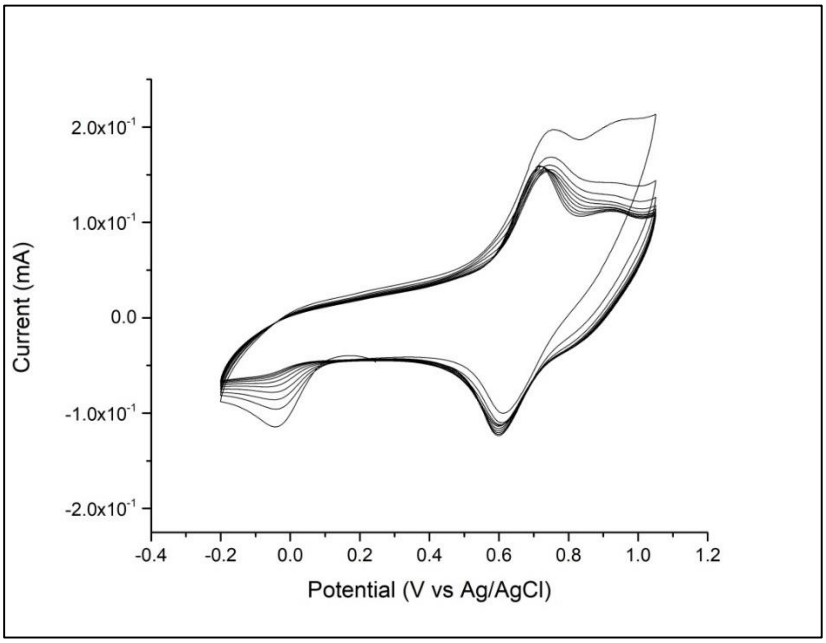

Figure 4.1.2: The graph represents the CV characterization in KNO_3 0.1M of the CuHCF method A film on Graphoil after the two deposition steps at the scan rate of 10 mV/s.

Figure 4.1.3 shows the CV characterization of a sample deposited on carbon tissue in KNO_3 0.1 M. Here too, it can be noticed that the first anodic segment has a higher current intensity value, also of that obtained on graphoil perhaps for some catalytic property of the support. The scan rate at which the cyclic voltammetry was done is 10 mV/s, also in this case. In the obtained voltammograms we get the same peaks of the previous tests, but one different shape due to the different used substrate.

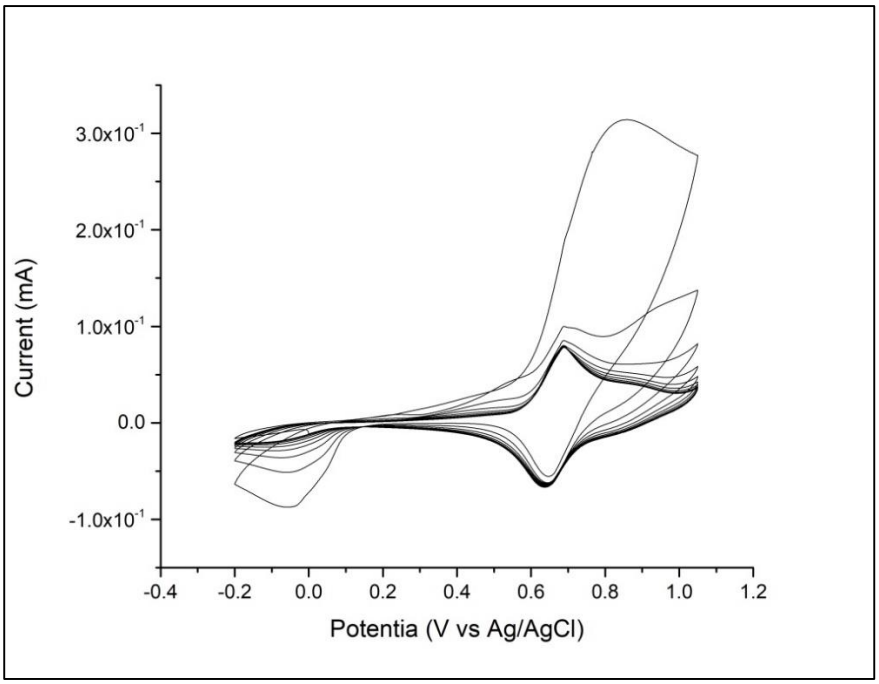

Figure 4.1.3: The graph represents the CV characterization in KNO_3 0.1M of the CuHCF method A film on Carbon Tissue after the two deposition steps at the scan rate of 10 mV/s.

COMPARISON BETWEEN THE TWO SUPPORTS

The table below shows the charges that pass through the different steps for each support. And we can observed that the amount of deposited metallic copper is lower on the graphoil than on the carbon tissue and this amount has been evaluated by the charge.

	Charge (C)	**Deposited Cu^0 (mg)**
	Step 1	
Graphoil	0.0366	0.0121
Carbon Tissue	0.2232	0.0735

On the sample deposited on carbon tissue, potential scans performed at different speeds (1 mV/s, 10 mV/s and 100 mV/s) allow us to see if the current is diffusive control (linear trend of the current intensity of the anodic peak with the square root of the scan speed) or whether it is a process confined to the surface (linear trend of the current intensity of the peak with scanning speed). Figure 4.1.4c shows the cyclic voltammetries performed on the same sample but at different speeds.

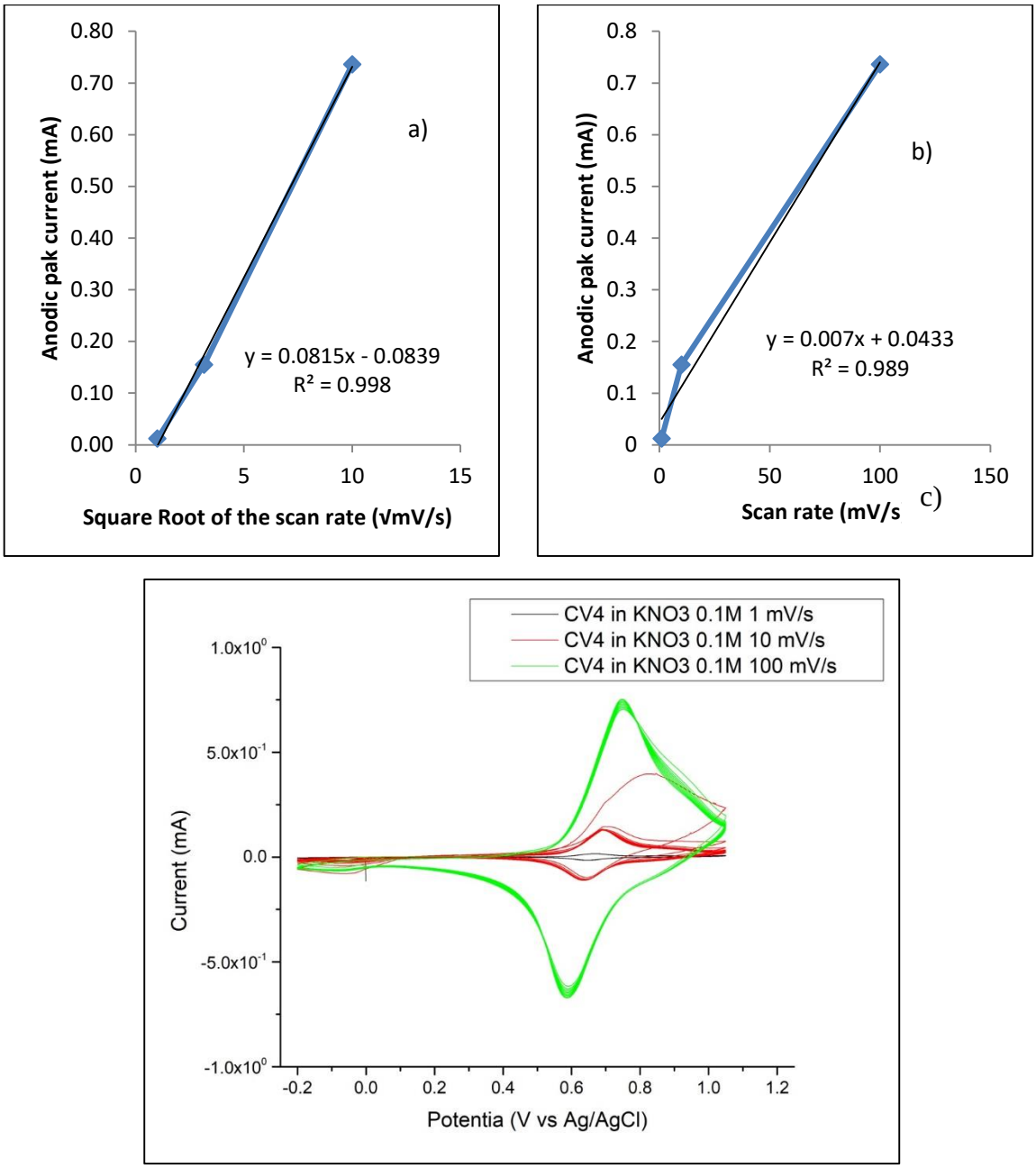

Figure 4.1.4: a) Anodic peak current trend with square root of the scan rate. b) Anodic peak current trend with the scan speed. c) CV in KNO_3 0.1 M at different scan speeds.

METHOD B

DEPOSITION

The deposition performed according to the method B is to deposit the metallic copper at higher potentials and for shorter application times than method A. The intent of depositing the metallic copper in smaller quantities is to avoid precipitation in the bulk of the solution and to obtain stable films that will give stable characterization voltammograms from the first cycle. In the first step the potentiostatic deposition of the metallic copper occurred at

a potential of -1 V for 4 seconds (Figure 4.5a) while for the second step +1 V for 15 seconds (Figure 4.1.5b).

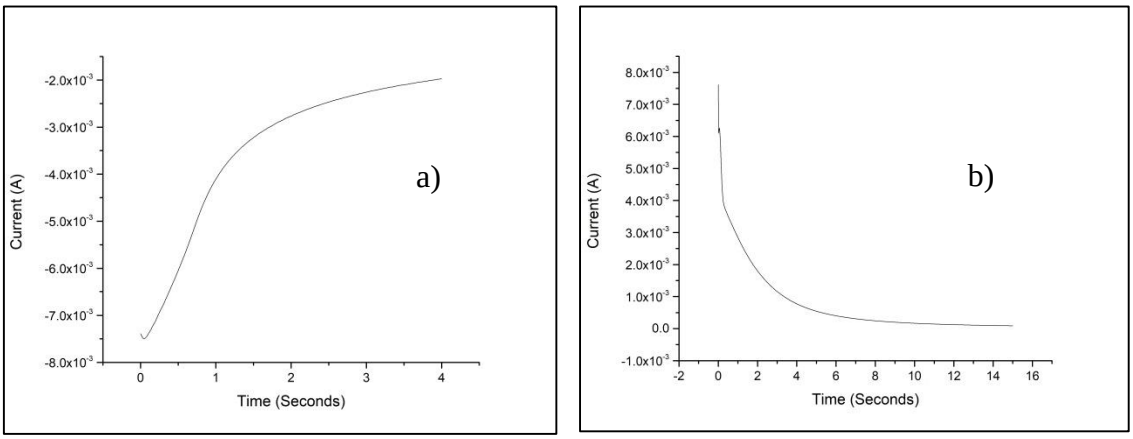

Figure 4.1.5: a) Chronoamperogram of metalic copper deposition process (-1 V for 4 seconds) in $CuSO_4$ 0.05 M + K_2SO_4 0.05 M solution. b) Chronoamperogram of the dissolution process of the film (+1 V for 15 seconds) in a solution of $K_3[Fe(CN)_6]$ 1 mM + K_2SO_4 0.25 M. Support: graphoil

ELECTROCHEMICAL CHARACTERIZATION

From the characterization we can see that there are substantial differences between the two methods. In addition to a lower current intensity and a stable voltammogram from the first segment, there is a peak at +0.4 V (Figure 4.1.6) that isn't present in the voltammograms of method A: The peaks at +0.4 V and 0.0 V are connected to the couple Cu^{2+}/Cu^{+} and the separation larger than 300 mV between the two has made many authors to suggest a possible structural reorganization.

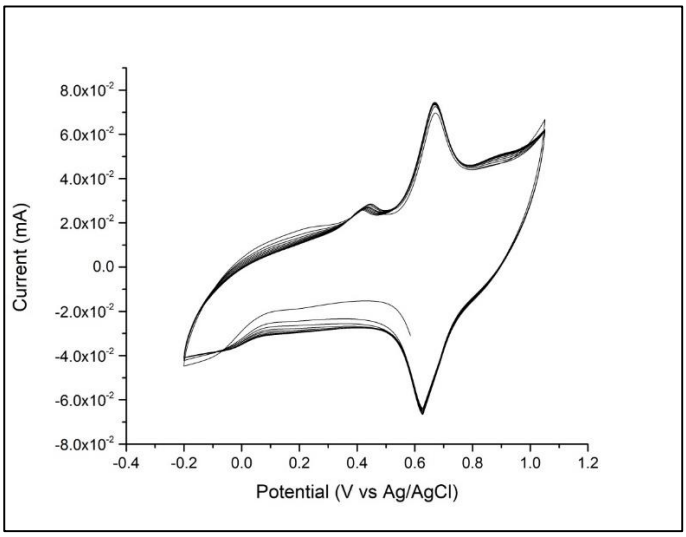

Figure 4.1.6: The graph represents the CV characterization in KNO_3 0.1M of the CuHCF method B film on Graphoil after the two deposition steps at the scan rate of 10 mV/s.

Figure 4.1.7 shows the cyclic voltammetries obtained on two other supports: carbon tissue and Toray carbon paper. The scan rate at which the cyclic voltammetry was done is 10

mV/s, also in this case. In the obtained voltammograms we get the same peaks of the previous tests, but one different shape due to the different used substrate. The compound deposited on the carbon tissue has a current intensity slightly lower than the one deposited on graphoil, and a good stability since the first cycle. As far as Toray Carbon Paper is concerned, here the currents are lower than those recorded in graphoil or carbon tissue and the first cycle has a much higher current than the following ones.

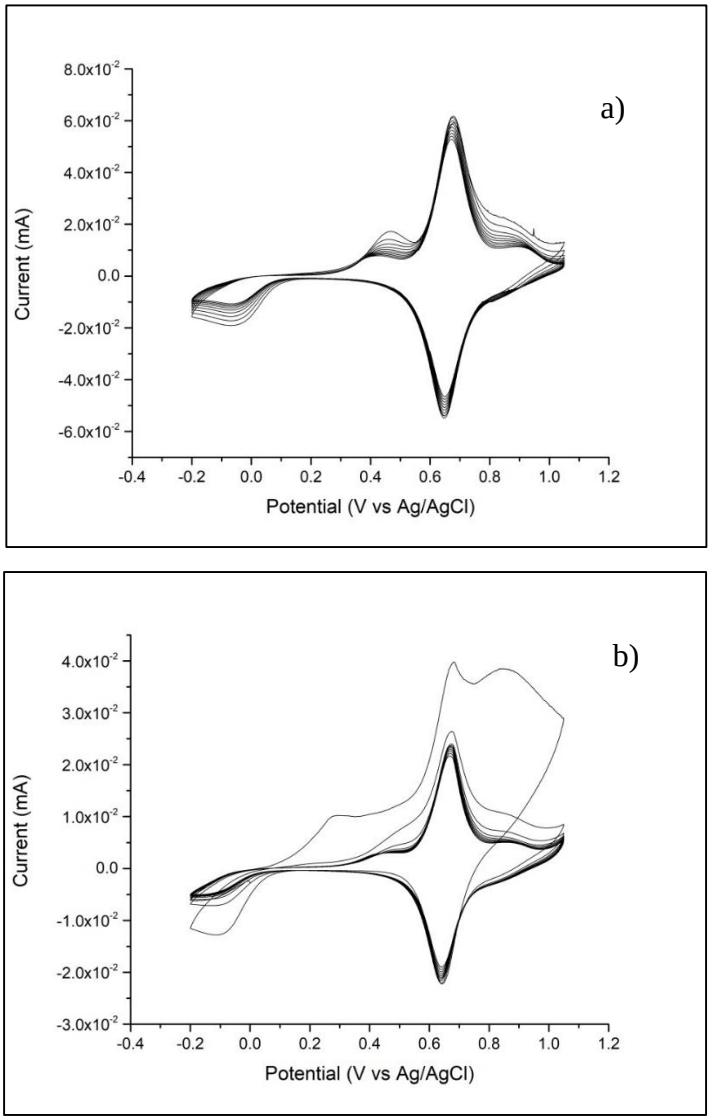

Figure 4.1.7: a) The CV characterization in KNO_3 0.1M of the CuHCF method B film on Carbon Tissue after the two deposition steps at the scan rate of 10 mV/s. b) The CV characterization in KNO_3 0.1M of the CuHCF method B film on Toray Carbon Paper after the two deposition steps at the scan rate of 10 mV/s

COMPARISON BETWEEN THE THREE SUPPORTS

The table below shows the charges that pass through the different steps for each support. And we can observed that the amount of deposited metallic copper is lower on the graphoil, followed by the one deposited on Toray Carbon Paper and the higher amount is obtained on the Carbon Tissue .

	Charge (C)		Deposited Cu^0 (mg)
	Step 1	Step 2	
Graphoil	0.0137	0.0113	0.0045
Carbon Tissue	0.0790	0.0302	0.0260
Toray Carbon Paper	0.0489	0.0237	0.0161

Also in this case, tests have been conducted on Carbon Tissue at different speeds (1 mV/s, 10 mV/s and 100 mV/s) to verify the nature of the deposition process. Figures 4.8a and 4.1.8b show that this method, unlike method A, in not under diffusive process but is confined to the surface.

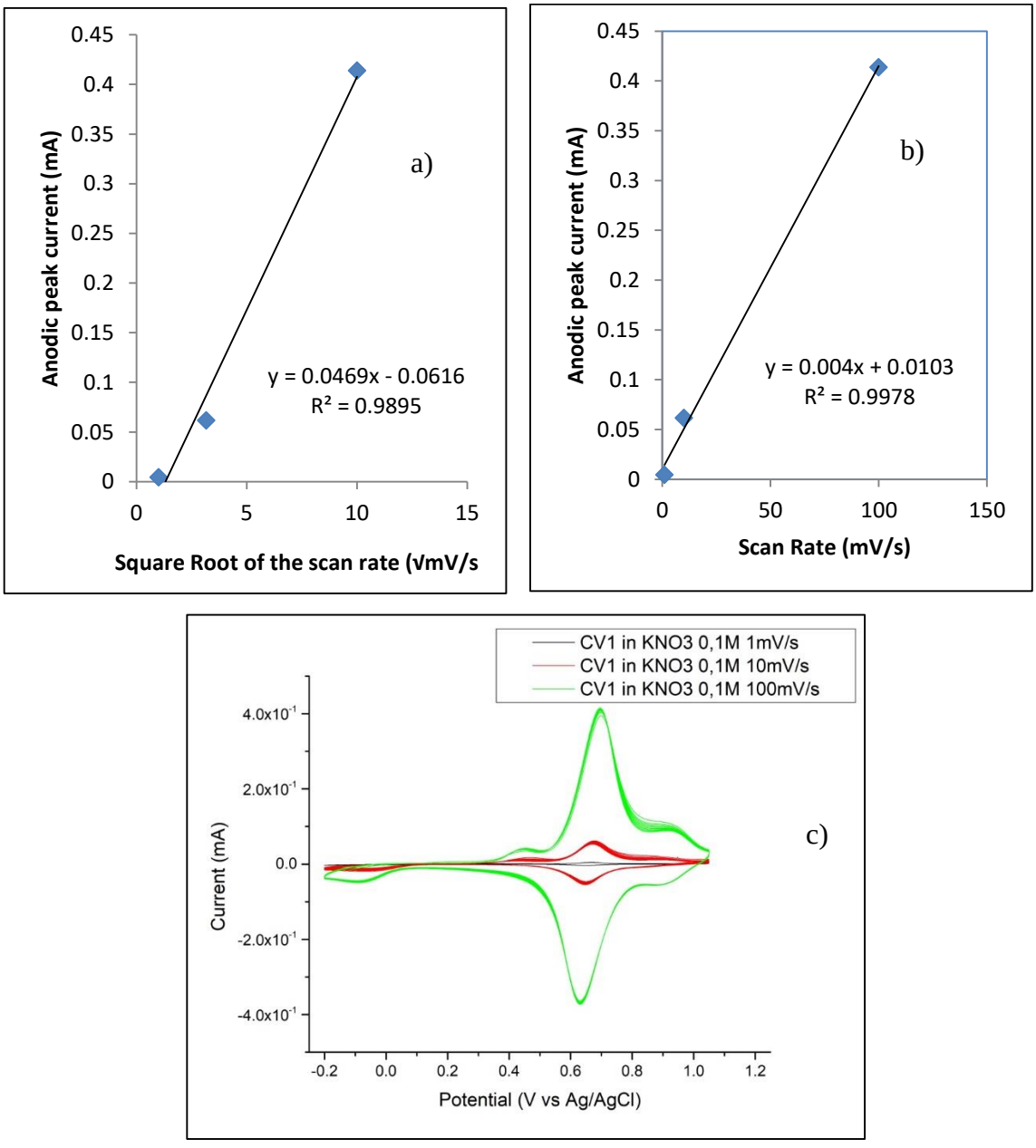

Figure 4.1.8: a) Anodic peak current trend with square root of the scan rate. b) Anodic peak current trend with the scan speed. c) CV in KNO_3 0.1 M at different scan speeds.

COMPARISON BETWEEN METHOD A AND B

In Figure 4.1.9 the voltammograms obtained with the two methods are compared. On both substrates we notice that the current intensity of the peak at + 0.6 V is greater for method A than for method B, and the peak at + 0.4 V is the difference between the two deposition methods. The intensity of the red curve at + 0.4 V exceed that of the black curve despite on the electrode modified with method B is present less electroactive material. This confirms that the + 0.4 V peak is not present in the voltammogram of method A.

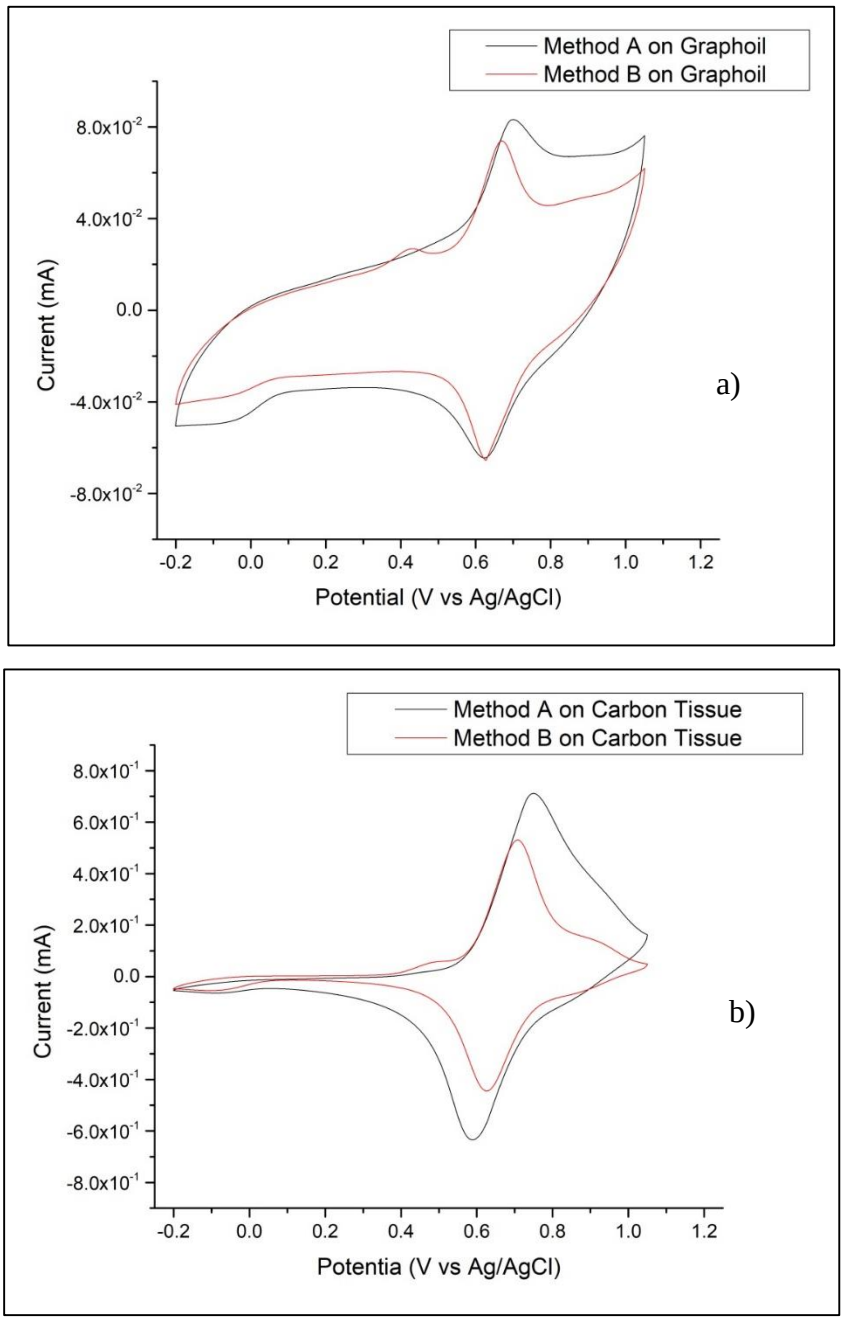

Figure 4.1.9: a) Comparison of CVs of method A and B deposited on graphoil at a scan rate of 10 mV/s. b) Comparison of CVs of method A and B deposited on Carbon Tissue at a scan rate of 100 mV/s. Average cyclic voltammetry is reported.

4.2 Nickel Hexacyanoferrate (NiHCF)

Deposition

Electrosynthesis was conducted in a solution of $K_3Fe(CN)_6$ 5 mM and KNO_3 0.1 M for 300 seconds, then applying a potential of 1.0 V for another 300 seconds. Is known from the literature that the electrosynthesis of nickel hexacyanoferrate by applying a constant potential for short time (around 50 seconds) or a cyclic one, brings to a product characterized by the presence of two different peaks at 0.45 V and 0.63 V if the CV is done in an aqueous solution of KNO_3 1M. The redox couple can be approximate to the $KNi[Fe^{III}(CN)_6]/K_2Ni[Fe^{II}(CN)_6]$ formulas and the insertion of Potassium resulting in a change of oxidation state and represented by the following reaction:

$$KNi[Fe^{III}(CN)_6] + K^+ + e^- \leftrightarrow K_2Ni[Fe(CN)_6]$$

By applying a constant potential for longer times, we can obtain a more resistant compound, the $Ni_{1.5}[Fe^{III}(CN)_6]$, greater thickness and better mechanical properties. This form of NiHCF, characterized by a voltammogram that, under the same conditions listed previously, has only a peak of approximately 0.45 V (80) corresponding to the reaction:

$$Ni_{1.5}[Fe^{III}(CN)_6] + K^+ + e^- \leftrightarrow KNi_{1.5}[Fe(CN)_6]$$

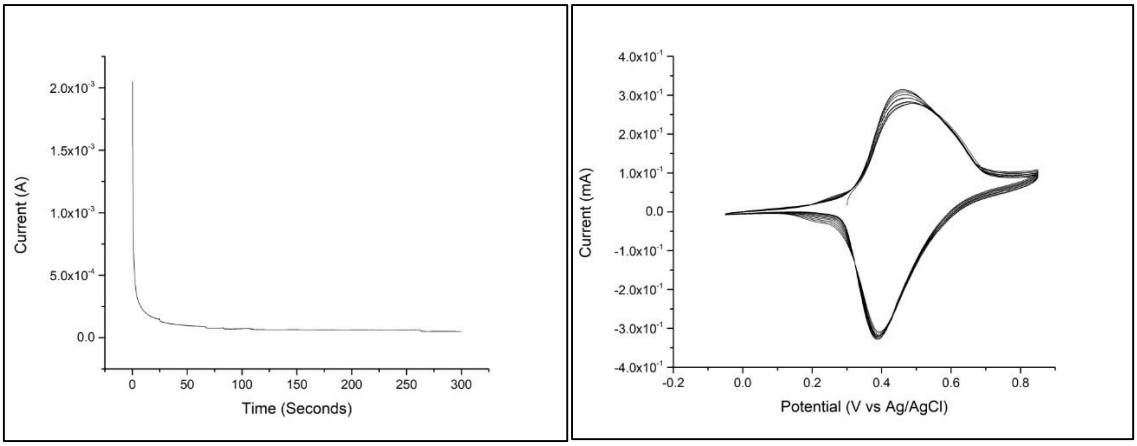

Figure 4.2.1: a) Chronoamperogram of nickel hexacyanoferrate deposition process (1 V for 300 seconds) in K3Fe(CN)6 5 mM and KNO3 0.1 M solution. b)) The CV characterization in $NaNO_3$ 1 M of the NiHCF on Nickel Foam at the scan rate of 50 mV/s

Electrochemical Characterization

The compound is the one expected as the characterization in $NaNO_3$ shows a single peak corresponding to the redox pair $Ni_{1.5}[Fe^{III}(CN)_6]$/ $NaNi_{1.5}[Fe^{II}(CN)_6]$ characteristic of this form of NiHCF. Figure 4.2.1b we can verify that the cathodic peak is at a potential of 0.45 V and the anodic one at 0.40 V. We can conclude that the reaction is reversible and it respects certain criteria of reversibility, such the relationship between the anodic current

peak and the cathodic one, that is equal to 1.09 , and ΔE_p (the difference between the cathodic and anodic peak) is 0.05 V.

Therefore was considered the cathodic peak of the last voltammogram to calculate the deposited mass of nickel hexacyanoferrate. From the integral of this peak, the number of exchanged electrons was calculated with the following formula:

$$n = \frac{integral}{F * v}$$

Where F is the Faraday's constant (96485 C/mol) and v is the scan rate. If we consider that every mole of NiHCF exchange a mole of electrons to pass from the oxidized form $NaNi_{1.5}[Fe^{III}(CN)_6]$ to the reduced one $Ni_{1.5}[Fe^{II}(CN)_6]$, is possible to equate the electrons moles just found to those of NiHCF present on the electrode surface. Through the molar mass of $Ni_{1.5}[Fe^{II}(CN)_6]$ that is 299.99 g/mol we can find the deposited mass of the product, that in this case is 3.57 mg.

However it have to be reminded that this procedure is an approximation as it is considered that all the current passing through the electrode is due to faradic reaction of oxidation and reduction of the iron from the nickel hexacyanoferrate, there are always present some dissipative current and it is possible that at the same time competitive reaction are taking place. So it is possible that the results are slightly overestimated.

COMPARISON IN DIFFERENT ELECTROLYTES

Characterization were also performed in other electrolytes. Figure 4.2.2 shows the various voltammograms obtained in different electrolytes with a scan speed of 50 mV/s. The position of the peak may vary and depend not only on the nature of the analysed material but also on the material of which the working electrode is done and the electrolyte solution in which the characterization occurs.

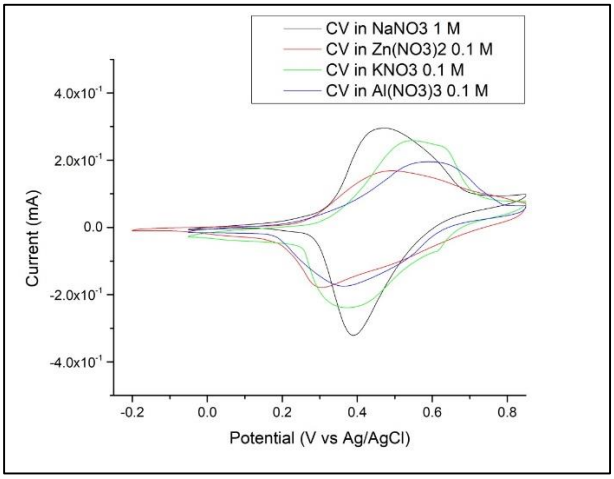

Figure 4.2.2: Comparison of the CVs obtained in the different electrolytes at the scan rate of 50 mV/s. Average cyclic voltammetry is reported.

On the sample characterized in KNO_3 0.1 M, potential scans performed at different speeds (1 mV/s, 10 mV/s and 50 mV/s) allow us to see if the current is diffusive control (linear trend of the current intensity of the cathodic peak with the square root of the scan speed) or whether it is a process confined to the surface (linear trend of the current intensity of the peak with scanning speed). Figure 4.2.3c shows the cyclic voltammetries performed on the same sample but at different speeds.

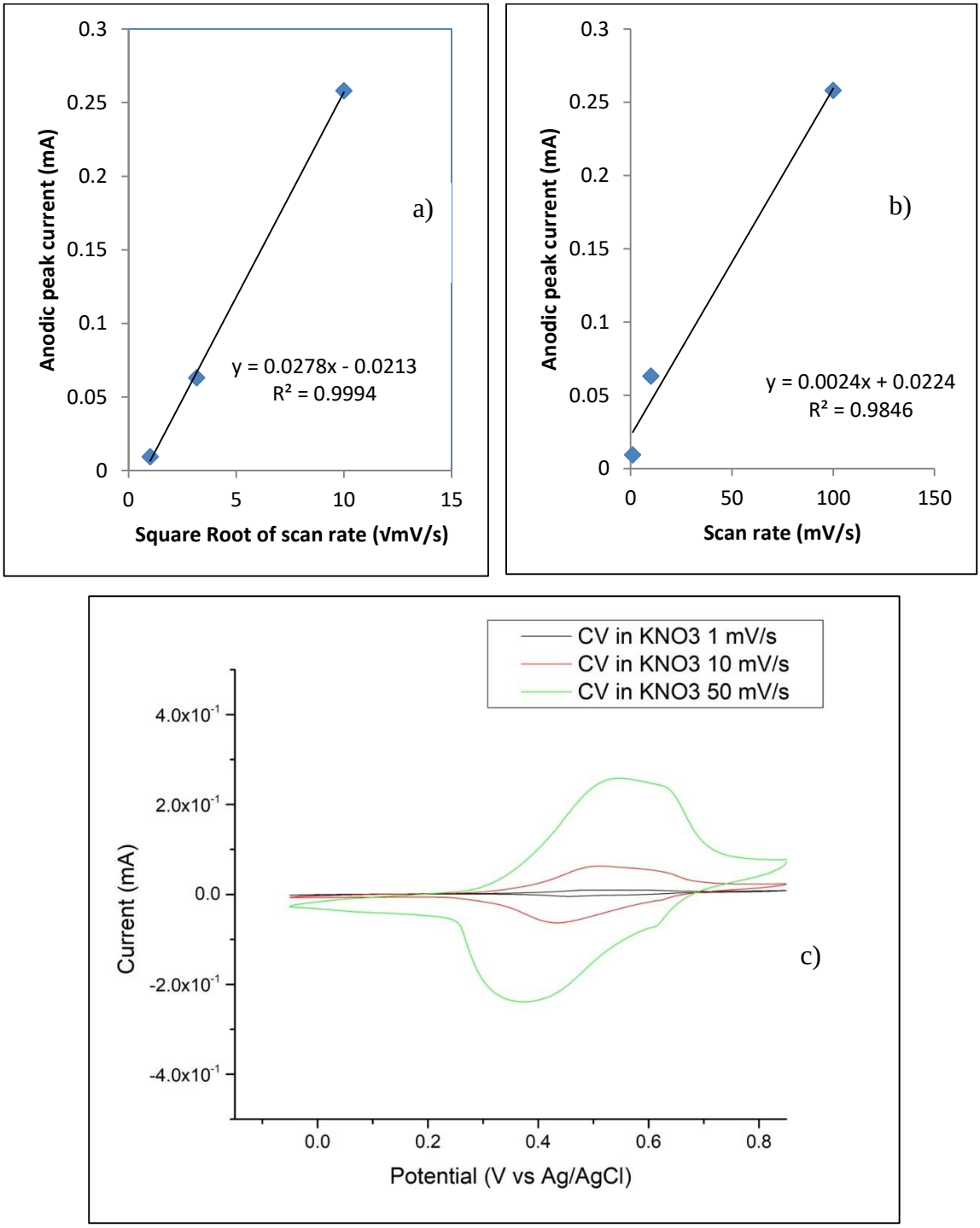

Figure 4.2.3: a) Anodic peak current trend with square root of the scan rate. b) Anodic peak current trend with the scan speed. c) CV in KNO_3 0.1 M at different scan speeds. Average cyclic voltammetry is reported.

4.3 Double Layer Hydroxide (LDH)

Here too, the intent is to apply the deposition protocol to different substrates, (graphoil with graphite on both sides, carbon tissue, Toray carbon paper and nickel foam) and then compare the results obtained to figure out which present the best performance.

DEPOSITION

The Co/Al and Co/Fe LDH were synthesized by electrochemical way, applying a constant cathodic potential (-1.15 V) for fixed times (30s, 60s or 120s) to a solution that contained the metal nitrates of interest. The bivalent and trivalent metal concentration were respectively 0.0225 M and 0.0075 M, in a molar ratio of 3/1 and a total concentration of 0.03 M. Figure 4.3.1 shows the chronoamprerograms of the two compounds on graphoil.

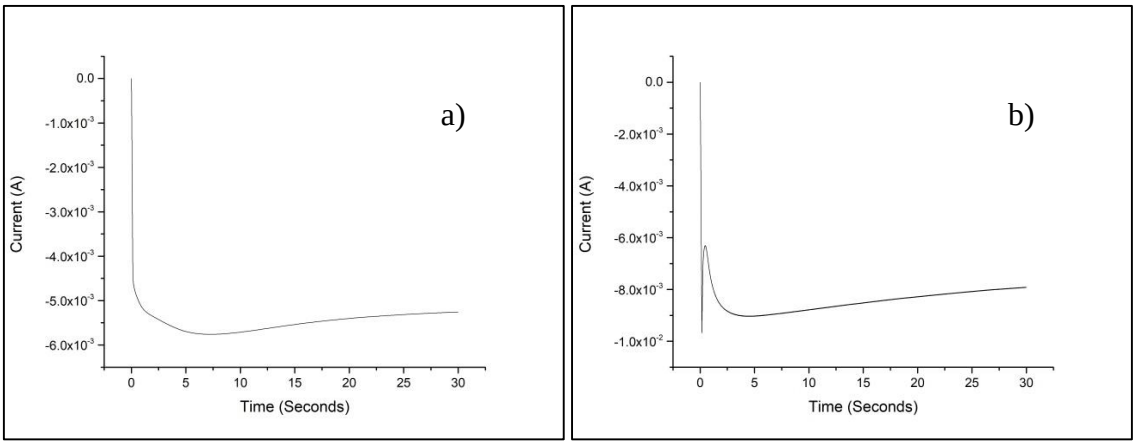

Figure 4.3.1: a) Chronoamperogram of CoAl deposition process (- 1.15 V for 30 seconds) in $Co(NO_3)_2$ and $Al(NO_3)_3$ 0.03 M solution in a molar ration of 3/1. b)) Chronoamperogram of CoFe deposition process (- 1.15 V for 30 seconds) in $Co(NO_3)_2$ and $Fe(NO_3)_3$ 0.03 M solution in a molar ration of 3/1.

ELECTROCHEMICAL CHARACTERIZATION

All electrodes modified with LDH were electrochemically characterized by running 10 cycles in a solution of KOH 1 M in a suitable potential windows.

4.3.1 Cobalt Aluminium (CoAl)

In the Figure 4.3.2 we can see that in the first cycle we observe an irreversible peak attributable to the partial oxidation of most centers of Co (II). This is in agreement with previous research work in which it was shown that 80% of the Co (II) sites undergoes oxidation during the first anodic scanning in which the hydrotalcite evolve in a more stable form γ-Co(III)OOH (81). The obtained signal stays stable after the first cycle and remains unchanged even after many others cycles, indicating the good stability of the electrodeposited film on the electrode.

depending on the deposition conditions and the pretreatment of the support, we can observe one single expanded system or two almost separate systems, due to Co(II)/Co(III) and Co(III)/Co(IV). The two peaks are respectively at around 0.17V and 0.29V, due to the following oxidation reactions:

$$\text{Co(II)-LDH} + OH^- \rightleftarrows \text{Co(III)-LDH-OH} + e^- + H_2O$$

$$\text{Co(III)-LDH} + OH^- \rightleftarrows \text{Co(IV)-LDH-OH} + e^- + H_2O$$

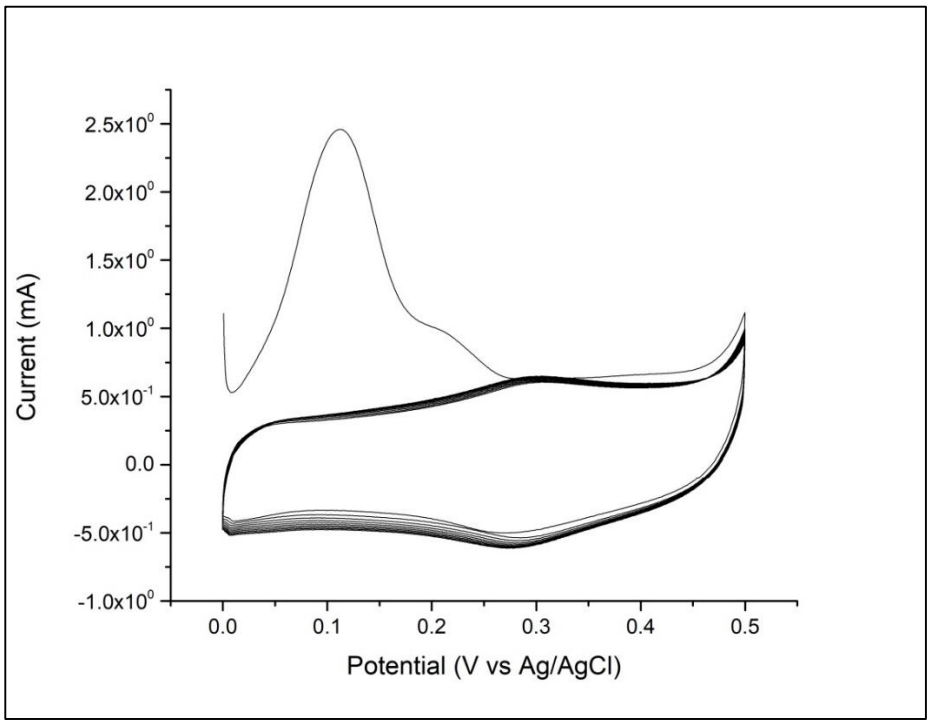

Figure 4.3.2: The CV characterization in KOH 1 M of the CoAl (deposition time: 30 seconds) on Graphoil at the scan rate of 10 mV/s.

Figure 4.3.3 shows the comparison between voltammograms of electrodes obtained with different deposition time, that is 30, 60 and 120 seconds. We can see the presence of the irreversible peak and the same form of the voltammetry, but the current intensity increases with the deposition time, as expected.

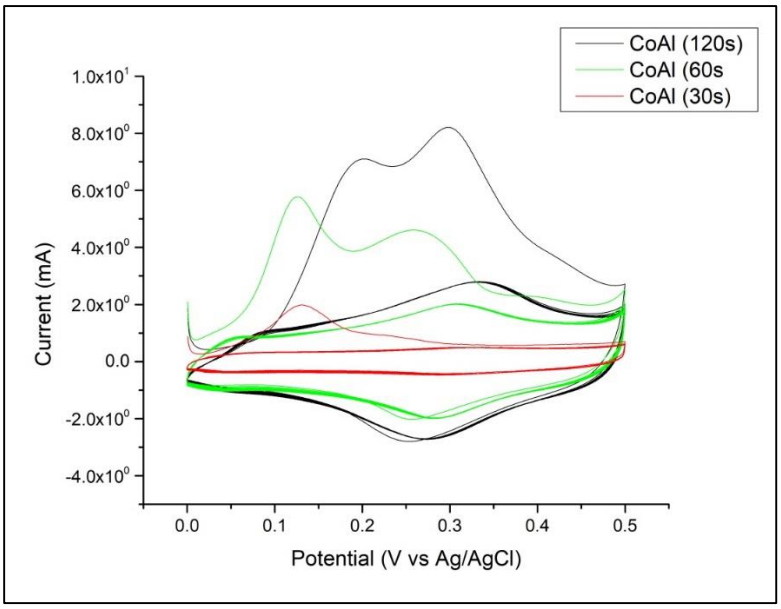

Figure 4.3.3: Comparison of the CV characterization in KOH 1 M of the CoAl obtained with different deposition time on Graphoil at the scan rate of 10 mV/s.

Electrodeposition for more than 120 seconds haven't been performed because, beyond that time, a spontaneous deposition of the deposit from the support is noticeable due to the high thickness of the film, worsening the mechanical proprieties and adhesion to the electrode surface of the material.

COMPARISON BETWEEN THE FOUR SUPPORTS

Figure 4.3.4 shows the voltammograms obtained on other supports at the scan speed of 10 mV/s and deposition time of 30 seconds. We can observe that all the voltammograms have the same shape, instead the performance, in terms of current intensity, nickel foam is placed at first place followed by graphoil.

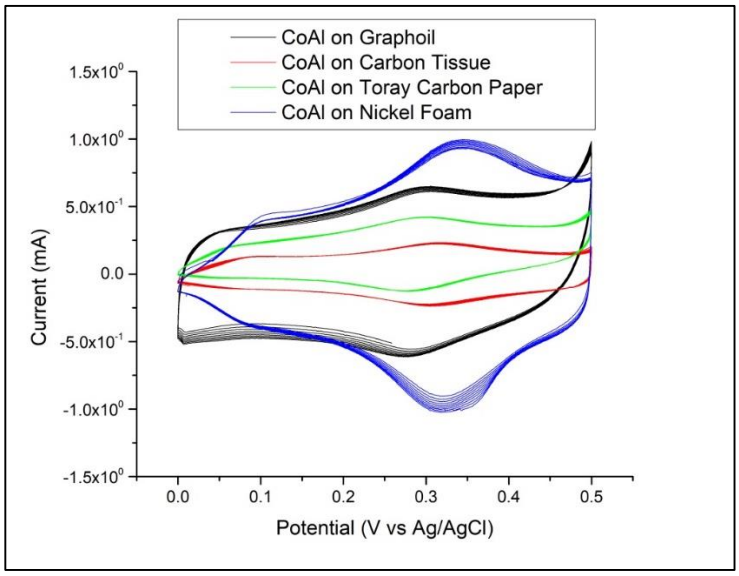

Figure 4.3.4: Comparison of CVs of CoAl deposited for 30 seconds on different supports and at a scan rate of 10 mV/s

Co/Al LDH deposited for 60 seconds on graphoil has also been characterized at different scan rate (5, 10, 20, 50 and 100 mV/s). The plot of the anodic current as a function of either scan rate or to the square root of the scan rate (Figure 4.3.4) a linear correlation is observed in the former case, indicating that the electroactive species is confined on the surface of the electrode.

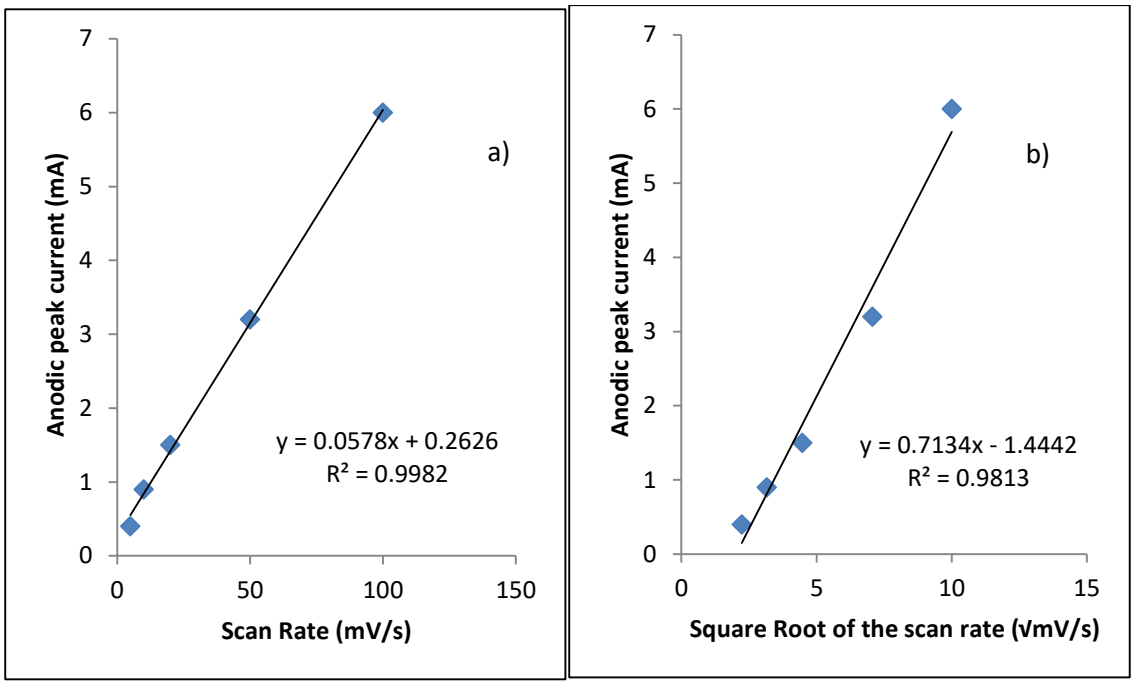

Figure 4.3.4: a) Anodic peak current trend with square root of the scan rate. b) Anodic peak current trend with the scan speed.

Regarding the reproducibility of deposited masses for a certain synthesis time quite satisfactory results have been achieved for the graphoil, but not so good for the carbon tissue. Is was therefore decided to study the correlation between the synthesis time and the mass obtained by weighing the electrodes before and after deposition, and to use this data to determine the specific capacity of the material. To study the possible correlation between deposition time and mass obtained, several samples were prepared depositing LDHs for the following times: 30, 60 e 120 seconds In the case of carbon tissue, deposited masses are higher and decrease with the increasing of deposition time, although data is not reproducible how we can see from the table below, perhaps because of the very porous material where not always enter the same amount of compound and there isn't linearity with the deposition time. In the case of graphoil instead, deposited masses are lower and reproducible and have good linearity with deposition time.

Support	Deposition time (s)	Deposited mass (mg)	Average mass (mg)
Graphoil	30	0.08	
	30	0.06	0.07
	30	0.07	
Carbon Tissue	30	0.37	
	30	0.41	0.356
	30	0.29	

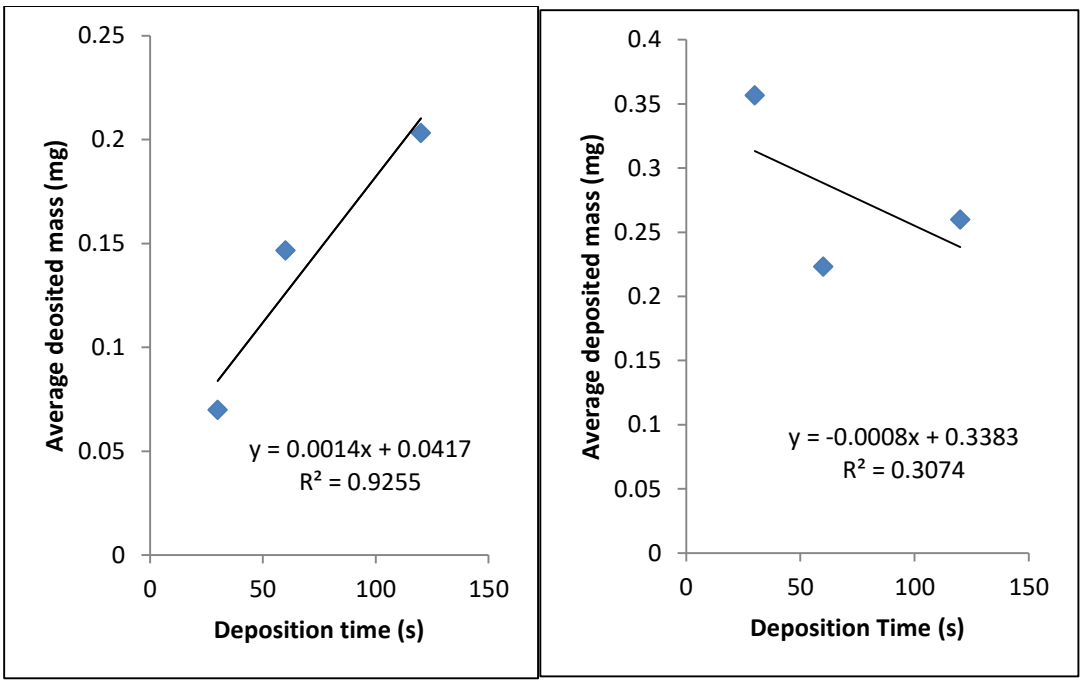

Figure 4.3.5: a) Dependence of the average deposited mass with deposition time on graphoil. b) Dependence of the average deposited mass with deposition time on carbon tissue.

4.3.2 Cobalt Iron (CoFe)

Subsequently, was studied under the same conditions the behaviour of Co/Fe LDH film after deposition time of 30 seconds. In characterization CV present a single pair of peaks, around a potential of + 0.1 V. It is known in the literature that iron inside the hydrotalcitic structure is not electroactive, so we can attribute the pair of observed peaks to the redox process of the cobalt. It is, however, observed how the presence of iron leads in advance the cobalt oxidation. A good reversibility can be observed and how the process is stable from the first cycle, unlike the Co/Al LDH, and currents are also higher than the CoAl. We also note how the recorded curves of the electrode's characterization with Co/Fe LDH interest a larger potential window, indicating capacitive behaviour in a larger ΔV than Co/Al LDH.

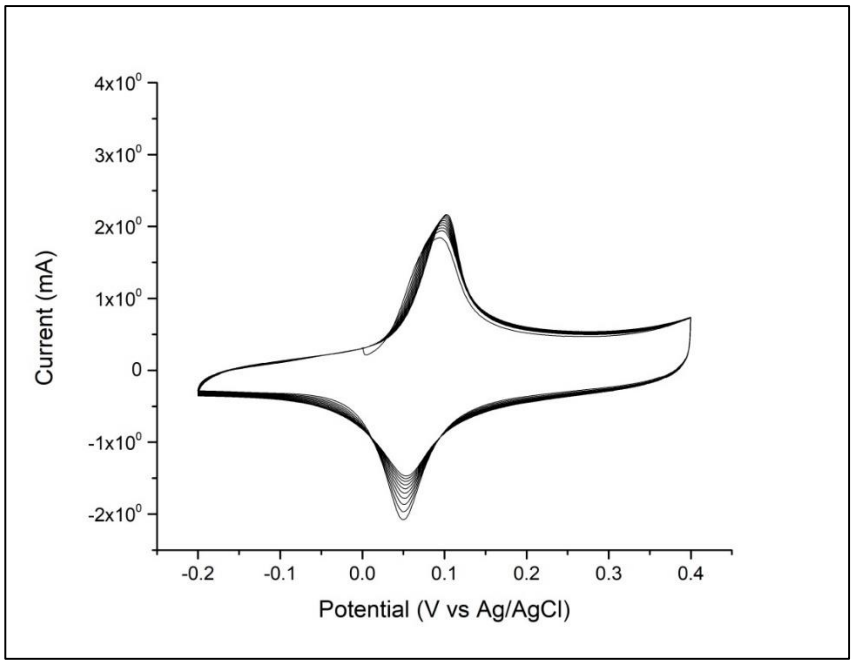

Figure 4.3.6: The CV characterization in KOH 1 M of the CoFe (deposition time: 30 seconds) on Graphoil at the scan rate of 10 mV/s.

Figure 4.3.7 shows the voltammograms of electrodes obtained with different deposition time, that is 60 and 120 seconds. We can see that the shape of the voltammogram is the same, but the current intensity increases with the deposition time, as expected.

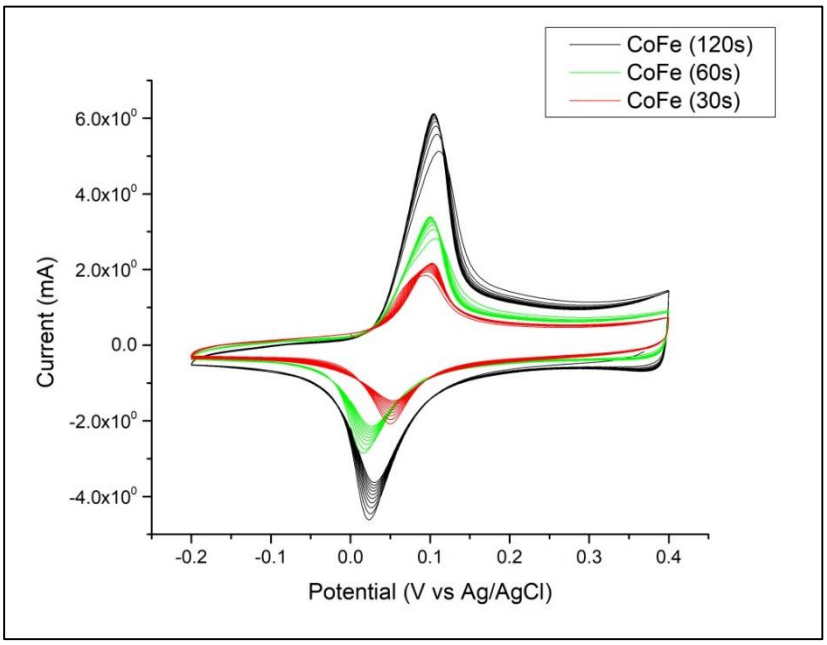

Figure 4.3.7: Comparison of the CV characterization in KOH 1 M of the CoFe obtained with different deposition time on Graphoil at the scan rate of 10 mV/s.

COMPARISON BETWEEN THE FOUR SUPPORTS

Figure 4.3.8 shows the voltammograms obtained on other supports at the scan speed of 10 mV/s and deposition time of 30 seconds. We can observe that all the voltammograms have

the same shape, instead the performance, in terms of current intensity, graphoil is placed at first place.

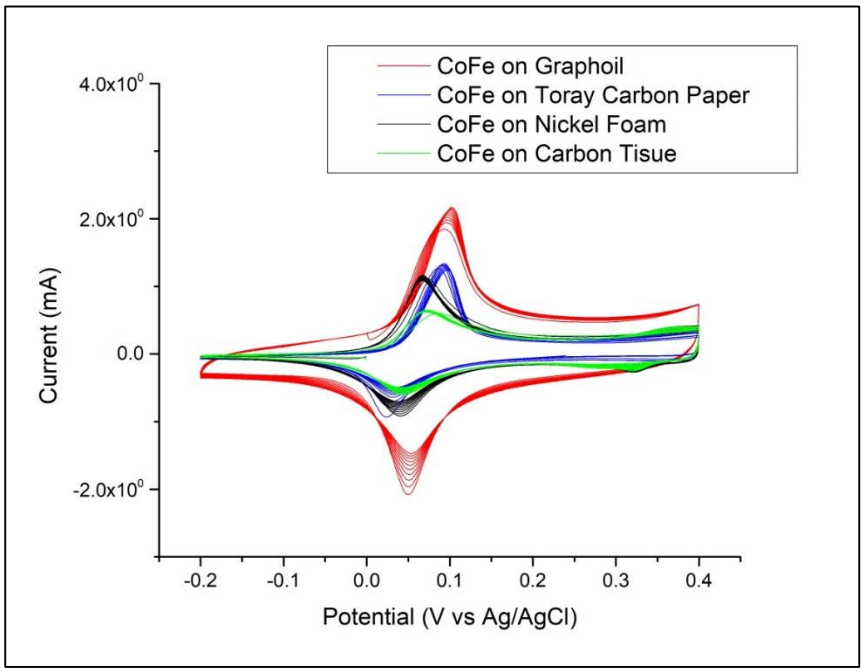

Figure 4.3.8: Comparison of CVs of CoFe deposited for 30 seconds on different supports and at a scan rate of 10 mV/s.

Co/Fe LDH deposited for 60 seconds on graphoil has also been characterized at different scan rate (1, 2, 5, 10, 20, 50 and 100 mV/s). In this case, however, drawing the anode peak current based on the potential scan rate, no linear correlation is obtained, but the current is proportional to the square root of the potential scan speed (Figure 4.3.9). This indicates that in this case the faradic redox reaction of cobalt prevails and the current follows the expected theoretical dependence (equation of Randles – Sevcik):

$$I_p = 2.686 * 10^5 * z^{3/2} * A * D^{1/2} * C * v^{1/2}$$

Where:

- ip = current maximum in Ampere
- z = number of electrons transferred in the redox event (usually 1)
- A = electrode area in cm2
- D = diffusion coefficient in cm2/s
- C = concentration in mol/cm3
- ν = scan rate in V/s

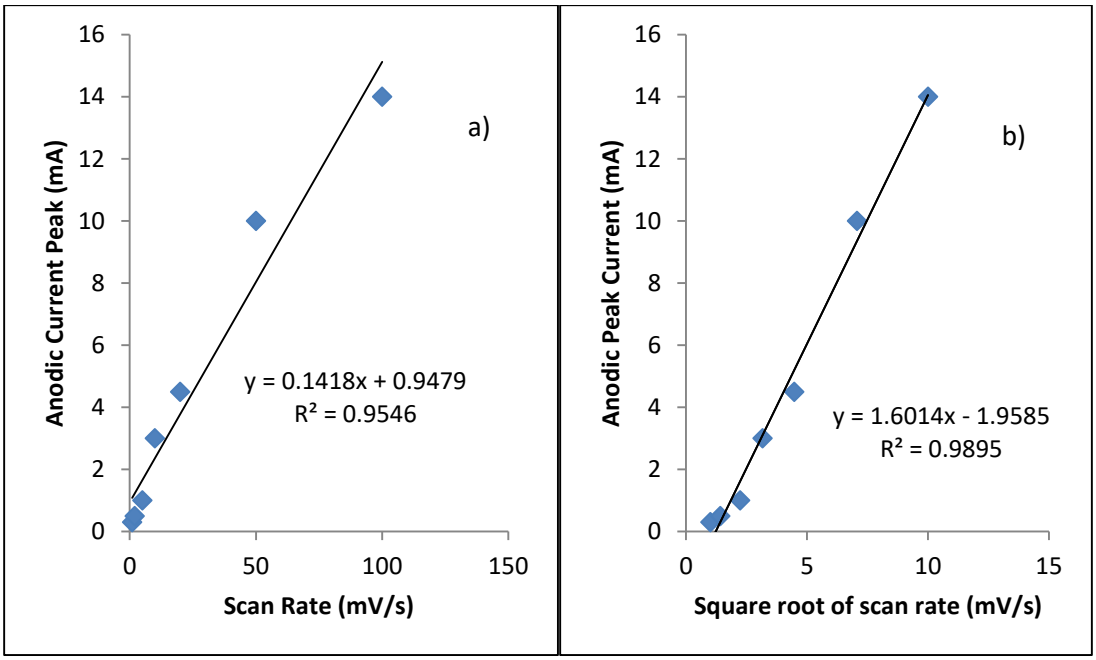

Figure 4.3.9: a) Anodic peak current trend with square root of the scan rate. b) Anodic peak current trend with the scan speed.

Regarding the reproducibility of deposited masses for a certain synthesis time, also here, quite satisfactory results have been achieved for the graphoil, but not so good for the carbon tissue, how Figure 4.3.10 shows. In the case of carbon tissue, deposited masses are higher, although data is not reproducible how we can see from the table below, perhaps because of the very porous material where not always enter the same amount of compound and there isn't linearity with the deposition time. In the case of graphoil instead, deposited masses are lower and reproducible and have good linearity with deposition time.

Support	Deposition time (s)	Deposited mass (mg)	Average mass (mg)
Graphoil	30	0.06	
	30	0.05	0.053
	30	0.05	
Carbon Tissue	30	0.15	
	30	0.44	0.263
	30	0.20	

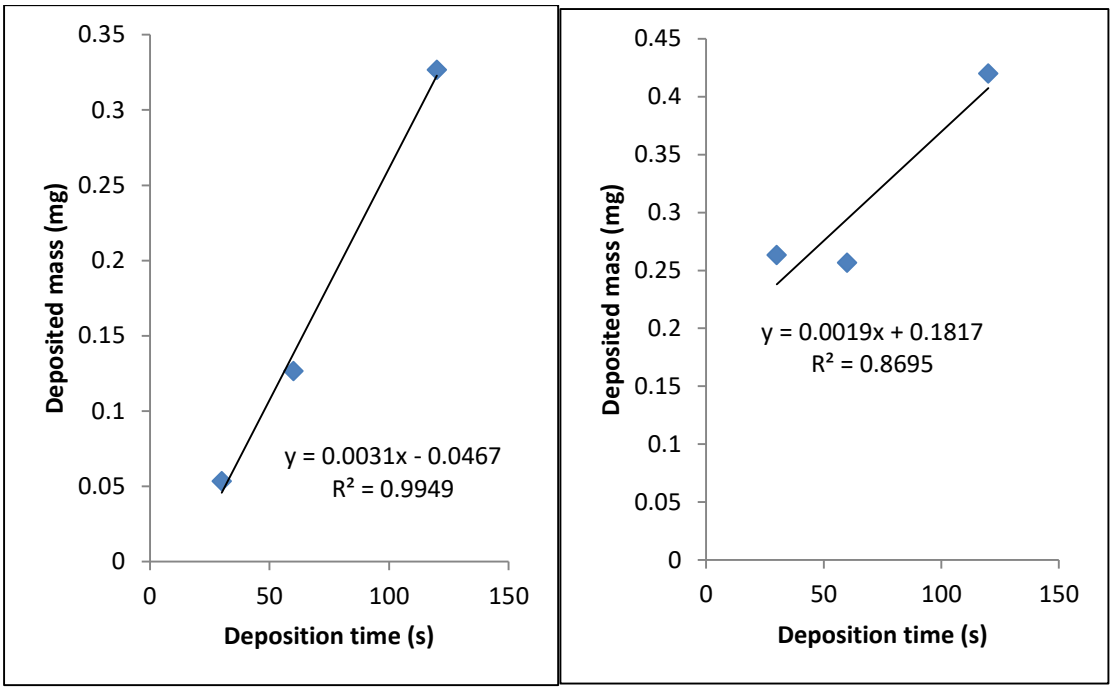

Figure 4.3.5: a) Dependence of the average deposited mass with deposition time on graphoil. b) Dependence of the average deposited mass with deposition time on carbon tissue.

CALCULATION OF THE CAPACITY OF LDH FROM CVS

Since the charge accumulated in the material is related to the underlying area of the cyclic voltammograms, the specific capacity of the electrodes was calculate using the following equation:

$$C_S = \frac{I}{v * m}$$

Where I (A) is the current, m (g) is the electrodeposited mass and v is the scan rate (V/s). Considering the calculated masses and the scanning speed ν = 0.01 V / s, the specific capacity of the modified electrode on graphoil are reported in the following table:

Deposition Time (s)	CoAl (F/g)	CoFe (F/g)
30	746	891
60	1116	932
120	1526	1600

In Figure 4.3.6 are reported the values of specific capacities calculated from the CVs recorded at different scan rates (from 0.001 to 0.05 V/s) in 1 M KOH. In case of Co/Al LDH the capacity is almost independent from the scan rate whereas the opposite is worth for the Co/Fe based material, for which a sudden drop of the Cs value is observed from 0.01 to 0.05 V/s. This result is a common phenomenon in supercapacitors since at high scan rates, the mass-transport of ions (from the electrolyte)

to the interior (bulk) of the electrode limits the electrochemical performance, which leads to a lower capacity. (82)

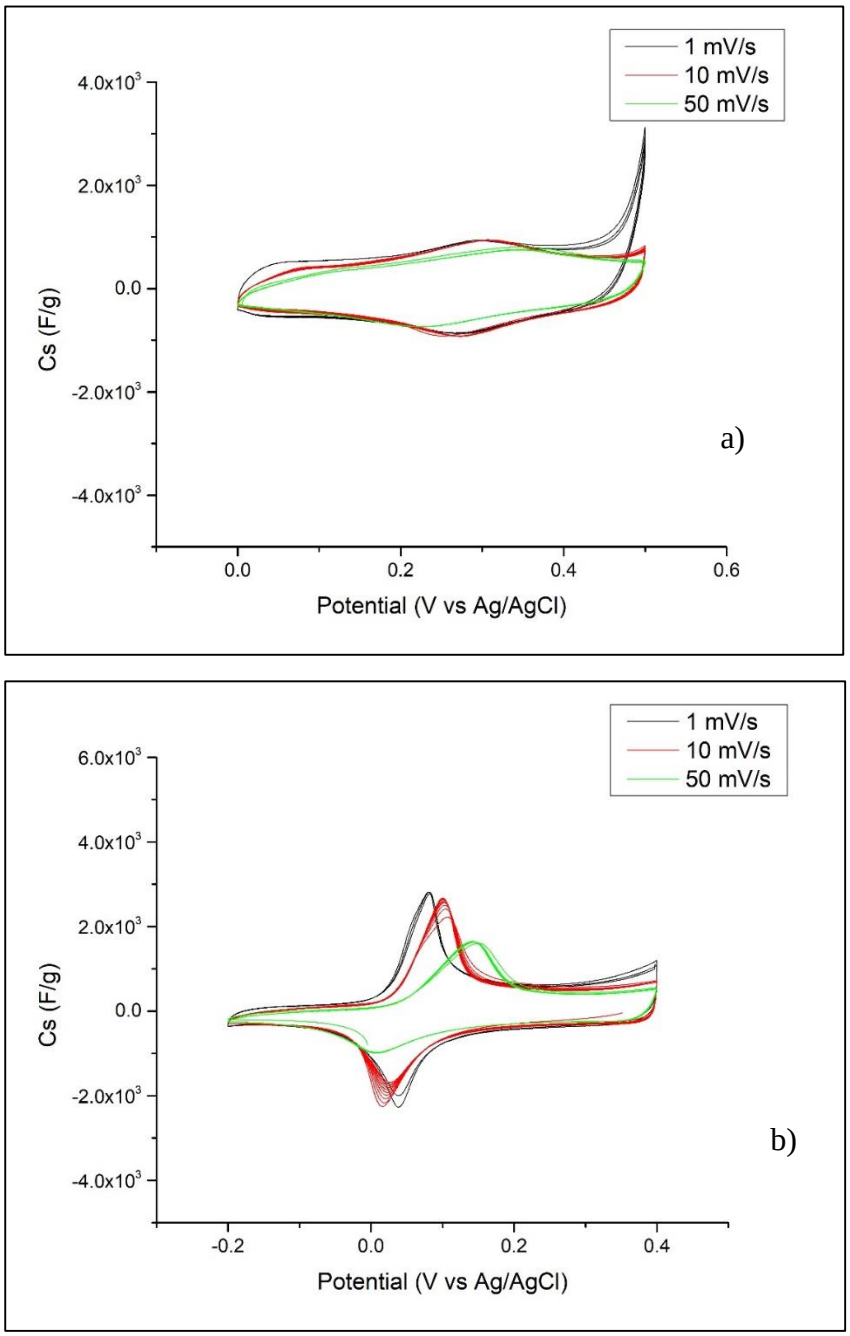

Figure 4.3.6: Dependence of the specific capacity on the scan rate for the Co/Al (a) and Co/Fe LDH (b).

Below is reported the same, but as support is used carbon tissue:

Deposition Time (s)	CoAl (F/g)	CoFe (F/g)
30	100	87
60	195	260
120	308	320

4.4 Morphological and structural characterization

4.4.1 SEM/EDX

SEM

From the morphological analysis of the electronic scanning microscope, the following images were obtained.

CuHCF

Samples were prepared following methods A and B depositing on graphoil and carbon tissue. Observing the images we notice a substantial difference in the amount of deposited material on the surface and presence of agglomerates. On both substrates it can be seen that the amount of deposition obtained with Method A is greater than that obtained with Method B. Moreover, on carbon tissue is observed for both methods as deposition does not occur uniformly and mainly affects the outer parts of the support, those in direct contact with the solution.

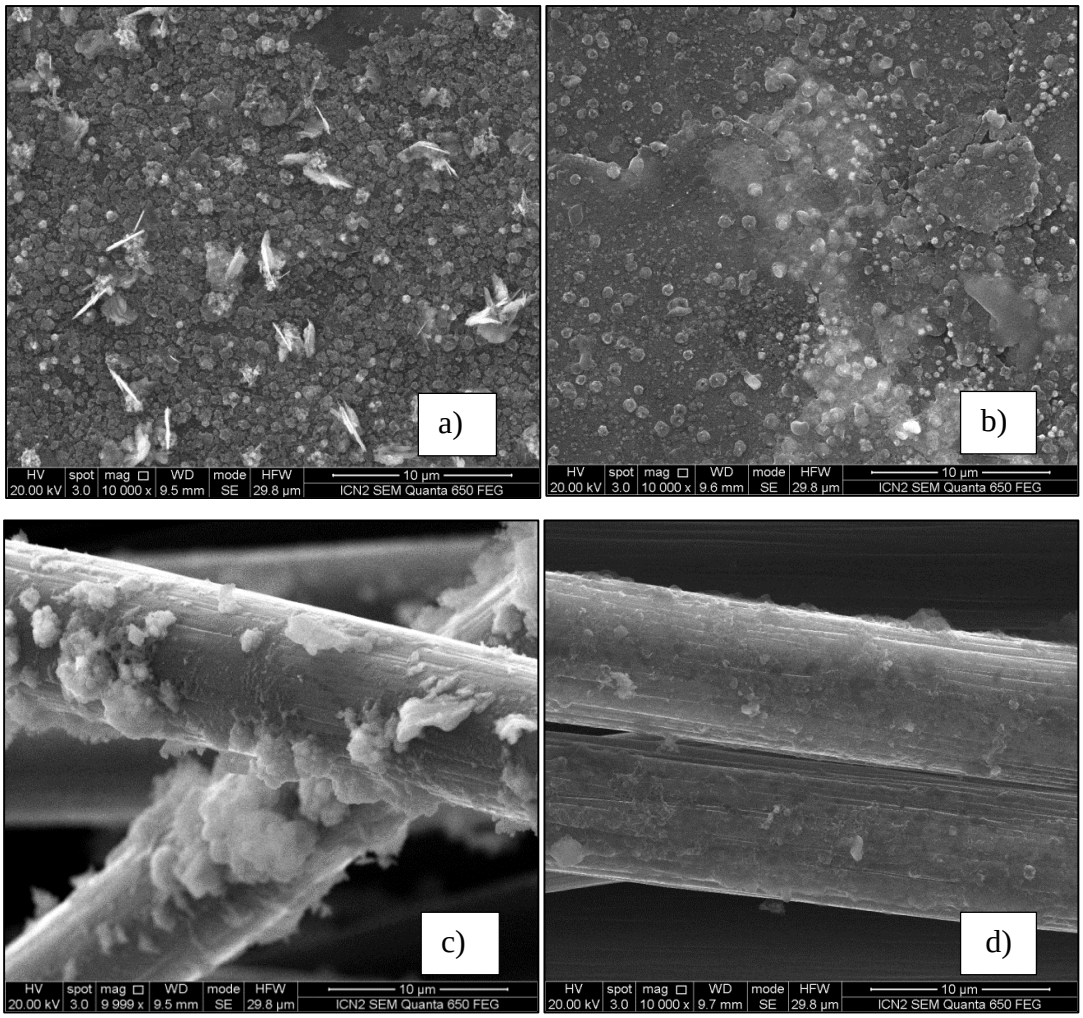

Figure 4.4.1: SEM images of CuHCF: a) film obtained by Method A on graphoil. b) film obtained by Method B on graphoil. c) film obtained by Method A on carbon tissue. d) film obtained by Method B on carbon tissue

NiHCF

Again, there is a non-homogeneity of the deposit that has agglomerates in some parts.

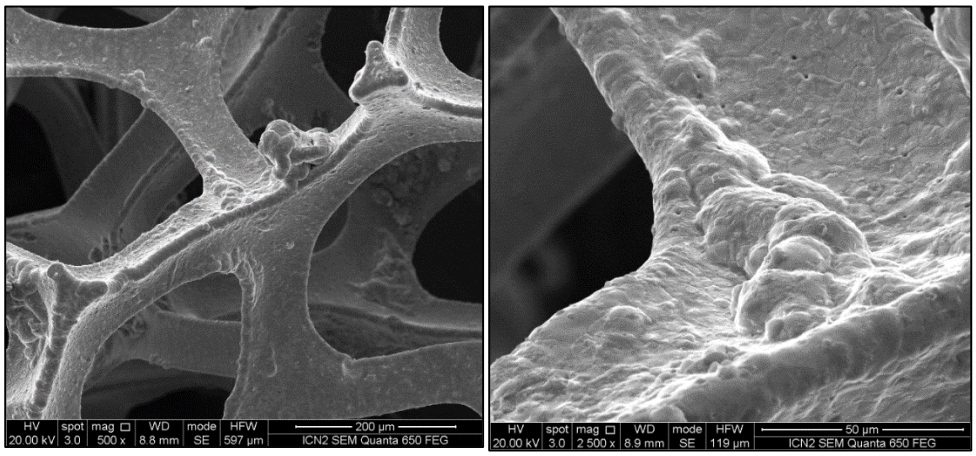

Figure 4.4.2: SEM images of NiHCF

LDH

From the images obtained by analysing the Co/Al LDH deposited for 30 seconds on the various supports we can observe that the film is rather homogeneous but not continuous, especially on porous supports (nickel foam, carbon tissue and toray paper) where a deposition is observed on the outer parts of these.

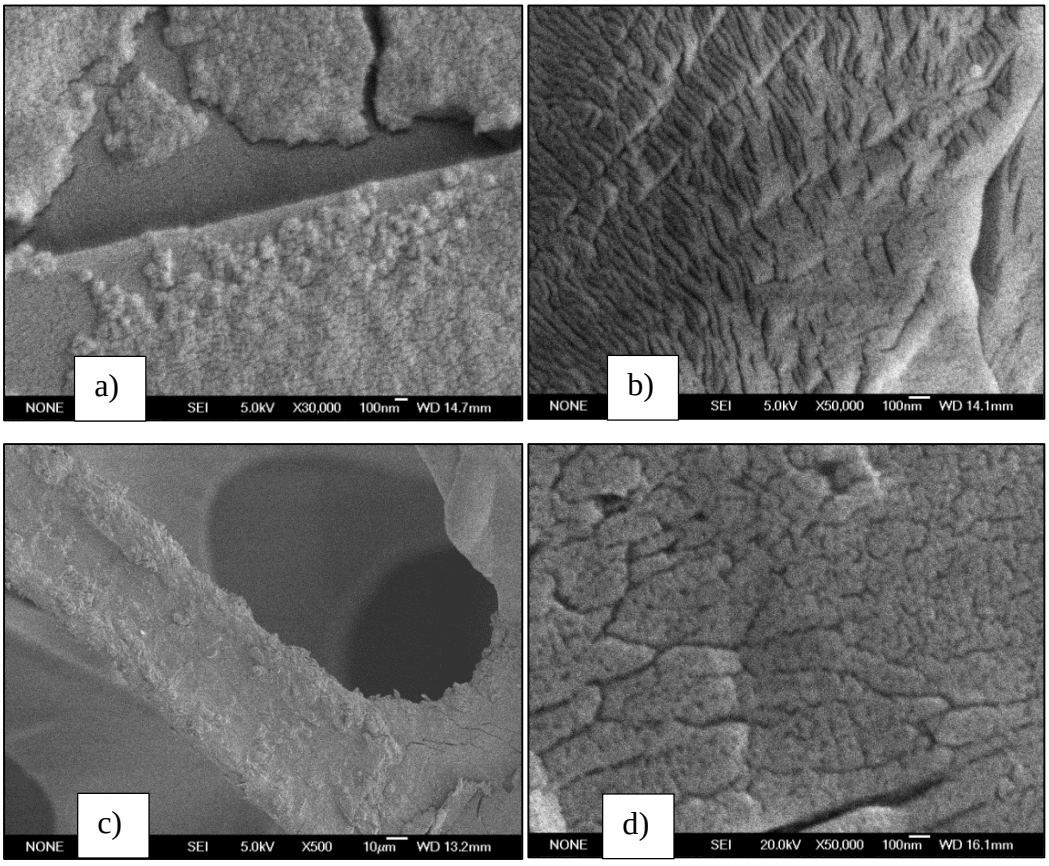

Figure 4.4.3: SEM images of CoAl LDH electro synthesized for 30 seconds: a) on Graphoil. b) Carbon Tissue. c) on Nickel Foam. d) on Toray Carbon Paper

Samples of CoFe LDHs deposited on graphoil for several times were analysed with SEM and it was noted that that increasing the deposition time also increases the amount of material covering the support, decreasing the holes shown in Figure 4.4.4a.

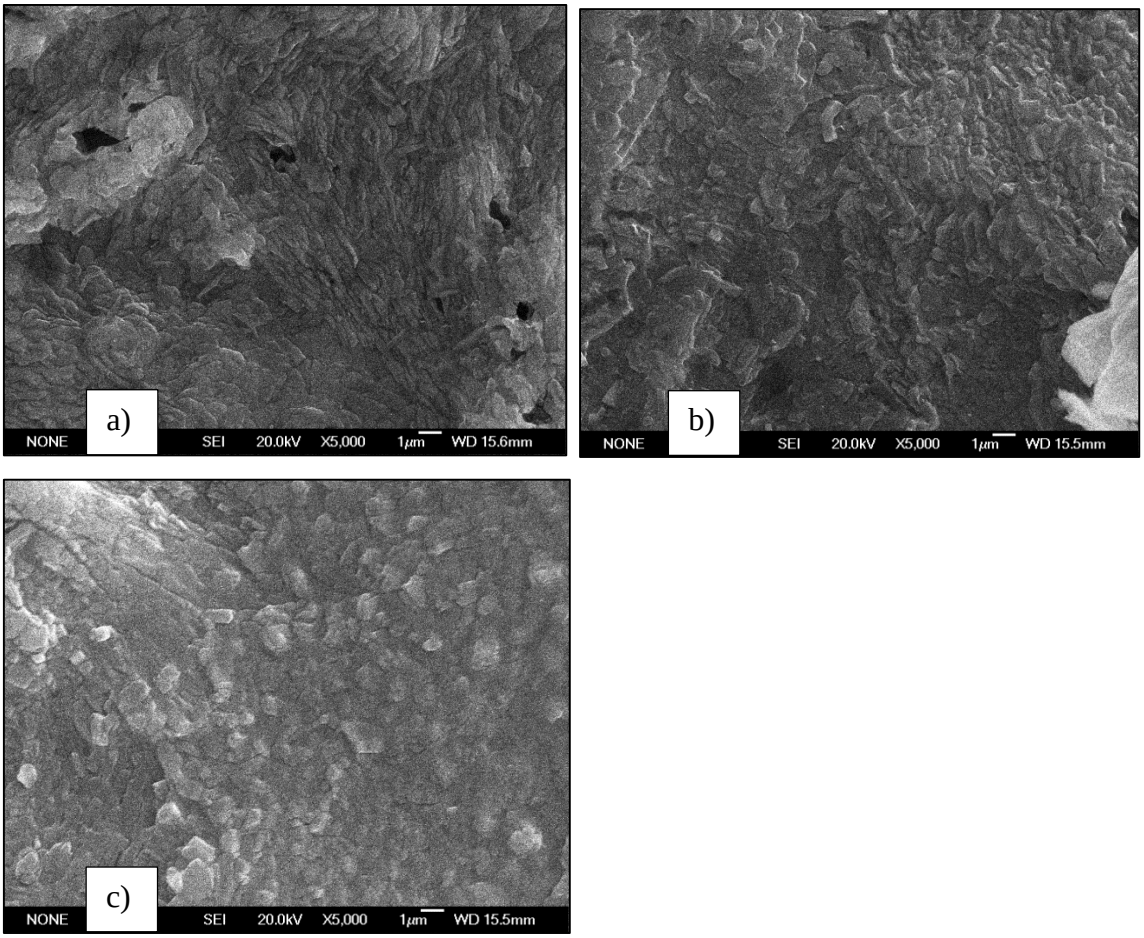

Figure 4.4.4: SEM images of CoFe LDH electro synthesized on Graphoil for different times: a) 30 seconds. b) 60 seconds. c) 120 seconds.

EDX

Elemental composition was studied by submitting samples to EDX analysis. In the case of CuHCF the ratio of Cu : Fe is seen to be somewhat variable (it has been calculated in various parts for the same sample) and except in one case (Carbon Tissue, Method B) is never the 2:1 or 1:1 stoichiometry. This is because not all the metallic copper deposited in the first step dissolves in the second one to form the metal hexacyanoferrate. Actually, a large fraction remains as such, i.e.: electrodeposited Cu. This, in turn, makes the EXD measure to probe not only the CuHCF on the surface but also the undissolved layer of Cu. Moreover, the ratio is greater for Method A than B because of the longer deposition times, and therefore more material deposits. Pollution of carbonaceous materials with metallic

impurities is reported in literature (83) and could be one of the causes of contamination. The data is also in agreement with the mass of metallic copper calculated before from the chronoamperometric curves.

Method	Support	Ratio (Cu:Fe)
A	Graphoil	7 : 1
		6 : 1
		11 : 1
	Carbon Tissue	16 : 1
		28 : 1
B	Graphoil	7 : 1
		9 : 1
	Carbon Tissue	1 : 1
		6 : 1

The same was done for the NiHCF but no trace of iron was found.

4.4.2 XRD

The measurements made with XRD are reported below. Figure 4.4.5a a is a comparison of samples with different deposits on the same support, i.e. carbon tissue. While in Figure 4.4.5b was analysed a sample of CoFe deposited for 120 on graphoil.

All samples show two broad graphite reflections at about 26.5º (002) and 54.5º (004). On these, there are many other smaller and with different intensity between one sample and the other, probably due to the different amount of material exposed to X - rays. The obtained peaks shape suggest a well-crystallized materials in some extent.

The CuHCF is the least crystalline one: additional peaks are not very intense but rather tight, so it would seem rather a matter of quantity of material.

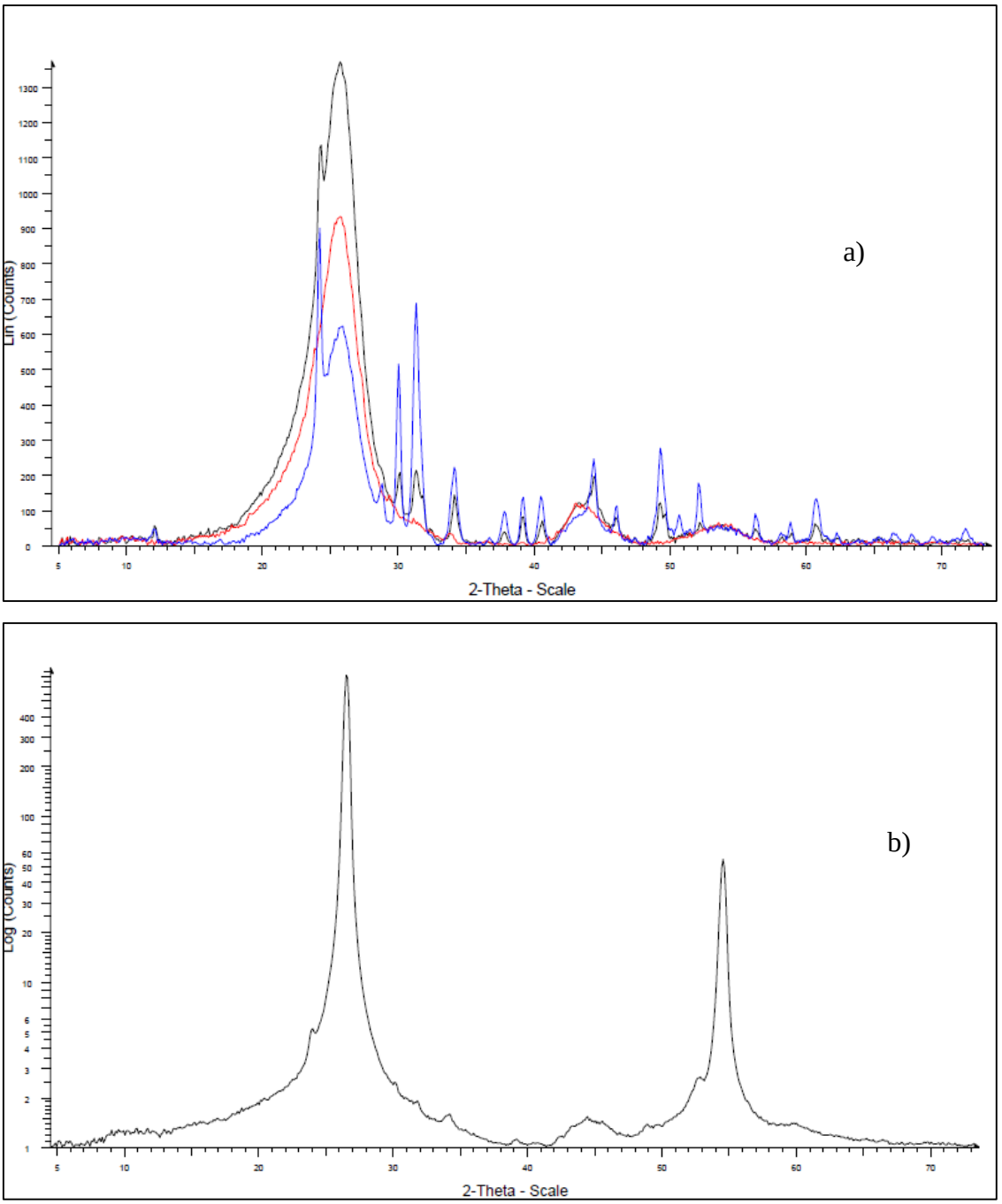

Figure 4.4.5: XRD images. a) of different compounds on Carbon Tissue: black line CoFe (120s), blue line CoAl (120s) and red line CuHCF A. b) of CoFe (120s) deposited on graphoil.

4.5 Testing the materials in a battery assembly

Using the support as cathode, there were carried out cyclic voltammetries in argon and in oxygen to understand the "basic" performance of the different supports. The three supports that have been tested are graphoil, carbon tissue and nickel foam. The last one gave very low current, inferior to an order than the other two, so it was decided not to proceed with subsequent analysis. In both of them there is an anodic peak only in oxygen while in argon

does not appear. Graphoil shows greater stability than carbon tissue but slightly lower currents.

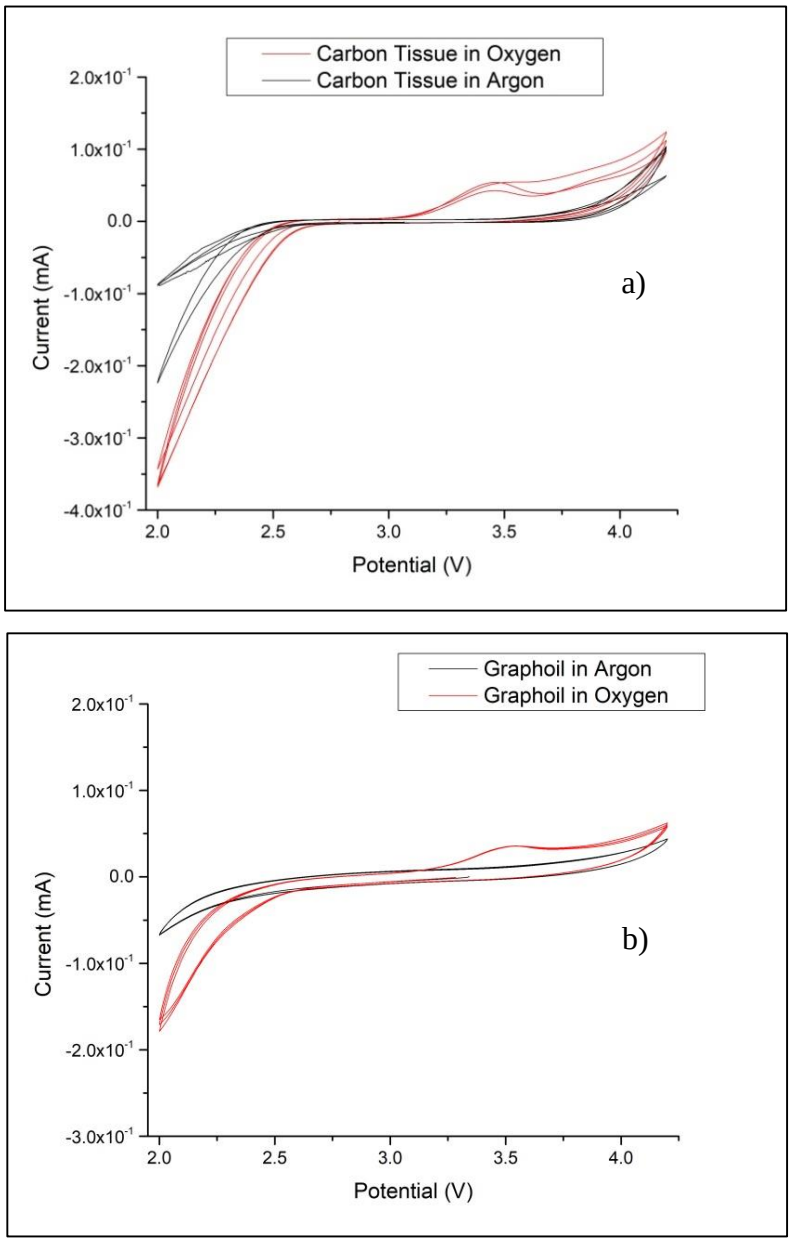

Figure 4.5.1: a) CVs of Carbon Tissue. b) CVs of Graphoil.

Multirate is useful to evaluate rate capability and reversibility. Several tests have been carried out at different densities of current values (0.01, 0.02, 0.05 and 0.1 mA/cm^2) Graphoil shows the smallest overpotentials and is less affected by current increase.

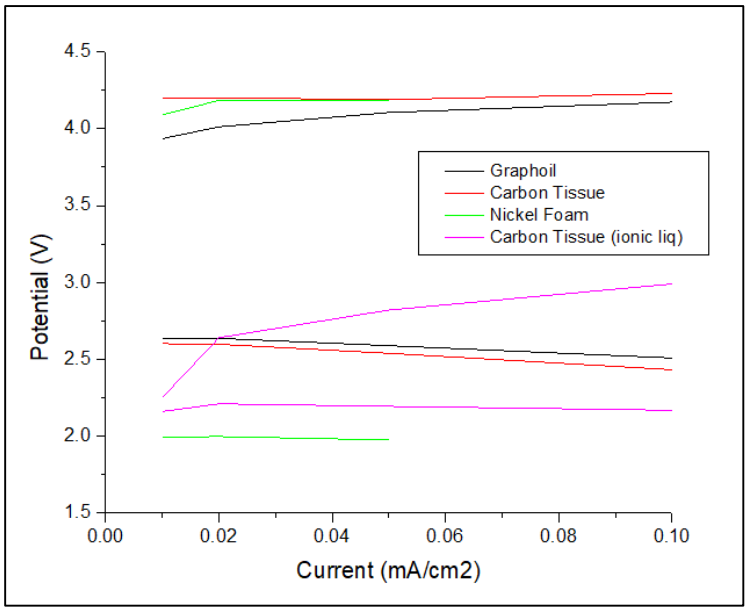

Figure 4.5.2: Multirate of the different supports.

From the Figure 4.5.3 it is observed that the carbon tissue gives greater capacity but there is also a great loss of capacity between one cycle and another. While the grahoil has a slightly lower capacity but with less leakage over time. Nickel foam does not even compete with these capacities that are anyway very low.

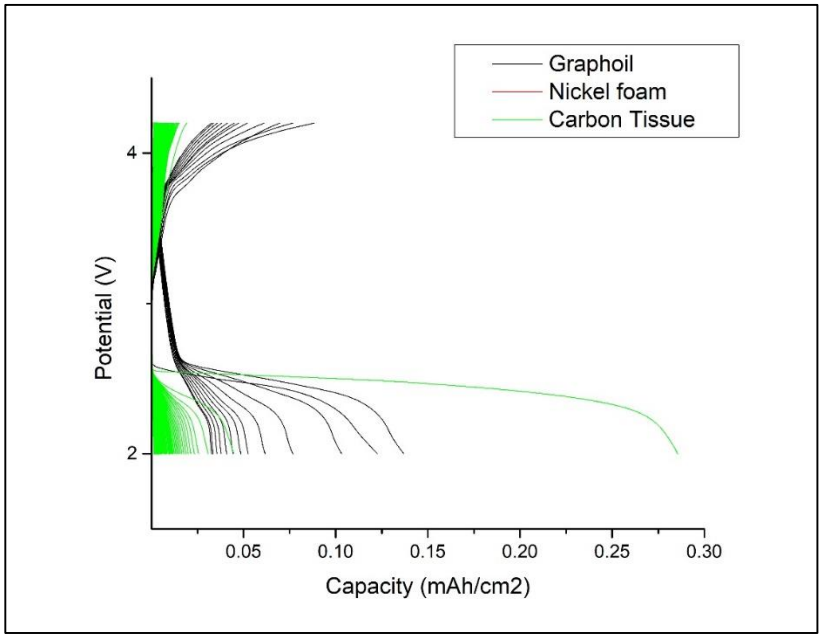

Figure 4.5.3: Full discharge of the different supports.

The redox activity of the deposited compounds was expected to intervene and facilitate the charge process. However, contrarily to the case of the aqueous electrolyte, no redox peaks were observed for any sample in this ether – based electrolyte in Ar, implying that also no Li^+ intercalation is occurring. Assuming that hindered intercalation supresses the charge transfer, a modification of the Li^+ solvation was attempted: 1) by using ionic liquids as

solvent or 2) by adding a small amount of water, which has been also suggested to assist cation intercalation. At the beginning 1000 ppm of water was added to the previous electrolyte, consisting of lithium triflate salt (CF3SO3Li) in DEGDME 1 M concentration. Then another electrolyte was prepared which consisted of a 0.6 M solution of triflate salt in ionic liquid. In this latter case, all the analyses were carried out at a temperature of 60 ° C because it is here that the ionic liquid, by decreasing its viscosity gives the best performance. By using water in the electrolyte, no oxygen peak is observed, but the cathodic currents in oxygen increase. In the case of ionic liquid, a peak in oxygen with a higher intensity than in the previous cases and even a small in argon is observed. Reduction currents are smaller, but oxidation is similar. There is therefore a better balance between discharge and charge which should lead to improved cycle life.

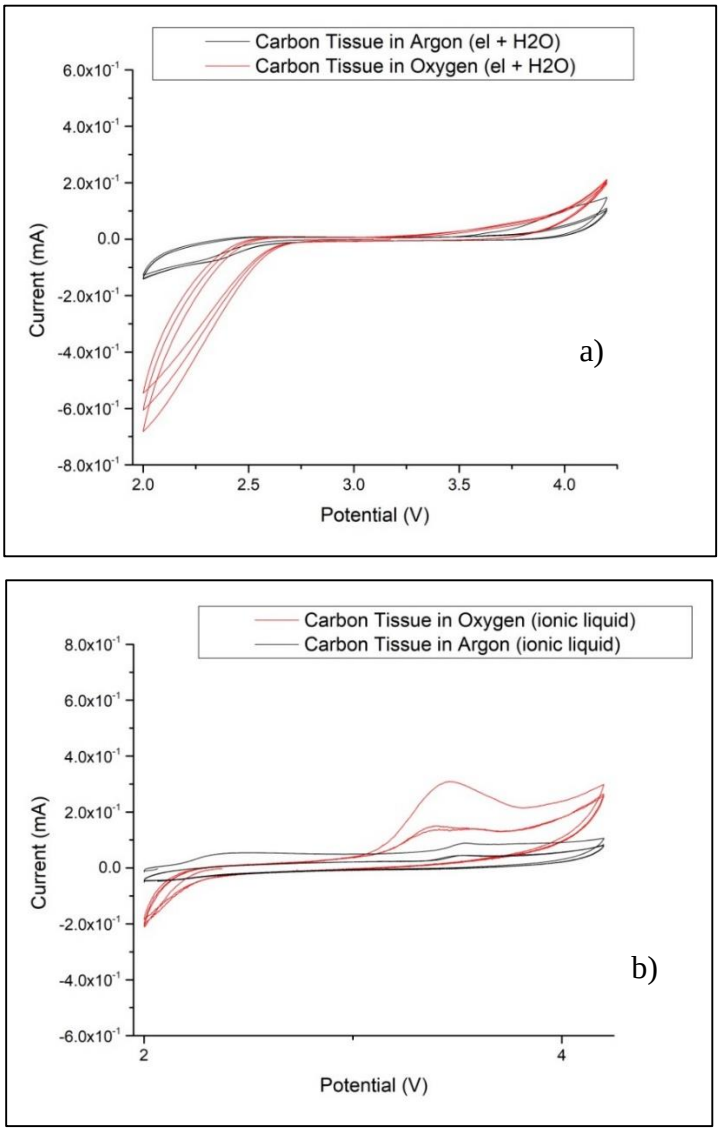

Figure 4.5.4: CVs of Carbon Tissue: a) in lithium triflate salt (CF3SO3Li) in DEGDME 1 M concentration with H_2O. b) in lithium triflate salt (CF3SO3Li) in ionic liquid 0.6 M concentration and a temperature of 60 °C.

The full discharges of the different compounds are compared below. We can notice how capacities, in both cases, are reduced if something is deposited over the support. Particularly in the case of graphoil, the deposits appear to be detrimental to the capacity, probably because they act as passivation covers on a flat surface.

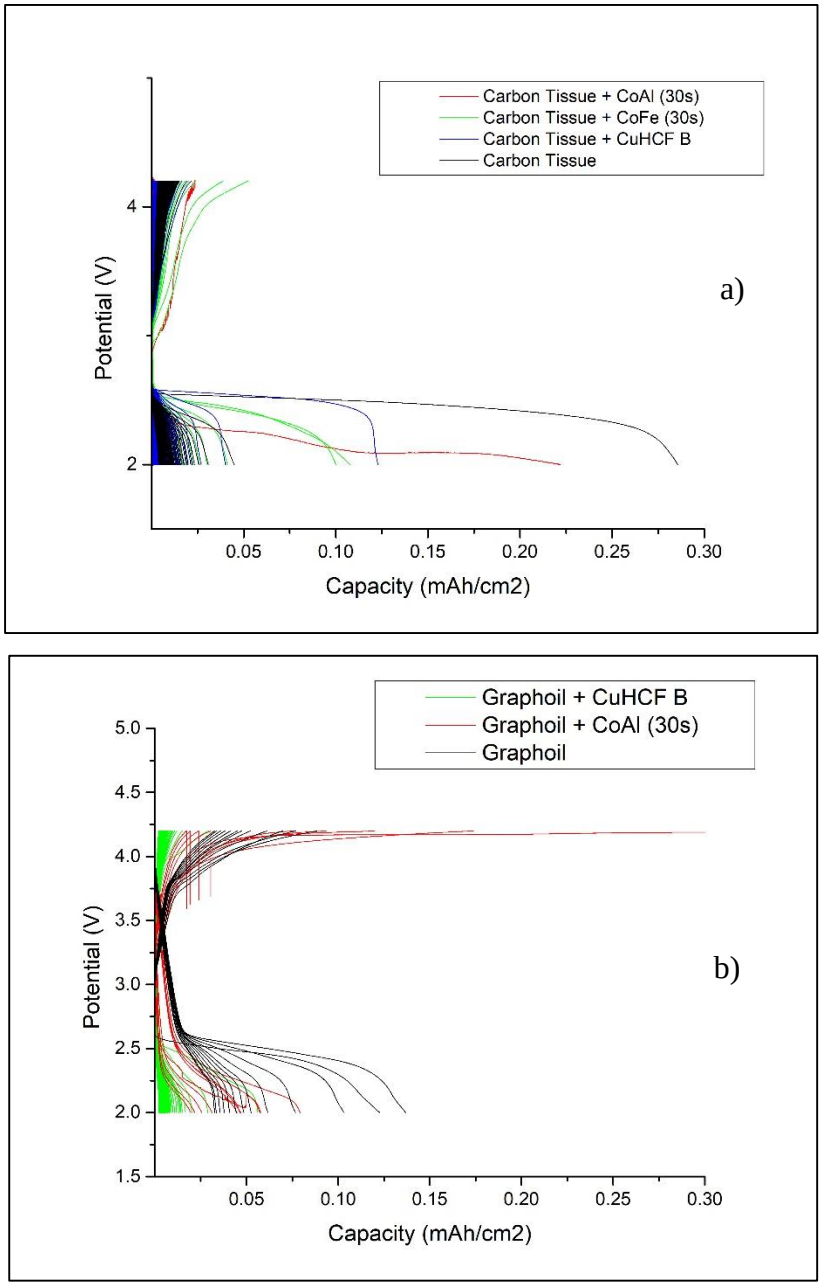

Figure 4.5.5: Comparison of full discharges: a) on Carbon Tissue. b) on Graphoil.

Next, those in other electrolytes are reported. In the case of the CuHCF in the electrolyte that contains water (Figure 4.5.6a) there would seem to be a positive response with the galvanostatics: the discharge is bigger, and above all, a first partial recharge is noted within the upper limit of potential. This allows a second discharge with less loss of capacity.

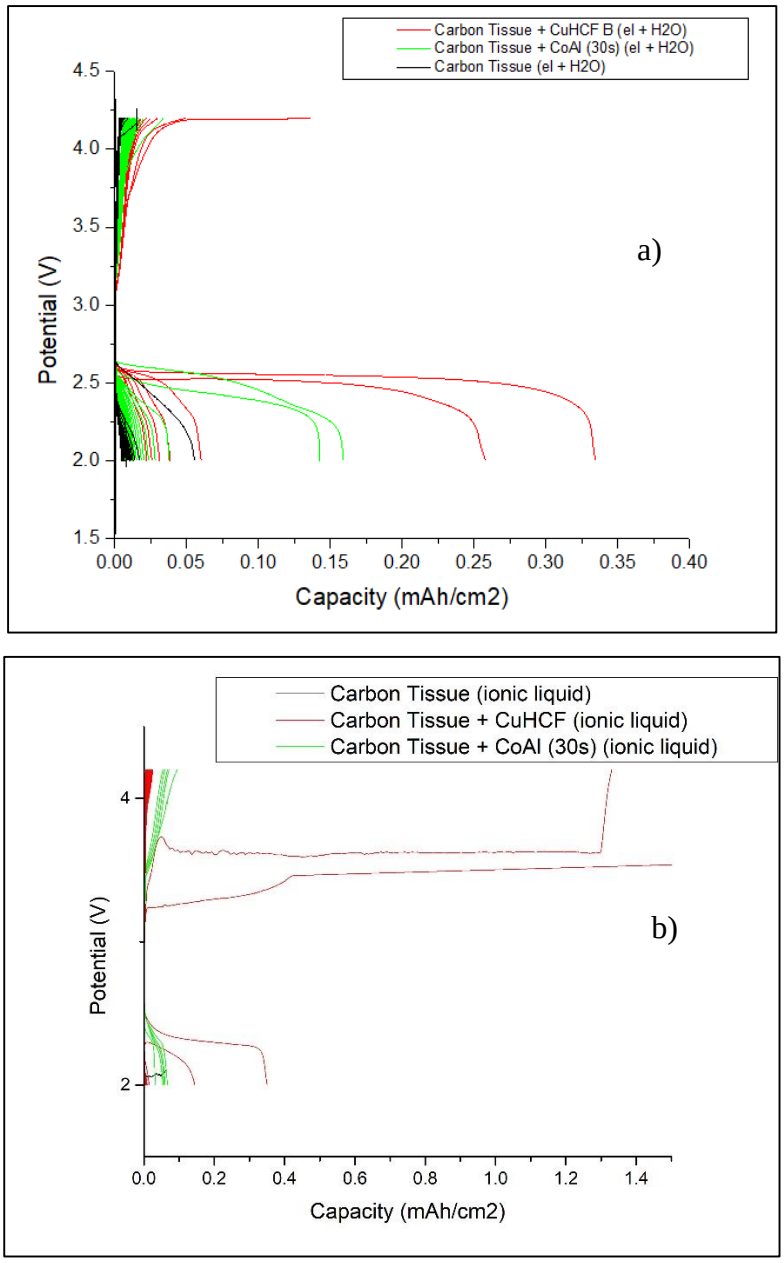

Figure 4.5.6: Comparison of full discharges of Carbon Tissue: a) in lithium triflate salt (CF3SO3Li) in DEGDME 1 M concentration with H_2O. b) in lithium triflate salt (CF3SO3Li) in ionic liquid 0.6 M concentration and a temperature of 60 °C.

4.6 Hair as a substrate

The hair was washed with soap and dried. Once dried it was placed in ceramic bowls and introduced into the oven. Here, a stabilization treatment has taken place up to a temperature of 300 °C in presence of oxygen with an increase in temperature of 1 °C per minute. Once reached the temperature of 300 °C this was maintained for 1 hour, after which the temperature was lowered to 20 °C with a ramp of 5 °C per minute. Small amounts of stabilized hair mixture and KOH were prepared in different ratios (1 to 2, 1 to 1.25, 1 to 1, 1 to 0.5, 1 to 0.25 and 1 to 0). After mixing well in a mortar, they were reintroduced into

the oven and subjected to activation treatment that bring to a temperature of 900 °C with an increase ramp of 3 °C per minute, keeping it for 3 hours and then bring it back to 20 °C with a ramp of 5 °C per minute, all in the presence of nitrogen with a flow of 28/30 bubbles every quarter of a minute. Taken out of the oven before it was neutralized with a solution of HCl 2M until it reached a pH of about 6, after which it was washed twice with water using a centrifuge. The first table shows the yield of the stabilized mass (SM) as a function of the initial one and we can see how it is fairly constant.

Test number	Yield (%)	Test number	Yield (%)
1	63	**7**	59
2	55	**8**	57
3	55	**9**	57
4	56	**10**	61
5	56	**11**	57
6	57		

Regarding the yield of the product obtained at the end of the thermal treatment with respect to the stabilized mass is quite variable, it is thought may be due to considerable leakage of material during the various steps.

The figure 4.6.1 shows the absorption isotherm of a sample with a ratio SM : KOH of 1: 1. The sample exhibit a IV type isotherm, typical of micro – mesoporous materials, where a hysteresis loop is associated with a mesopore filling process, governed by the phenomenon of capillary condensation. This type of isotherm is governed by a capillary condensation due to the filling (condensation) and emptying of pores (evaporation) occurs with different capillary rays, as a consequence of the type of pores that the material possesses.

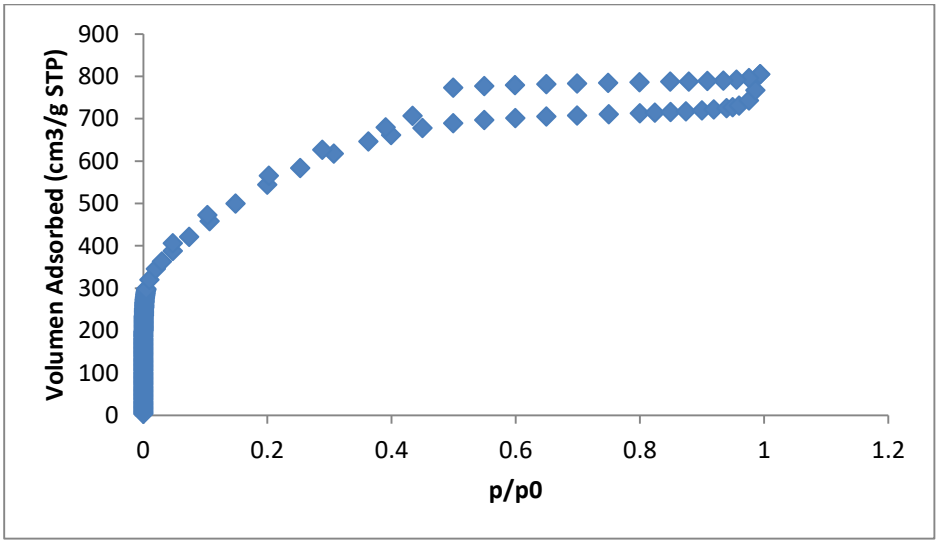

Figure 4.6.1: Nitrogen absorption isotherm of an hair sample with a ratio of 1 : 1 (SM : KOH).

Test were carried out on several samples with the aim of comparing the results for the same ratio (stabilized hair mass : KOH) and below is reported the average BET area for every ratio. Although yields are not always in agreement, it is noticed that this doesn't affect the properties of the material and that the values (of the different test with the same ratio) are quite similar.

Ratio (SM : KOH)	Average BET Surface Area (m^2/g)
1 : 0	4.63
1 : 0.5	1178
1 : 0.75	1764.5
1 : 1	1893.2
1 : 1.25	1316

A slurry was prepared using 5 mg of activated hair in the ratio of 1 : 1, 150 µL of Nafion perfluorinated resin solution 5 wt % in lower aliphatic alcohols and water. As solvent was used isopropanol. The mixture was stirred for 24 hours in a closed vessel. After the vessel was opened and the isopropanol has been left to evaporate until the slurry was dense enough.

The experiment was conducted in a three cell system where the working electrode was obtained after a drop of this slurry was put on a Glassy Carbon. The electrode was left to dry in the oven. The counter electrode was a platinum wire and the reference electrode an Ag/AgCl one. The specific capacitances were calculated according to the usual formula and reported according to the scan speed. Various tests were performed to see if there was reproducibility.

$$C_S = \frac{I}{v * m}$$

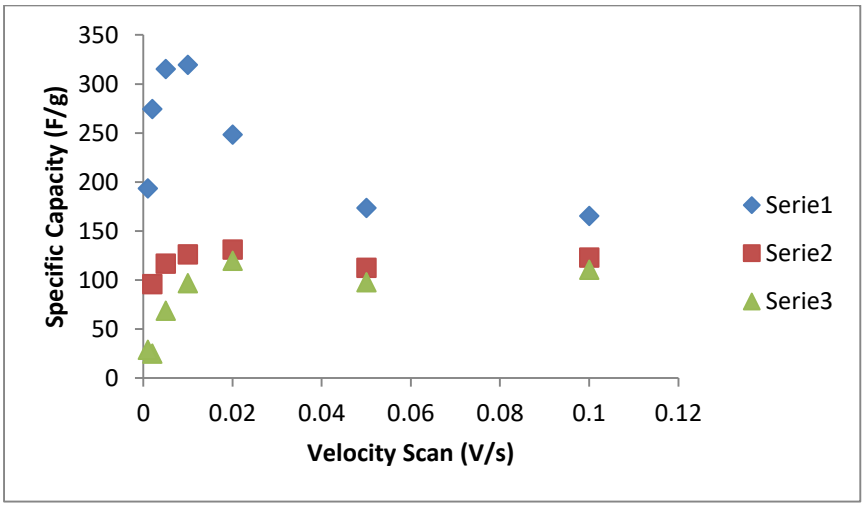

Figure 4.6.2: Specific capacity in function of velocity scan for the slurry of hair.

Chapter 5: Conclusions

Depositions and characterizations of CuHCF through two different protocols was conducted on several substrates. Method A consists of milder potentials for a longer time, while Method B applies extremes potentials for a short period of time. The two protocols lead to structural differences, as confirmed both by cyclic voltammetries and SEM – EDX characterizations. The shape of the cyclic voltammetry is the same regardless of the material used as a support, which leads us to conclude that the protocols developed can also be reproduced by changing the substrate. Method A has always given slightly higher currents than Method B, regardless of the support. However it is noted that with the carbon tissue the current are higher around an order of magnitude than those obtained with graphoil and carbon toray paper.

NiHCF electrosynthesis occurs only on a support, nickel foam. Electrochemical characterization by cyclic voltammetry has confirmed the reproducibility of the method. By changing the electrolyte we notice that the shape remains the same even if the peaks move to more positive potentials.

Also in the case of Co/Fe and Co/Al LDH various supports have been tested and it is observed that the cyclic voltammetries shape are retained. The first support studied was grahite and it has been proven to be an excellent support. The nickel foam, carbon tissue and carbon toray paper have the characteristic of high porosity and therefore exposed surface. This feature allows to obtain substantial large storage. In all cases, Co/Al and Co/Fe deposits were obtained, characterized by good reproducibility, and the specific capacitance were calculated from the characterizations performed, which is quite high.

Tests carried out on assembled Lithium – air battery using as cathode the various compounds have not given good results but allowed us to do an initial screening, paving the way for further testing.

Chapter 6: Bibliography

1. **Anonymou,** *"Miscellanea Berolinensia ad Incrementum Scientiarum(Berlin)", no.1, p. 377,* 1710

2. **Swiler, D. R.,** *"Pigments , Inorganic," Encyclopedia, Kirk-othmer Technology*, 2005

3. **E. Wiberg, N. Wiberg, and A. F. Holleman,** "*Inorganic chemistry", Academic Press,* 2001

4. **R. M. Izatt, G. D. Watt, C. H. Bartholomew, and J. J. Christensen,** *"A Calorimetric Study of Prussian Blue and Turnbull's Blue Formation", Inorganic Chemistry, vol. 9, no. 9, pp. 2019-2021,* 1970

5. **H.J. Busser, D. Schwarzenbach, W. Petter and A. Ludi,** *"The crystal structure of Prussian Blue: Fe4[Fe(CN)6] * xH2O", Inorganic Chemistry, pp 2704 - 2710,* 1977

6. **Miles, J. Keggin and F,** *"Structures and formulae of the Prussian blues and related compounds", Nature, vol. 137, no. 3466, pp 577-578,* 1936

7. **J. F. Duncan and P. W. R. Wigley,** *"The electronic structure of the iron atoms in complex iron cyanides", J. Chem. Soc., pp. 1120-1125,* 1963

8. **M. B. Robin and P. Day,** *"Mixed Valence Chemistry - A Survey and Classification", vol. 10 of Advances in Inorganic Chemistry and Radiochemistry, pp 247-422, Academic Press,* 1968

9. **H. J. Buser, D. Schwarzenbach, W. Petter, and a. Ludi,** *The crystal structure of Prussian Blue: Fe4[Fe(CN)6]3.xH2O", Inorganic Chemistry, vol. 16, no. 11, pp. 2704-2710,* 1977

10. **V. D. Neff,** *"Electrochemical Oxidation and Reduction of Thin Films of Prussian Blue", Journal of The Electrochemical Society, vol. 125, no. 6, p. 886,* 1978

11. **K. Itaya, H. Akahoshi, and S. Toshima,** *"Electrochemistry of Prussian Blue Modified Electrodes: An Electrochemical Preparation Method", Journal of The Electrochemical Society, vol. 129, no. 7, pp. 1498–1500,* 1982

12. **D. E. Ellis, M. A. Eckhoff, and V. D. Neff,** *"Electrochromism in the mixed-valence hexacyanides. 1. Voltammetric and spectral studies of the oxidation and reduction of thin films of Prussian blue", Journal of Physical Chemistry, vol. 85, no. 9, pp. 1225-1231,* 1981

13. **R. J. Mortimer and D. R. Rosseinsky,** *"Electrochemical polychromicity in iron hexacyanoferrate films, and a new film form of ferric ferricyanide", Journal of*

Electroanalytical Chemistry and Interfacial Electrochemistry, vol. 151, pp. 133–147, aug 1983

14. **L. Guadagnini, A. Maljusch, X. Chen, S. Neugebauer, D. Tonelli, andW. Schuhmann,** *"Visualization of electrocatalytic activity of microstructured metal hexacyanoferrates by means of redox competition mode of scanning electrochemical microscopy (RC- SECM)", Electrochimica Acta, vol. 54, no. 14, pp. 3753–3758,* 2009

15. **Y. Shan, G. Yang, J. Gong, X. Zhang, L. Zhu, and L. Qu,** *"Prussian blue nanoparticles potentiostatically electrodeposited on indium tin oxide/chitosan nanofibers electrode and their electrocatalysis towards hydrogen peroxide", Electrochimica Acta, vol. 53, no. 26, pp. 7751–7755,* 2008

16. **S. Lupu, L. Pigani, R. Seeber, F. Terzi, and C. Zanardi,** *"Study of Ultrathin Prussian Blue Films Using in situ Electrochemical Surface Plasmon Resonance", Collection of Czechoslovak Chemical Communications, vol. 70, no. 2, pp. 154–167,* 2005

17. **R. J. Mortimer Rosseinsky, D.R. and Glidle,** *"Polyelectrochromic Prussian blue: a chronoamperometric study of the electrodeposition", Sol. Energy Mater. Sol. Cells, vol. 25, pp. 211–230,* 1992

18. **M. Zadronecki, P. K. Wrona, and Z. Galus,** *"Study of Growth and the Electrochemical Behavior of Prussian Blue Films Using Electrochemical Quartz Crystal Microbalance", Journal of The Electrochemical Society, vol. 146, no. 2, pp. 620–627,* 1999

19. **J. Petersen, M. Michel, V. Toniazzo, D. Ruch, G. Schmerber, D. Ihiawakrim, D. Muller, A. Dinia, and V. Ball,** *"Atmospheric plasma polymer films as templates for inorganic synthesis to yield functional hybrid coatings", RSC Advances, vol. 2, no. 26, pp. 9860–9866,* 2012

20. **K. Itaya, T. Ataka, and S. Toshima,** *"Spectroelectrochemistry and electrochemical preparation method of Prussian blue modified electrodes", Journal of the American Chemical Society, vol. 104, no. 18, pp. 4767–4772,* 1982

21. **C. Kuhnhardt.** *"Nucleation and growth of Prussian Blue films on glassy carbon electrodes", Journal of Electroanalytical Chemistry, vol. 369, pp. 71–78,* may 1994

22. **E. C. Muñoz, R. A. Córdova, R. G. Henríquez, R. S. Schrebler, R. Cisternas, and R. E. Marotti,** *"Electrochemical synthesis and nucleation and growth mechanism of Prussian blue films on p-Si(100) electrodes", Journal of Solid State Electrochemistry vol. 16, no. 1, pp. 93–100,* 2012

23. **Y. Yao, X. Bai, and K.-K. Shiu,** *"Spontaneous Deposition of Prussian Blue on Multi-Walled Carbon Nanotubes and the Application in an Amperometric Biosensor", Nanomaterials, vol. 2, pp. 428–444,* 2012

24. **L. M. Siperko and T. Kuwana,** *"Electrochemical and Spectroscopic Studies of Metal Hexacyanometalate Films I. Cupric Hexacyanoferrate", Journal of The Electrochemical Society, vol. 130, no. 2, pp. 396-402,* 198

25. **H. Razmi and A. Azadbakht,** *"Electrochemical characteristics of dopamine oxidation at palladium hexacyanoferrate film, electroless plated on aluminum electrode", Electrochimica Acta, vol. 50, no. 11, pp. 2193–2201,* 2005

26. **V. Malev, V. Kurdakova, V. Kondratiev, and V. Zigel,** *"Indium hexacyanoferrate films,voltammetric and impedance characterization", Solid State Ionics, vol. 169, no. 1-4 SPEC. ISS., pp. 95–104,* 2004

27. **C. Liu, Y. Wang, G. Zhu, and S. Dong,** *"Study of cupric hexacyanoferrate-modified platinum electrodes using probe beam deflection and electrochemical quartz cry-stal microbalance techniques", Electrochimica Acta, vol. 42, no. 12, pp. 1795–1800,* 1997

28. **G. L. de Lara González, H. Kahlert, and F. Scholz,** *"Catalytic reduction of hydrogen peroxide at metal hexacyanoferrate composite electrodes and applications in enzymatic analysis", Electrochimica Acta, vol. 52, no. 5, pp. 1968–1974,* 2007

29. **A. V. Krylov and F. Lisdat,** *"Nickel hexacyanoferrate-based sensor electrode for the detection of nitric oxide at low potentials", Electroanalysis, vol. 19, no. 1, pp. 23–29,* 2007

30. **Z. Xun, C. Cai, W. Xing, and T. Lu,** *"Electrocatalytic oxidation of dopamine at a cobalt hexacyanoferrate modified glassy carbon electrode prepared by a new method",* 2003.

31. **C. G. Tsiafoulis, P. N. Trikalitis, and M. I. Prodromidis,** *"Synthesis, characterization and performance of vanadium hexacyanoferrate as electrocatalyst of H_2O_2", Electrochemistry Communications, vol. 7, no. 12, pp. 1398–1404,* 2005

32. **J. Joseph, H. Gomathi, and G. P. Rao,** *"Modification of carbon electrodes with zinc hexacyanoferrate", Journal of Electroanalytical Chemistry, vol. 431, no. 2, pp. 231– 235,* 1997

33. **H. Yu, Q. L. Sheng, and J. B. Zheng,** *"Preparation, electrochemical behavior and performance of gallium hexacyanoferrate as electrocatalyst of H_2O_2", Electrochimica Acta, vol. 52, no. 13, pp. 4403–4410,* 2007

34. **D. Jayasri and S. Sriman Narayanan,** *"Manganese(II) hexacyanoferrate based renewa-ble amperometric sensor for the determination of butylated hydroxyanisole in food products", Food Chemistry, vol. 101, no. 2, pp. 607–614,* 2007

35. **L. Guadagnini, M. Giorgetti, F. Tarterini, and D. Tonelli,** *"Electrocatalytic performances of pure and mixed hexacyanoferrates of Cu and Pd for the reduction of hydrogen peroxide", Electroanalysis, vol. 22, no. 15, pp. 1695–1701,* 2010

36. **X. Cui, L. Hong, and X. Lin,** *"Electrochemical preparation, characterization and application of electrodes modified with hybrid hexacyanoferrates of copper and cobalt",* 2002

37. **P. J. Kulesza, M. A. Malik, R. Schmidt, A. Smolinska, K. Miecznikowski, S. Zampo-ni, A. Czerwinski, M. Berrettoni, and R. Marassi,** *"Electrochemical preparation and characterization of electrodes modified with mixed hexacyanoferrates of nickel and palladium", Journal of Electroanalytical Chemistry, vol. 487, no. 1, pp. 57–65,* 2000

38. **P. J. Kulesza,** *"Hybrid Metal Cyanometallates Electrochemical Charging and Spectrochemical Identity of Heteronuclear Nickel/Cobalt Hexacyanoferrate", Journal of The Electrochemical Society, vol. 146, no. 10, p. 3757,* 1999

39. **R. Pauliukaite, S. B. Hocevar, E. A. Hutton, and B. Ogorevc,** *"Novel electrochemical microsensor for hydrogen peroxide based on iron-ruthenium hexacyanoferrate modified carbon fiber electrode", Electroanalysis, vol. 20, no. 1, pp. 47–53,* 2008

40. **Q. L. Sheng, H. Yu, and J. B. Zheng,** *"Sol-gel derived carbon ceramic electrode for the investigation of the electrochemical behavior and electrocatalytic activity of neodymium hexacyanoferrate", Electrochimica Acta, vol. 52, no. 13, pp. 4506–4512,* 2007

41. **D. Woermann,** *"Anorganische Fiillungsmembranen", Naturwissenschaften, pp. 528–535,* 1987

42. **M. Giorgetti, L. Guadagnini, D. Tonelli, M. Minicucci, and G. Aquilanti,** *"Structural characterization of electrodeposited copper hexacyanoferrate films by using a spectroscopic multi-technique approach", Physical chemistry chemical physics : PCCP, vol. 14, no. 16, pp. 5527–5537,* 2012

43. **Z. Jia, J. Wang, and Y. Wang,** *"Electrochemical sodium storage of copper hexacyanoferrate with a well-defined open framework for sodium ion batteries", RSC Adv., vol. 4, no. 43, pp. 22768–22774,* 2014

44. **S. Ayrault, C. Loos-Neskovic, M. Fedoroff, E. Garnier, and D. J. Jones,** *"Compositions and structures of copper hexacyanoferrates(II) and (III): experimental results", Talanta, vol. 42, no. 11, pp. 1581–1593,* 1995

45. **C. Loos-Neskovic, S. Ayrault, V. Badillo, B. Jimenez, E. Garnier, M. Fedoroff, D. J. Jones, and B. Merinov,** *"Structure of copper-potassium hexacyanoferrate (II) and sorption mechanisms of cesium", Journal of Solid State Chemistry, vol. 177, no. 6, pp 817–1828,* 2004

46. **D. R. Shankaran and S. S. Narayanan,** *"Characterization and application of an electrode modified by mechanically immobilized copper hexacyanoferrate", Fresenius' Journal of Analytical Chemistry, vol. 364, no. 8, pp. 686–689,* 1999

47. **O. Makowski, J. Stroka, P. J. Kulesza, M. a. Malik, and Z. Galus,** *"Electrochemical identity of copper hexacyanoferrate in the solid-state: Evidence for the presence and redox activity of both iron and copper ionic sites", Journal of Electroanalytical Chemistry, vol. 532, pp. 157–164,* 2002

48. **N. Zakharchuk, N. Naumov, R. Stoesser, U. Schroeder, F. Scholz, and H. Mehner,** *"Solid state electrochemistry, X-ray powder diffraction, magnetic susceptibility, electron spin resonance, Mossbauer and diffuse reflectance spectroscopy of mixed iron(III)-cadmium(II) hexacyanoferrates", Journal of Solid State Electrochemistry, vol. 3,* 1999

49. **R. Ojani, J.-B. Raoof, and B. Norouzi,** *"Cu(II) Hexacyanoferrate(III) Modified Carbon Paste Electrode; Application for Electrocatalytic Detection of Nitrite", Electroanalysis, vol. 20, no. 18, pp. 1996–2002,* 2008

50. **A. P. Baioni, M. Vidotti, P. A. Fiorito, E. A. Ponzio, and S. I. C. De Torresi,** *"Synthesis and characterization of copper hexacyanoferrate nanoparticles for building up long-term stability electrochromic electrodes", Langmuir, vol. 23, no. 12, pp. 6796–6800,* 2007

51. **M. A. Malik and P. J. Kulesza,** *"Preparation and characterization of Ag-intercalated copper hexacyanoferrate films on electrodes", Electroanalysis, vol. 8, no. 2, pp. 113– 116,* 1996

52. **L. Guadagnini, D. Tonelli, and M. Giorgetti,** *"Improved performances of electrodes based on Cu2+-loaded copper hexacyanoferrate for hydrogen peroxide detection", Electrochimica Acta, vol. 55, no. 17, pp. 5036–5039,* 2010

53. **S. M. Chen and C. M. Chan,** *"Preparation, characterization, and electrocatalytic properties of copper hexacyanoferrate film and bilayer film modified electrodes", Journal of Electroanalytical Chemistry, vol. 543, no. 2, pp. 161–173,* 2003

54. **R. Garjonyte and A. Malinauskas,** *“Operational stability of amperometric hydrogen peroxide sensors, based on ferrous and copper hexacyanoferrates”, Sensors and Actuators, B: Chemical, vol. 56, no. 1, pp. 93–97,* 1999

55. **I. L. De Mattos, L. Gorton, T. Laurell, A. Malinauskas, and A. A. Karyakin,** *“Development of biosensors based on hexacyanoferrates”, Talanta, vol. 52, no. 5, pp. 791–799,* 2000

56. **M. A. Lilga, R. J. Orth, J. P. H. Sukamto, S. D. Rassat, J. D. Genders, and R. Gopal,** *"Cesium separation using electrically switched ion exchange", Separation and Purification rechnology, pp 451-466,* 2001,

57. **Y. Lin and X. Cui,** *"Electrosynthesis, characterization, and application of novel hybrid materials based on carbon nanotube- polyaniline - nickel hexacyanoferrate nanocomposites", Journal of Materials Chemistry, p 585,* 2006,

58. **Y. Lin and X. Cui**, *"Novel hybrid materials with high stability for electrically switched ion exchange: carbon nanotube-polyaniline-nickel hexacyanoferrate nanocomposites", Chemical communications (Cambridge, England), pp 2226 - 2228,* 2005

59. **S. Zamponi, M. Berrettoni, P. J. Kulesza, K. Miecznikowski, M. A. Malik, O. Makowski, and R. Marassi,** *"Influence of experimental conditions on electrochemical behavior of Prussian blue type nickel hexacyanoferrate film", Elctrochimica Acta, pp 4261 - 4269,* 2003

60. **G. R. Chen, Y. R. Chang, X. Liu, T. Kawamoto, H. Tanaka, A. Kitajima, D. Parajuli, M. Takasaki, K. Yoshino, M. L. Chen, Y. K. Lo, Z. Lei, and D. J. Lee,** *"Prussian blue (PB) granules for cesium (Cs) removal from drinking water", Separation and Purification Technology, pp 146 - 151,* 2015

61. **D. Parajuli, A. Takahashi, H. Noguchi, A. Kitajima, H. Tanaka, M. Takasaki, K. Yoshino, and T. Kawamoto,** *"Comparative study of the factors associated with the application of metal hexacyanoferrates for environmental Cs decontamination", Chemical Engineering Journal, pp 1322 - 1328,* 2016,

62. **A. A. Karyakin,** *"Prussian blue and its analogues: Electrochemistry and analytical applications", Electroanalysis, pp 813 - 819,* 2001

63. **M. Orellana, R. Del Rio, R. Schrebler, and R. Cordova,** *"A potentiostatic and atomic force microscopy study of the nucleation and growth mechanisms of certain metallic cyanometalates", Journal of Physical Chemistry C, pp 17541 - 17550,* 2007

64. S. **Sinha and A. B. Bocarsly,** *"Effects of surface structure on electrode charge transfer properties", Journal of Electroanalytical Chemistry and Interfacial Electrochemistry, pp 167 - 172,* 1982

65. **F. Cavani, F. Trifirb, A. Vaccari,** *"Hydrotalcite-type anionic clays: preparation, properties and applications", Catal. Today11, pp 173-301,* 1991

66. **G. Henze,** *"Analytical Voltammetry and Polarography", in Ullmann's Encyclopedia of Industrial Chemistry, p. 431,* 2008

67. **J. C. Long and J. M. Criscione,** *"Carbon, Survey", in Kirk-Othmer Encyclopedia of Chemical Technology, vol. 4, pp. 733–741,* 2003

68. **G. M. Jenkins and K. Kawamura,** *"Structure of Glassy Carbon", Nature, vol. 231, no. 5299, pp. 175–176,* 1971

69. **P. J. F. Harris,** *"Fullerene-related structure of commercial glassy carbons", Philosophical Magazine, vol. 84, no. 29, pp. 3159–3167,* 2004

70. **Wenjin Qian, Fengxia Sun, Yanhui Xu, LIhua Qiu, Changhai Liu, Suidong Wang and Feng Yan,** *Human hair-derived carbon flakes for electrochemical supercapacitors,* 2014

71. **D. Engel and E.W. Grabner,** *"Charge Transfer at a Copperhexacyanoferrate-Modified Glassy Carbon Electrode", Zeitschrift für Physikalische Chemie, vol. 160, pp. 151–168,* 1988

72. **D. Engel and E. W. Grabner,** *"Copper Hexacyanoferrate-Modified Glassy Carbon: A Novel Type of Potassium-Seletive Electrode", Berichte der Bunsengesellschaft für physikalische Chemie, vol. 89, no. 9, pp. 982–986,* 1985

73. **Z. Jia, B. Wang, and Y. Wang,** *"Copper hexacyanoferrate with a well-defined open framework as a positive electrode for aqueous zinc ion batteries", Materials Chemistry and Physics, vol. 149, pp. 601–606,* 2015

74. **S. Liu, G. L. Pan, G. R. Li, and X. P. Gao,** *"Copper hexacyanoferrate nanoparticles as cathode material for aqueous Al-ion batteries", J. Mater. Chem. A, vol. 3, no. 3, pp. 959–962,* 2014

75. **D.G. Kwabi, N. Ortiz - Vitoriano, S.A. Freunberger, Y. Chen, N. Imanishi, P.G. Bruce and Y. Shao - Horn,** *"Material challenges in rechargeable lithium - air batteries",* 2014

76. **M. Gong, Y. Li, H. Wang, Y. Liang, J.Z. Wu, J. Zhou, J. Wang, T. Regier, F. Wei, H. Dai,** *"An advanced Ni–Fe Layered Double Hydroxide electrocatalyst for water oxidation", J. Am. Chem. Soc. 135,* 2013

77. **Junke Ou, Yongzhi Zhang, Li Chen, Hongyan Yuan and Dan Xiao,** *"Heteroatom doped porous carbn derived from hair as an anode with high performance for lithium ion batteries", RSC Adv, 4, 63784,.* 2014

78. **Stephen Brunauer, P. H. Emmett, Edward Teller,** *"Adsorption of gases in multimolecular layers", J. Am. Chem. Soc., 60 (2), pp 309 -319,* 1938

79. **M.M. Dubinin, E.D. Zaverina, L.V. Radushkevich,** *"Sorption and structure of active carbons. I. Adsorption of organic vapors", Zh. Fiz. Khim., pp 1351 - 1362,* 1947

80. **S. Zamponi, M. Berrettoni, P. J. Kulesza, K. Miecznikowski, M. A. Malik, O. Makowski,** *"Influence of experimental conditions on electrochemical behaviour of Prussian Blue tyoe nickel hexayanoferrate film", Electrochimica Acta, pp 4261 - 4269,* 2003

81. **Ylea Vlamidis, Erika Scavetta, Massima Gazzano, Domenica Tonelli,** *"Iron vs aluminium based layered double hydroxides as water splitting ctatlysts", Electrochimica Acta, Vol 188, pp 653 - 660,* 2016

82. **Hao Chen, Linfeng Hu, Min Chen, Yan Yan, Limin Wu,** *"Nickel–cobalt layered double hydroxide nanosheets for high-performance supercapacitor electrode materials", Adv. Funct. Mater., pp 934–942,* 2014

83. **Y. Lum, Y. Kwon, P. Lobaccaro, L. Chen, E. L. Clark, A. T. Bell, and J. W. Ager,** *"Trace Levels of Copper in Carbon Materials Show Significant Electrochemical CO2 Reduction Activity", ACS Catalysis,* 2015

Acknowledgments

I would first like to thank my thesis advisor Prof. Marco Giorgetti for the continuous support, his patience and motivation. Without his encouragement, I would not have taken part in that wonderful experience called Erasmus, which not only made me grow professionally but also personally.

Besides my advisor, I would like to thank the rest of my thesis committee: Prof Eduardo Enciso Rodriguez for his availability and patience not only in helping me with the thesis but also in giving me life-advice. My sincere thanks also goes to Dino Tonti for offering me the opportunity to work with him. A special thanks goes to Ylea Vlamidis for being there for me, helping and giving advice on my thesis and reassuring me.

I must express my very profound gratitude to my parents and grandmother for providing me with unfailing support and continuous encouragement throughout my years of study and through the process of researching and writing this thesis. This accomplishment would not have been possible without them. Thank you.

Finally, I would like to acknowledge all my friends and people I have met during this time, who support me all the time and without whom everything would have been more difficult. A special thanks to Mae Charef that shared my Erasmus experience and helped me in different ways and also to Tommaso Salzillo who has been a dear friend and a confidant.